The University of Southern Mississippi
The Aquila Digital Community

Dissertations

Fall 2018

Effect of Network Structure on Free Volume and Gas Transport Properties of Thiol-Ene and Epoxy-Amine Networks

Ramesh Krishnan Ramakrishnan
University of Southern Mississippi

Follow this and additional works at: https://aquila.usm.edu/dissertations

 Part of the Physical Chemistry Commons, and the Polymer Chemistry Commons

Recommended Citation

Ramakrishnan, Ramesh Krishnan, "Effect of Network Structure on Free Volume and Gas Transport Properties of Thiol-Ene and Epoxy-Amine Networks" (2018). *Dissertations*. 1601.
https://aquila.usm.edu/dissertations/1601

This Dissertation is brought to you for free and open access by The Aquila Digital Community. It has been accepted for inclusion in Dissertations by an authorized administrator of The Aquila Digital Community. For more information, please contact Joshua.Cromwell@usm.edu.

EFFECT OF NETWORK STRUCTURE ON FREE VOLUME AND GAS TRANSPORT PROPERTIES OF THIOL-ENE AND EPOXY-AMINE NETWORKS

by

Ramesh Krishnan Ramakrishnan

A Dissertation
Submitted to the Graduate School,
the College of Arts and Sciences
and the School of Polymer Science and Engineering
at The University of Southern Mississippi
in Partial Fulfillment of the Requirements
for the Degree of Doctor of Philosophy

Approved by:

Dr. Sergei Nazarenko, Committee Chair
Dr. Sarah Morgan
Dr. Jeffrey Wiggins
Dr. James Rawlins
Dr. Gopinath Subramanian

Dr. Sergei Nazarenko Committee Chair	Dr. Jeffrey Wiggins Director of School	Dr. Karen S. Coats Dean of the Graduate School

December 2018

COPYRIGHT BY

Ramesh Krishnan Ramakrishnan

2018

Published by the Graduate School

ABSTRACT

Network parameters such as cross-link density or intermolecular interactions were used as effective parameters to control polymer chain packing or free volume and thereby control the mass transport properties of networks.

A series of polyethylene glycol (PEG) based thiol-ene elastomeric networks having a broad range of molecular weight between cross-links, M_c, (inverse of cross-link density) was prepared. The specific volume of the networks was studied as a function of temperature and pressure using high pressure dilatometry, and the obtained PVT data was fit using Simha-Somcynsky equation of state (S-S eos) analysis. Fractional free volume, quantified through S-S eos analysis, changed linearly as a function of cross-link density of the networks proving that the system obeyed Fox and Loshaek model. Average free volume hole size, $<v_h>$, of the networks was directly probed using positron annihilation lifetime spectroscopy (PALS). $<v_h>$ of the networks also changed linearly as a function of cross-link density. Typically, in traditional elastomers, changing cross-link density also causes simultaneous changes in chemical nature or polarity of the system, therefore those systems deviate from Fox and Loshaek model. Internal pressure P_i of the networks, calculated from PVT data, showed similar values for all networks, and the same was the case for storage permittivity values obtained from dielectric spectroscopy analysis. This proved that the chemical nature of the networks was unaffected and cross-link density was the only parameter controlling the free volume of the networks. Gas diffusivity of the networks obeyed Cohen Turnbull model, and thus the experimental gas diffusivity trends were modeled as a function of molecular weight between cross-links of the networks.

The effect of intermolecular (repulsive) interactions on free volume and gas transport was studied in a series of perfluorinated thiol-ene elastomers. Perfluorinated thiol-ene elastomers were prepared via 2-step synthesis. In the first step, a four-functional thiol was converted into a three functional thiol containing a perfluorinated dangling moiety via Thio Michael addition reaction with a perfluorinated acrylate. The modified thiol monomer was then reacted with triene to obtain perfluorinated thiol-ene networks. Fluorine content was varied by changing the length of perfluorinated moiety used in Thio Michael addition and this enabled the synthesis of a series of perfluorinated networks containing perfluorinated dangling moieties of different lengths. Fast reaction kinetics of thiol-ene chemistry prevented the phase separation of perfluorinated moieties and locked-in the thermodynamically frustrated perfluorinated moieties within the thiol-ene scaffold. The repulsive interactions between highly non-polar perfluorinated moieties and polar thiol-ene backbone created huge free volume pockets in the network. For the biggest perfluorinated dangling moiety used in this study, $<v_h>$ increased by four times in comparison to an unmodified network. The gas transport properties showed a significant improvement as a function of the length of the dangling moiety. But gas diffusivity of the networks did not obey Cohen Turnbull model. The deviation was explained by the static nature of free volume pockets around perfluorinated moieties, and percolation of free volume pockets as the sizes of free volume cavities increased.

The 2-step synthetic approach was taken a step further to prepare a series of hybrid thiol-ene elastomers containing varying concentrations of polar PEG moieties and non-polar perfluorinated moieties. The effect of PEG and perfluorinated concentrations (or attractive and repulsive interactions) on chain packing was studied. PEG moieties

improved CO_2 gas permeability and selectivity because of the Lewis acid-base type interactions between PEG and CO_2.

In the final chapter, the effect of moisture sorption on free volume, oxygen, and water vapor transport was studied on five different epoxy-amine networks having T_gs in the range between -11 °C to 227 °C. Water sorption did not show any effect on $<v_h>$ of elastomeric networks. Whereas, glassy networks showed a V-shaped trend when $<v_h>$ was plotted as a function of relative humidity or water content. The decrease in $<v_h>$ was due to water molecules filling free volume holes. Increasing water concentration in the networks beyond 75% relative humidity (RH) resulted in swelling of the networks and thereby $<v_h>$ increase. Effect of water sorption on oxygen permeability of the glassy networks also showed a similar V-shaped trend, but the mechanism was more complex as water sorption affected both oxygen diffusivity and solubility. Water vapor permeability of the glassy networks was unaffected until 75% RH. Beyond 75% RH, free volume increase due to swelling resulted in water vapor permeability increase.

ACKNOWLEDGMENTS

I am extremely grateful to my advisor, Dr. Sergei Nazarenko on many accounts. Over the course of the past five years, he has guided me to become a better researcher, presenter, writer, and overall a better professional. I am very indebted for all the wonderful opportunities that he provided me such as mentoring undergrads, presenting research at numerous conferences, making me a part of several research collaborations, and providing me with opportunities to learn numerous technical skills through my graduate student career. But most important of all, he was always there to discuss and share his ideas and abundant knowledge, and by virtue of which I was able to get my dissertation to the level you see here.

I want to thank my other dissertation committee members, Dr. Morgan, Dr. Wiggins, Dr. Rawlins, and Dr. Subramanian for all the constructive inputs that they have given me for my previous presentations and documents, which has helped me to improve my research comprehension and communication.

I was very fortunate to have had Jim Goetz as my mentor when I started my research work at USM. He taught me many of the experimental and research skills that I have used to get data for this dissertation. He went out of his way to train me and get me up to speed to generate highly valuable data from very complex analytical techniques that I have used for this research. I am very grateful to Vivek for helping me with sample preparation and data generation, and for being a great teammate and colleague. I am very glad that I got to work with Steven Wand, Dr. Rawlins and Mr. Michael Blanton for the work on epoxy amine networks that you will see in this dissertation. I also would like to thank current and past members of Nazarenko research group, Kevin Meyers, Maliha

Syed, Beibei Chen, and Jacob Schekman who have all helped me with experiments for my research.

I had the chance to mentor highly motivated undergraduate students Tyler Haddock, Zari Davis, Andrew Hoff (REUs), and Aaron Maliden, high school teachers Ms. Rebecca Hooper, and Ms. Robin Lewis (RETs). They have immensely helped me with many of the experiments that you will see in this dissertation. Also, mentoring them has enabled me to better comprehend my research.

I want to especially thank our lab manager Ms. Jody for making our lives so much easier in the lab. Finally, I would like to thank all the professors, staff and students of the Polymer department who have helped me in some way or other during my graduate education.

I want to acknowledge the financial support of this research from the National Science Foundation's Center for Layered Polymeric Systems Center (CLiPS) program, and Department of Defense.

DEDICATION

To my mother, Remadevi and my wife, Arya.

For their unconditional support and love.

TABLE OF CONTENTS

LIST OF TABLES

LIST OF ILLUSTRATIONS

CHAPTER I - FREE VOLUME AND GAS TRANSPORT IN POLYMERS: BACKGROUND

1.1 Introduction

Free volume is one of the most critical parameters in polymers which has a strong influence on gas transport, mechanical, rheological properties etc. among many others. But the property of interest for this thesis is gas or vapor transport in polymers. The gas or vapor permeation requirements of a polymer material obviously would depend on the type of application. Typically high permeation or flux is required for membrane or gas separation applications, and therefore membrane scientists strive to develop high flux polymers that selectively permeate the gas of interest. In chapters 2-4 we discuss the development of high flux polymer networks for membrane applications. Whereas low flux or high barrier is required for packaging or coating applications, and therefore there are needs for new packaging materials that can enhance the shelf life of foods or new coating resins that can further enhance barrier against corrosive species and prevent metals from corroding for longer durations. In Chapter 5 we discuss how the presence of moisture in epoxy amine networks affects polymer chain packing, and thereby its complex effect on oxygen permeation.

1.2 Free volume in polymers

The free volume of a polymer is the difference between its specific volume V_{sp} and the volume occupied by its molecules, i.e., V_{occ}.[1]

$$V_{sp} = V_{occ} + V_f \qquad (1)$$

Where V_f is the specific free volume. Furthermore, V_f is the product of concentration, N_h', and the average size of free volume holes $\langle v_h \rangle$.

$$V_{sp} = V_{occ} + N_h' \langle v_h \rangle \qquad (2)$$

Occupied volume V_{occ} is the product of van der Waal's volume V_{vdw} of the polymer and interstitial free volume.

Different natures of free volume in amorphous glasses and elastomers (liquids) can be understood from Figure 1.1. In elastomers ($T>T_g$) (Figure 1.1), the overall volume change has a higher slope (liquid line V_l), i.e., thermal expansivity is higher in elastomers. As the chain mobility increases (when $T> T_g$), the polymer expands because of the expansion of free volume holes. In this state, because of the higher mobility of the chains, the free volume holes in the polymer is dynamic in nature, i.e. it is constantly getting redistributed. Whereas, as the polymer is cooled down to a temperature below glass transition temperature ($T<T_g$), the long-range and the segmental mobility of the chains cease, and therefore the polymer has lower thermal expansivity (glassy line V_g). In this nonequilibrium state, free volume holes are frozen-in or static in nature because of the cessation of chain motions. This different nature of free volume states (i.e. static in glasses compared to dynamic in elastomers) influences the way gas transport happens through the polymer, which is briefly discussed in chapter 5.

1.3 Factors affecting free volume in elastomers

In linear polymers, i.e., liquids, according to Fox and Loshaek, free volume (or specific volume) is usually dictated by the molecular weight of the chains.[2] That is, as the number of chain ends decrease (or as molecular weight increases), the free volume of a polymer decreases and this has been proved experimentally as well.[3]

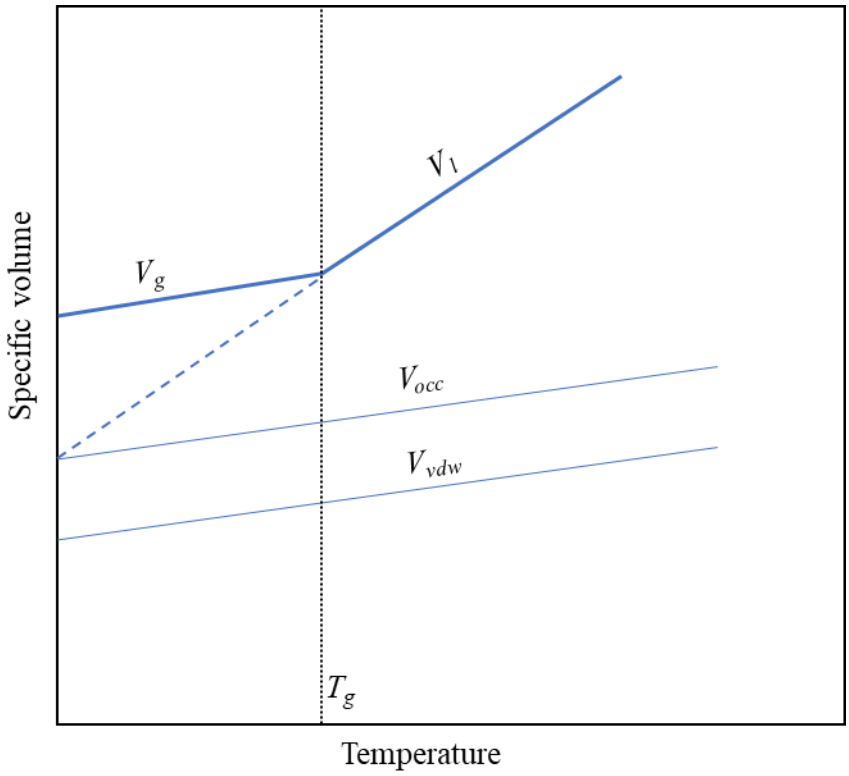

Figure 1.1 Schematic representation of V_{sp} vs. temperature following the concepts of Simha and Boyer[4].

But the focus of this thesis is on cross-linked polymers or thermosets. For cross-linked polymers, according to the classical Fox Loshaek equation, increasing cross-link density results in free volume or specific volume decrease.[2] That is, replacement of van der Waal's or other intermolecular interactions with covalent bonds results in a decrease of free volume.[2] Most studies agree with Fox Loshaek theory, i.e., increasing cross-link density of elastomers results in a decrease of free volume.[5-9] But there are a few studies which showed no effect[10] or contradictory results (i.e., increase in free volume with increasing cross-link density).[11] Usually, elastomers are cross-linked by cross-linking agents or hardeners which along with cross-link density might also change the chemical nature of the system. For example, the concentration of sulfur is increased in a nonpolar

elastomer such as polybutadiene to increase cross-link density, and this increase in sulfur will also change the polarity or chemical nature of the elastomer along with cross-link density. Polarity or chemical nature of cross-linking moieties can affect the intermolecular interactions, and thereby affect chain packing or free volume. Therefore, two parameters, i.e., cross-link density and chemical nature change are together affecting free volume or chain packing in most polymer systems, when cross-link density is changed. This results in the deviation from the model derived by Fox and Loshaek which relates cross-link density to free volume in polymer networks.[2] In chapter 2 of this thesis, we describe a series of polymer elastomeric networks prepared using thiol-ene chemistry, where molecular weight between cross-links M_c was changed by an order of magnitude without changing the chemical nature across the series. By doing that, we showed that this system obeys the Fox and Loshaek model. Whereas, in chapter 3 through perfluoriantion of thiol-ene networks, we discuss the effect of intermolecular interactions (repulsive interactions), i.e., the effect of changing chemical nature on free volume while cross-link density was kept constant. Chapter 4 gives insight on the synthesis and properties of hybrid thiol ene networks containing perfluorinated and polyethylene glycol moieties, which are polar opposite to each other.

As mentioned earlier, free volume in elastomers is dynamic in nature, but in the case of perfluorinated thiol-ene elastomers, we surprisingly found that the huge free volume pockets formed, because of the repulsive interactions, around perfluorinated moieties are mostly static in nature. Altogether, chapters 2-4 of this thesis will shed light on how parameters such as cross-link density, and altering chemical nature of networks

can be effectively used to tune free volume, and thereby the gas transport properties of elastomers.

1.4 Factors affecting free volume in glassy networks

Typically, in glasses, free volume scales as a function of T_g or chain rigidity.[12-15] When the chains are made by more rigid components, chain mobility ceases at a higher temperature (i.e., the material will have a higher T_g), and this results in accumulation of higher amounts of frozen-in or static hole free volume at room temperature (or any temperature below T_g). In chapter 5, there is a discussion in regards to the free volume in glassy epoxy-amine networks having different T_g values or chain rigidity. But the major focus of that chapter is to understand the effect of moisture sorption on free volume in glassy networks.

It has been shown in linear polymers that, moisture sorption results in a V-shaped trend. That is, initially as the glassy polymer absorbs water, free volume decreases. And beyond a particular moisture concentration, free volume of the polymer increases. It is mostly accepted that the initial decrease in free volume is due to water molecules filling free volume holes.[16-17] But the possibility of moisture induced aging is also considered as a cause for this decrease.[18] To the best of our knowledge, we could not find any studies on the effect of the moisture concentration on free volume of network (or crosslinked) polymers. Therefore, chapter 5 dwells about a comprehensive study on the effect of moisture sorption on free volume, oxygen, and water vapor transport of glassy epoxy-amine networks.

1.5 Gas transport through polymers

The transport of small molecules through polymers occurring as a result of the difference in partial pressures on either side of the material is commonly described by the solution-diffusion model where small molecule gases first sorb into the material, diffuse across free volume holes of sufficient size and desorb on the lower pressure side. Barrer described this phenomenon using the equation $P = D \times S$, where *P* is the permeability coefficient, *D* is the diffusion coefficient and *S* is the solubility coefficient.[19] Figure 1.2 shows a schematic of this model.

Permeability *P* is a proportionality coefficient of the material that defines the number of gas molecules that permeate a thickness, *l*, across a partial pressure differential, *Δp*, at a constant flux, *J*. The diffusion coefficient *D* of the material defines the random walk of small molecule gases through a polymer film with the total jump length, *l (i.e film thickness)*, and a time lag, *θ*. The solubility coefficient *S* is Henry's law constant for a given gas-polymer pair describing the amount of gas sorbed, *C*, into a polymer at a given external pressure, *p*.

$$P = \frac{J \cdot l}{\Delta p} \qquad D = \frac{l^2}{6 \cdot \theta} \qquad S = \frac{C}{p} \qquad (3)$$

In amorphous polymers, the diffusion process of light or small gases is considered to be a random walk of jumps between free volume elements of sufficient size at a given distance apart.

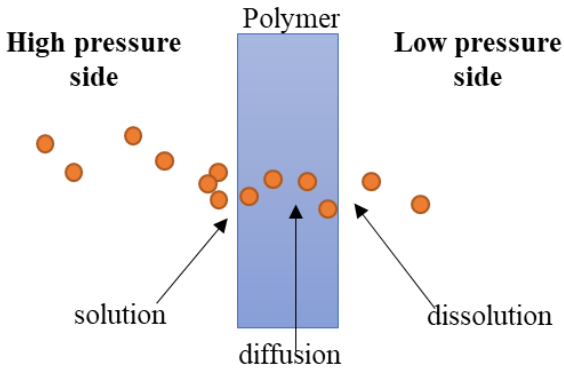

Figure 1.2 Schematic of the solution-diffusion model

1.6 The relationship between gas transport and free volume in polymers

Typically, gas diffusivity is related to free volume in the material by Cohen Turnbull model[1] which is written as follows:[20-24]

$$D = D_h e^{\left(\frac{-B_h}{h}\right)} \qquad (4)$$

Where D is gas diffusivity, h is the fractional free volume of the material. D_h, and B_h are parameters which depend on penetrant gas. Therefore according to equation 4, the logarithm of gas diffusivity should change linearly as a function of *1/free volume* according to equation 4, and it is well known that elastomers do obey this relationship.[25] In chapter 2, we show that the family of elastomers having a broad range of cross-link density did obey this model. But, the perfluorinated thiol-ene networks discussed in chapter 3 and alkylated thiol-ene networks discussed in a previous manuscript[26] from our lab shows deviation from Cohen Turnbull model. This deviation is explained through the static nature of free volume pockets around the perfluorinated and alkylated moieties. Because of the static nature, these free volume holes cannot be redistributed and thereby results in lower gas diffusivity values than what it is supposed to be.

Glassy polymers typically show good correlation between the free volume hole size and gas solubility.[27-28] In chapter 5, we discuss the complex effect that water sorption has on free volume and thereby, gas transport properties in epoxy amine networks, and in particular on glassy epoxy amine networks.

1.7 Thiol-ene Chemistry

Thiol-ene reactions fall under Sharpless' description of click chemistry.[29-31] Click chemistry is the category wherein selective, highly efficient, modular, and orthogonal reactions that give no by-products can be found. Thiol-ene reactions occur under mild conditions and produce nearly 100% yields, which allows for the development and study of various network systems without intense chemical synthesis or purification methods. Also, thiol-ene reactions require no solvents, can be performed in air and at room temperature.

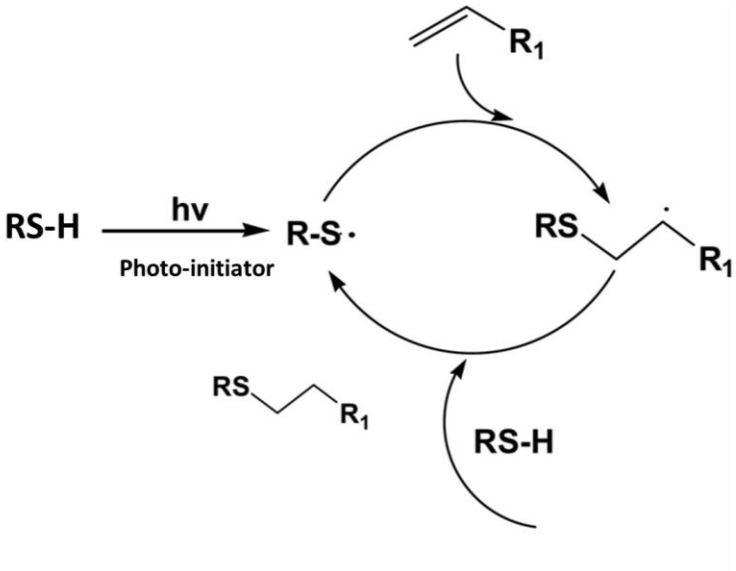

Figure 1.3 Mechanism of thiol-ene reactions

The UV initiated radical addition of a thiol to a carbon-carbon double bond, known as a thiol-ene reaction, has seen a revival in research in recent years.[30, 32-33] Figure

1.3 shows the mechanism of reaction between any thiol and an ene during UV polymerization. The key step in this reaction is the chain transfer from carbon-centered radical to thiyl radical via abstraction of hydrogen from thiol. The benefits of this reaction come from the radical step-growth nature of this polymerization. Contrary to oxygen inhibition in acrylates, where peroxy radicals cannot add to a double bond, in thiol-ene systems, peroxy radicals are able to extract hydrogen radicals from thiol moieties, allowing for the continuation of the polymerization. Also, thiol-ene chemistry produces more uniform networks with better control over cross-link density, which was taken advantage of for the preparation of a family of networks having a broad range of cross-link density described in chapter 2. Another biggest advantage of thiol-ene chemistry is the modularity, as there are a lot of thiol and ene functional monomers that are available commercially and also the monomers can be further modified to incorporate different functionalities.

The reaction between acrylate and thiol via thio Michael addition allows for the expansion of thiol monomer toolbox. With the wide variety of monoacrylates available, different functionalities can be incorporated into the thiol-ene networks via the preparation of modified thiol monomers using the aforementioned thio Michael addition, which can significantly impact the intermolecular interaction within the network. Our group has previously shown this through the use of variety of different functional acrylates having widely different polarities, which were successfully incorporated into thiol-ene network scaffold.[26, 34-35] In chapters 3 and 4, this method was utilized in creating perfluorinated and PEG modified thiol monomers to create perfluorinated and hybrid thiol-ene networks.

1.8 Pressure-Volume-Temperature High Pressure Dilatometry (PVT)

Zoller developed a high pressure mercury dilatometer specifically for polymeric materials where mercury is mostly used as the confining fluid.[36] This dilatometer measures the volume change of a polymer as a function of pressure and temperature. The resulting data can be used for calculating fundamental thermodynamic parameters of polymers such as coefficient of thermal expansion, compressibility, bulk modulus, and internal pressure. Figure 1.4 shows an example of special volume (V_{sp}) data collected from a standard isothermal run at pressures from 10 MPa to 140 MPa and in the temperature range of 30 °C to 150 °C. Gnomix software using Tait extrapolation then gives data extrapolated to 0.1 MPa. V_{sp} data obtained from this instrument is accurate to within ± 0.0015 cm^3/g.[36]

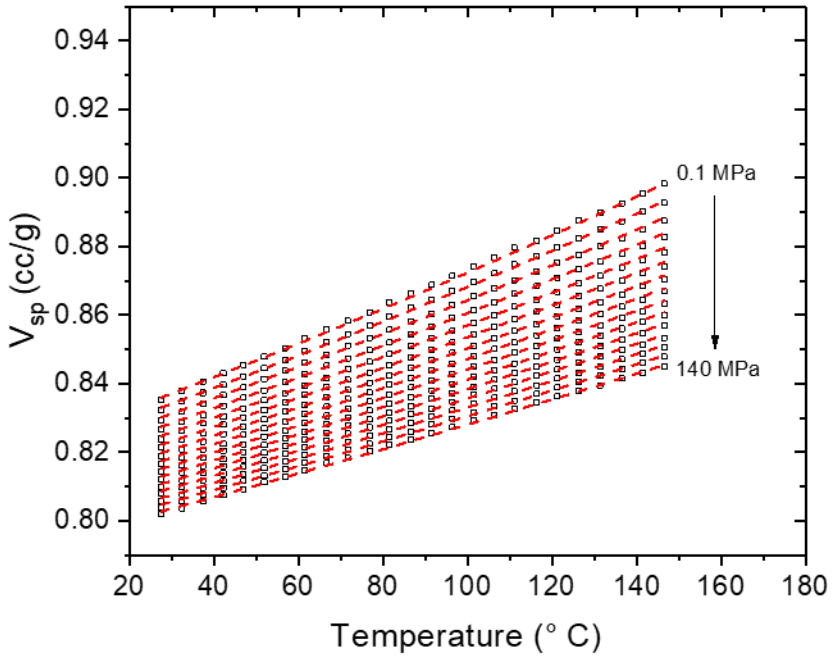

Figure 1.4 Example of PVT data obtained from Gnomix dilatometer.

This sample is D1E00 discussed in chapter 2. Dotted lines are S-S eos fits of the data

PVT data is typically fit using Simha Somcynsky equations of state (S-S eos)[37] to obtain the fractional free volume and a few other important molecular parameters of polymers. The equation of state is described in greater detail in chapter 2.

1.9 Positron Annihilation Lifetime Spectroscopy (PALS)

Positron annihilation lifetime spectroscopy is a technique that can directly probe the free volume elements in a polymer sample. The radioactive decay of ^{22}Na (source) results in a gamma quantum of energy 1.28 MeV and a positron, e^+. The gamma quanta are detected by a BaF_2 equipped photomultiplier tube (PMT) assembly tuned with a constant fraction discriminator (CFD) and is used to signify the "birth" of o-Ps.[38] In a polymer sample, positron couples with an electron to form an ortho-Positronium species which has a radius close to that of a hydrogen atom, 0.529 Å. In a vacuum, o-Ps has an intrinsic lifetime of 142 ns but in condensed matter, such as polymers, the lifetime is reduced to a few nanoseconds or lower. Upon the "death" of o-Ps, caused by a pick-off of the positron by an electron in the surrounding medium, two gamma quanta of energy 0.511 MeV are emitted and that is detected by another tuned PMT assembly. The time between these "birth" and "death" events is recorded using a time-to-amplitude converter (TAC) and compiled using a multi-channel analyzer (MCA). The frequency of these lifetime events is plotted as counts vs. lifetime as shown in Figure 1.5. Typical spectra are collected over one hour and the instrument is tuned to collect greater than 10^6 counts over that period of time. Figure 1.6 shows a typical PALS setup where the photomultipliers are aligned to the sample chamber and the figure also shows a general schematic of the fast-fast coincidence system.

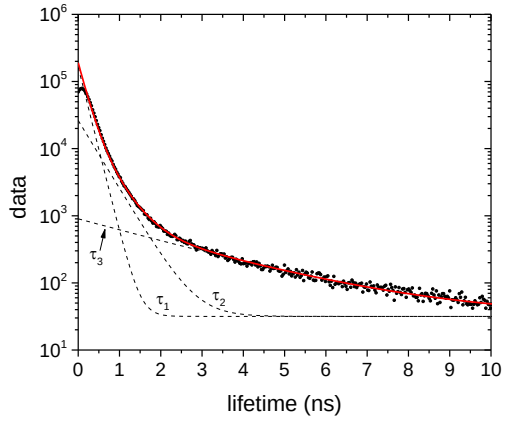

Figure 1.5 Typical PALS spectrum of the frequency of an event vs.. the lifetime of that event.

Discs having a diameter of 1 cm are prepared for this analysis. The minimum sample thickness has to be at least 1 mm to ensure all Ps are annihilated within the polymer sample and not in the surrounding media. Two such disks are prepared. For thin films, disks can be stacked together to form 1 mm in thickness and then wrapped using aluminum foil. A foil-wrapped ^{22}Na source packet is sandwiched between the two sample disks, and the sample source assembly is held together by a non-adhesive Teflon tape. The sample source assembly is then placed in the sample chamber, between the PMTs as shown in Figure 1.6.

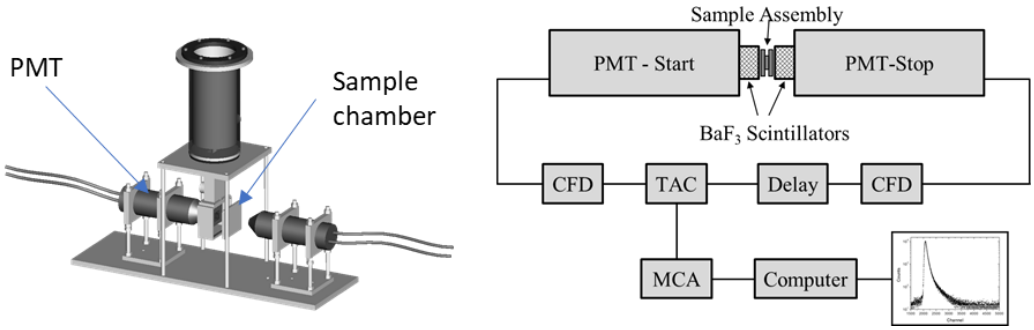

Figure 1.6 Schematic of a typical PALS instrument setup where temperature-controlled sample chamber is utilized for the tests.

The schematic on the right shows the different components of a typical PALS spectrometer.

A typical PALS spectrum includes the lifetime contributions of three annihilation events: the short-lived para-Positronium annihilation, free positron annihilation, and the long-lived ortho-Positronium annihilation. The deconvolution of the three lifetimes from a spectrum is performed using PATFIT-88 software[39] which outputs the average lifetime and relative fraction of positrons that annihilate from each of these Ps events. The resulting lifetimes (τ_1, τ_2, and τ_3) and intensities (I_1, I_2, and I_3) are obtained from the software. Since the first two annihilation events occur at lifetimes much shorter than the long-lived o-Ps annihilation, polymer data analysis only focuses on the o-Ps lifetime and intensity, τ_3 and I_3. Eldrup and Tao correlated τ_3 with void volumes in zeolite membranes with the assumption that the voids are spherical.[40] The radius of a free volume element, *R*, can be obtained from the experimentally determined τ_3 using eq 5.

$$\tau_3 = \frac{1}{2}\left[1 - \frac{R}{R_o} + \frac{1}{2\pi}\sin\left(\frac{2\pi R}{R_o}\right)\right]^{-1} \qquad (5)$$

In chapter 5, the effect of moisture sorption on free volume is discussed. To study that accurately, moisture desorption or adsorption should not happen during the testing of a moisture sorbed sample. To address that issue, a novel PALS humidity chamber was designed and fabricated in-house, and chapter 5 discusses the methodology of humidity control within that chamber.

1.10 Constant Volume Variable Pressure (CVVP) instrument

The transport phenomena of light gases through polymers can be studied using various techniques, CVVP is one among them. The constant volume variable pressure (CVVP), or diffusion lag technique allows for the determination of all three transport properties, i.e., *P*, *D*, and *S*, from one single experiment.[19, 41] In this test high pressure gas is applied to the upstream side of a polymeric film. The desorbed gas is collected in a

downstream vessel which has a calibrated volume. The downstream pressure increases as a function of time and is recorded using a differential pressure transducer where the reference pressure is a high vacuum. Figure 1.7 shows a typical CVVP data collected for a polymer film. First the gas sorbs into the upstream surface, then it diffuses through and desorbs on the downstream side of the film. The pressure in the downstream slowly increases until a steady state pressure increase versus time, dp_1/dt, is achieved. Steady-state pressure vs time is fit using first order linear regression. The permeability coefficient P is then calculated using:

$$P = \frac{V_d l}{p_2 ART}\left[\left(\frac{dp_1}{dt}\right)_{ss} - \left(\frac{dp_1}{dt}\right)_{leak}\right] \qquad (6)$$

where V_d is the downstream volume, l is the film thickness, A is the film area exposed to the permeate gas, R is the gas constant, and T is the absolute temperature.[41] The linear extrapolation of the steady state pressure to x-axis will give time lag, θ, which is then used to calculate the diffusion coefficient according to Equation 2. Applying the solution-diffusion model, the solubility of the gas can be determined using $S = P/D$.

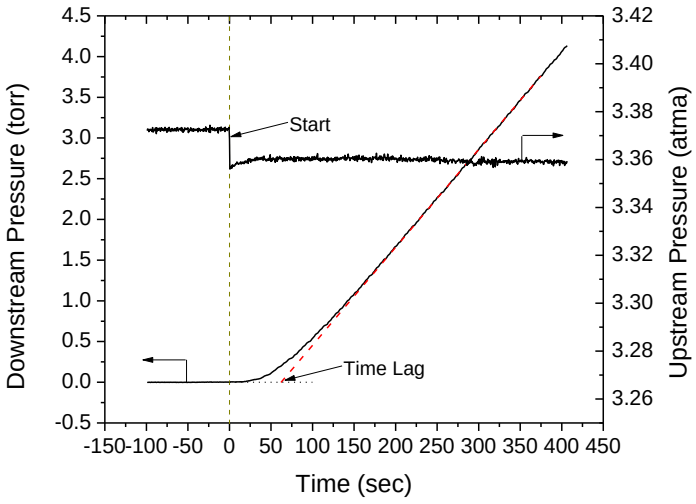

Figure 1.7 A standard downstream and upstream pressures as a function of time collected during a CVVP test.

Figure 1.8 shows a schematic of the instrument used in our lab which is based on Pye's description of the instrument.[41] In this experimental setup, there are two sample cells to allow for the testing of two samples simultaneously. Samples are typically degased overnight or for greater than 12 hours.

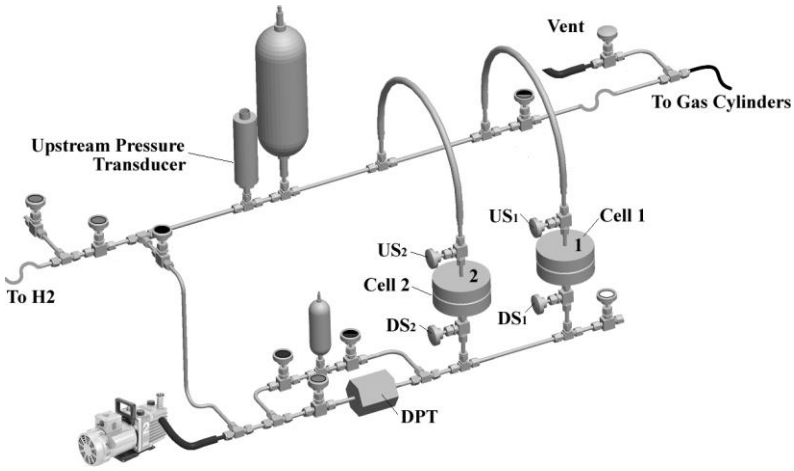

Figure 1.8 Schematic of a constant volume variable pressure apparatus.

1.11 Summary

Therefore, based on the background, the objectives of this research were devised as follows:

- To quantify free volume in a family of networks having a broad range of cross-link density using thiol-ene chemistry and to check if the networks obey Fox Loshaek model (Chapter 2).
- To synthesize a series of perfluorinated thiol-ene networks containing varying lengths of the perfluorinated dangling moiety, and therefore study the effect of repulsive intermolecular interactions on free volume and gas transport properties of networks (Chapter 3).
- To synthesize hybrid networks containing perfluorinated and PEG dangling moieties, and to study the effect of intermolecular interactions on free volume and gas transport properties (Chapter 4).
- To study the effect of moisture sorption on free volume, oxygen, and water vapor transport of epoxy-amine networks (Chapter 5).

1.12 References

1. Cohen, M. H.; Turnbull, D., Molecular Transport in Liquids and Glasses. *The Journal of Chemical Physics* **1959,** *31* (5), 1164-1169.

2. Fox, T. G.; Loshaek, S., Influence of molecular weight and degree of crosslinking on the specific volume and glass temperature of polymers. *Journal of Polymer Science* **1955,** *15* (80), 371-390.

3. Yu, Z.; Yahsi, U.; McGervey, J. D.; Jamieson, A. M.; Simha, R., Molecular weight-dependence of free volume in polystyrene studied by positron annihilation

measurements. *Journal of Polymer Science Part B: Polymer Physics* **1994,** *32* (16), 2637-2644.

4. Simha, R.; Boyer, R., On a general relation involving the glass temperature and coefficients of expansion of polymers. *The Journal of Chemical Physics* **1962,** *37* (5), 1003-1007.

5. Morgan, D. R.; Stejskal, E. O.; Andrady, A. L., 129Xe NMR Investigation of the Free Volume in Dendritic and Cross-Linked Polymers. *Macromolecules* **1999,** *32* (6), 1897-1903.

6. Consolati, G.; Kansy, J.; Pegoraro, M.; Quasso, F.; Zanderighi, L., Positron annihilation study of free volume in cross-linked amorphous polyurethanes through the glass transition temperature. *Polymer* **1998,** *39* (15), 3491-3498.

7. Dlubek, G.; Stejny, J.; Alam, M. A., Effect of Cross-Linking on the Free-Volume Properties of Diethylene Glycol Bis(allyl carbonate) Polymer Networks: A Positron Annihilation Lifetime Study. *Macromolecules* **1998,** *31* (14), 4574-4580.

8. Srithawatpong, R.; Peng, Z.; Olson, B.; Jamieson, A.; Simha, R.; McGervey, J.; Maier, T.; Halasa, A.; Ishida, H., Positron annihilation lifetime studies of changes in free volume on cross-linking cis-polyisoprene, high-vinyl polybutadiene, and their miscible blends. *Journal of Polymer Science Part B Polymer Physics* **1999,** *37* (19), 2754-2770.

9. Jean, Y. C.; Sandreczki, T. C.; Ames, D. P., Positronium annihilation in amine-cured epoxy polymers. *Journal of Polymer Science Part B: Polymer Physics* **1986,** *24* (6), 1247-1258.

10. Lin, H.; Kai, T.; Freeman, B. D.; Kalakkunnath, S.; Kalika, D. S., The Effect of Cross-Linking on Gas Permeability in Cross-Linked Poly(Ethylene Glycol Diacrylate). *Macromolecules* **2005,** *38* (20), 8381-8393.

11. Mansilla, M. A.; Rodríguez Garraza, A. L.; Silva, L.; Salgueiro, W.; Macchi, C.; Marzocca, A. J.; Somoza, A., Evolution of the free volume and glass transition temperature with the degree of cure of polybutadiene rubbers. *Polymer Testing* **2013,** *32* (4), 686-690.

12. Paul, D. R.; Yampol'skii, Y. P., *Polymeric gas separation membranes*. CRC press: 1993.

13. Freeman, B.; Yampolskii, Y.; Pinnau, I., *Materials science of membranes for gas and vapor separation*. John Wiley & Sons: 2006.

14. Finkelshtein, E. S.; Makovetskii, K.; Gringolts, M.; Rogan, Y. V.; Golenko, T.; Starannikova, L.; Yampolskii, Y. P.; Shantarovich, V.; Suzuki, T., Addition-type polynorbornenes with Si (CH3) 3 side groups: synthesis, gas permeability, and free volume. *Macromolecules* **2006,** *39* (20), 7022-7029.

15. Yu, X.; Jia, J.; Xu, S.; Lao, K. U.; Sanford, M. J.; Ramakrishnan, R. K.; Nazarenko, S. I.; Hoye, T. R.; Coates, G. W.; DiStasio, R. A., Unraveling substituent effects on the glass transition temperatures of biorenewable polyesters. *Nature communications* **2018,** *9* (1), 2880.

16. Muramatsu, M.; Okura, M.; Kuboyama, K.; Ougizawa, T.; Yamamoto, T.; Nishihara, Y.; Saito, Y.; Ito, K.; Hirata, K.; Kobayashi, Y., Oxygen permeability and free volume hole size in ethylene–vinyl alcohol copolymer film: temperature and humidity dependence. *Radiation Physics and Chemistry* **2003,** *68* (3), 561-564.

17. Xie, W.; Ju, H.; Geise, G. M.; Freeman, B. D.; Mardel, J. I.; Hill, A. J.; McGrath, J. E., Effect of free volume on water and salt transport properties in directly copolymerized disulfonated poly (arylene ether sulfone) random copolymers. *Macromolecules* **2011,** *44* (11), 4428-4438.

18. Dlubek, G.; Redmann, F.; Krause-Rehberg, R., Humidity-induced plasticization and antiplasticization of polyamide 6: A positron lifetime study of the local free volume. *Journal of Applied Polymer Science* **2002,** *84* (2), 244-255.

19. Barrer, R.; Rideal, E. K., Permeation, diffusion and solution of gases in organic polymers. *Transactions of the Faraday Society* **1939,** *35*, 628-643.

20. Park, J. Y.; Paul, D. R., Correlation and prediction of gas permeability in glassy polymer membrane materials via a modified free volume based group contribution method. *Journal of Membrane Science* **1997,** *125* (1), 23-39.

21. Haraya, K.; Hwang, S.-T., Permeation of oxygen, argon and nitrogen through polymer membranes. *Journal of Membrane Science* **1992,** *71* (1), 13-27.

22. Tanaka, K.; Kawai, T.; Kita, H.; Okamoto, K.-i.; Ito, Y., Correlation between Gas Diffusion Coefficient and Positron Annihilation Lifetime in Polymers with Rigid Polymer Chains. *Macromolecules* **2000,** *33* (15), 5513-5517.

23. Nagel, C.; Günther-Schade, K.; Fritsch, D.; Strunskus, T.; Faupel, F., Free Volume and Transport Properties in Highly Selective Polymer Membranes. *Macromolecules* **2002,** *35* (6), 2071-2077.

24. Sanders, D. F.; Smith, Z. P.; Guo, R.; Robeson, L. M.; McGrath, J. E.; Paul, D. R.; Freeman, B. D., Energy-efficient polymeric gas separation membranes for a sustainable future: A review. *Polymer* **2013,** *54* (18), 4729-4761.

25. Lin, H.; Wagner, E. V.; Swinnea, J. S.; Freeman, B. D.; Pas, S. J.; Hill, A. J.; Kalakkunnath, S.; Kalika, D. S., Transport and structural characteristics of crosslinked poly(ethylene oxide) rubbers. *Journal of Membrane Science* **2006,** *276* (1–2), 145-161.

26. Kwisnek, L.; Kaushik, M.; Hoyle, C. E.; Nazarenko, S., Free Volume, Transport, and Physical Properties of n-Alkyl Derivatized Thiol−Ene Networks: Chain Length Effect. *Macromolecules* **2010,** *43* (8), 3859-3867.

27. Hu, Y. S.; Mehta, S.; Schiraldi, D. A.; Hiltner, A.; Baer, E., Effect of water sorption on oxygen-barrier properties of aromatic polyamides. *Journal of Polymer Science Part B: Polymer Physics* **2005,** *43* (11), 1365-1381.

28. Hiltner, A.; Liu, R.; Hu, Y.; Baer, E., Oxygen transport as a solid-state structure probe for polymeric materials: A review. *Journal of Polymer Science Part B: Polymer Physics* **2005,** *43* (9), 1047-1063.

29. Kolb, H. C.; Finn, M.; Sharpless, K. B., Click chemistry: diverse chemical function from a few good reactions. *Angewandte Chemie International Edition* **2001,** *40* (11), 2004-2021.

30. Hoyle, C. E.; Bowman, C. N., Thiol–Ene Click Chemistry. *Angewandte Chemie International Edition* **2010,** *49* (9), 1540-1573.

31. Hoyle, C. E.; Lee, T. Y.; Roper, T., Thiol–enes: Chemistry of the past with promise for the future. *Journal of Polymer Science Part A: Polymer Chemistry* **2004,** *42* (21), 5301-5338.

32. Hoyle, C. E.; Lowe, A. B.; Bowman, C. N., Thiol-click chemistry: a multifaceted toolbox for small molecule and polymer synthesis. *Chemical Society Reviews* **2010,** *39* (4), 1355-1387.

33. Nair, D. P.; Podgórski, M.; Chatani, S.; Gong, T.; Xi, W.; Fenoli, C. R.; Bowman, C. N., The thiol-Michael addition click reaction: a powerful and widely used tool in materials chemistry. *Chemistry of Materials* **2013,** *26* (1), 724-744.

34. Kwisnek, L.; Nazarenko, S.; Hoyle, C. E., Oxygen Transport Properties of Thiol−Ene Networks. *Macromolecules* **2009,** *42* (18), 7031-7041.

35. Clark, T.; Kwisnek, L.; Hoyle, C. E.; Nazarenko, S., Photopolymerization of thiol-ene systems based on oligomeric thiols. *Journal of Polymer Science Part A: Polymer Chemistry* **2009,** *47* (1), 14-24.

36. Zoller, P.; Bolli, P.; Pahud, V.; Ackermann, H., Apparatus for measuring pressure–volume–temperature relationships of polymers to 350 C and 2200 kg/cm2. *Review of Scientific Instruments* **1976,** *47* (8), 948-952.

37. Simha, R.; Somcynsky, T., On the Statistical Thermodynamics of Spherical and Chain Molecule Fluids. *Macromolecules* **1969,** *2* (4), 342-350.

38. Pethrick, R. A., Positron annihilation—a probe for nanoscale voids and free volume? *Progress in Polymer Science* **1997,** *22* (1), 1-47.

39. Kirkegaard, P.; Eldrup, M.; Mogensen, O. E.; Pedersen, N. J., Program system for analysing positron lifetime spectra and angular correlation curves. *Computer Physics Communications* **1981,** *23* (3), 307-335.

40. Tao, S. J., Positronium Annihilation in Molecular Substances. *The Journal of Chemical Physics* **1972,** *56* (11), 5499-5510.

41. Pye, D.; Hoehn, H.; Panar, M., Measurement of gas permeability of polymers. II. Apparatus for determination of permeabilities of mixed gases and vapors. *Journal of Applied Polymer Science* **1976,** *20* (2), 287-301.

CHAPTER II - PROBING FREE VOLUME IN MODEL PEG CONTAINING THIOL-ENE NETWORKS: THE EFFECT OF CROSSLINK DENSITY

2.1 Abstract

A family of PEG based elastomeric networks having a broad range of molecular weight between cross-links M_c was produced by gradually decreasing the ratio of trifunctional to bifunctional thiol monomers, and curing with a bifunctional ene monomer while maintaining 1:1 thiol:ene stoichiometry. Dielectric spectroscopy studies revealed similar dielectric permittivity values for the networks, which indicated uniformity in chemical nature across the series. High pressure dilatometry studies were performed to study the effect of temperature and pressure on the specific volume of the networks (PVT analysis). The Simha-Somcynsky equation of state theory was used to fit the PVT data of the networks and to extract the fractional free volume of the networks. The fractional free volume of the networks changed linearly as a function of cross-link density, which agrees with the Fox and Loshaek theory. Average free volume hole size of the networks probed using positron annihilation lifetime spectroscopy, also changed linearly as a function of cross-link density. A free volume based model was developed to describe the gas diffusivity trends of the networks as a function of cross-link density.

2.2 Introduction

Polymer membranes offer several important advantages, i.e., lower energy consumption and environmental footprint, over more traditional gas separation methods such as distillation and pressure swing adsorption.[1-3] In the gas separation industry, carbon dioxide separation from other important light gases such as methane, nitrogen, and hydrogen has been an important domain for natural gas enrichment, flue gas capture,

hydrogen purification industries respectively.[4-6] Over the last few years, a considerable amount of research has been carried out towards the development of polymer membranes for CO_2 separation.[7-11] It is well known that the addition of poly(ethylene glycol) (PEG) units improves the CO_2 selectivity of the membranes, because of the Lewis acid-base type interaction between the PEG units and CO_2.[7-8, 11]

Recently, our group developed and studied the gas transport and gas selectivity of a series of elastomeric networks containing PEG units, which were synthesized using thiol-ene chemistry.[8] In these networks, PEG content was increased by increasing the ratio of a PEG containing dithiol to a trithiol crosslinker, which were then UV cured with a PEG containing diene, while maintaining 1:1 thiol:ene stoichiometry (Figure 2.1). This method produced a series of networks, in which increases in PEG content led to simultaneous increases in molecular weight between cross-links (M_c). The experimental gas diffusivities of these networks showed outstanding dependence on M_c, which was hypothesized as a free volume effect. A free volume based model was developed to describe the gas diffusivities of these networks as a function of their M_c, assuming that the system obeyed Fox Loshaek model.[8]

Fox and Loshaek studied the effect of cross-link density on changes in specific volume and glass transition temperature. According to their model, the specific volume of the networks should linearly decrease and glass transition temperature should linearly increase with cross-link density. But if the changes in cross-link density also cause simultaneous changes in chemical nature (or polarity), the linearity between the aforementioned parameters gets affected.[12] There have been quite a few studies, in the past, on the effect of cross-link density on either free volume or gas transport in polymer

networks.[13-19] As expected, most of these studies showed that decreases in cross-link density led to increases in free volume or gas diffusivity (or permeability), but there were very few attempts to show if the system obeys the Fox and Loshaek model.[17] This might be because, changes in cross-link density, in most cases, causes simultaneous changes in chemical nature (or polarity). For example, if the amounts of polar cross-linking agents like sulfur, isocyanate or peroxides etc. are varied to change the cross-link density of predominantly hydrocarbon networks, it can dramatically affect the chemical nature as well, alongside the cross-link density. The chemical nature or polarity can also affect the chain packing and free volume. Thereby, the linear relationship between free volume and cross-link density can get affected, as mentioned earlier and the system might not obey the Fox and Loshaek model. In some cases, changes in cross-link density are made by varying the ratio of a difunctional monomer to a monofunctional monomer.[7, 20-22] In such cases, apart from cross-link density, the chain ends of the mono-functional monomer will also affect the free volume.[12] Also, networks synthesized through step growth or chain growth cross-linking produces heterogeneous networks. Thus, the task of studying the effect of cross-link density alone on free volume becomes arduous.

In the PEG based thiol-ene networks, though M_c was changed by an order of magnitude, we assumed that the chemical nature (or polarity) remained uniform across the entire series.[8] Also, it is well known that thiol-ene chemistry produces more uniform networks when compared to the step growth or chain growth cross-linking.[23-25] Owing to the uniformity and chemical similarity of the networks, it was hypothesized that these PEG based thiol-ene networks will obey Fox and Loshaek model, and therefore the diffusivity trends were excellently modeled as a function of Mc (or cross-link density),

but free volume parameters were not quantified in the previous paper.[8] Thus, the goal of this work was to quantify the free volume parameters of the PEG based thiol-ene networks and to check if the system obeys the Fox and Loshaek model, as hypothesized in the previous paper.

2.3 Experimental

2.3.1 Materials

Monomers triethylene glycol divinyl ether (TEGDVE), 2,2′-(ethylenedioxy)diethanethiol (EDDT) and photo-initiator 2,2-dimethoxy-2-phenylacetophenone (DMPA) were obtained from Aldrich. Trithiol cross-linker trimethylolpropanetri(3- mercaptopropionate) (3T) was provided by Bruno Bock. All materials were used as received and their chemical structures are shown in Figure 2.1.

2.3.2 Sample preparation

The recipes used for sample preparation are shown in Table 2.1. The amounts of bifunctional thiol (EDDT) and trifunctional cross-linker thiol (3T) were varied to change the concentration of cross-links in the networks while maintaining 1:1 thol:ene stoichiometry. Films were prepared by UV curing using the procedure shown elsewhere.[8] Monomers were taken in a vial in accordance with the recipes shown in Table 2.1 along with 1wt% DMPA photoinitiator for preparing the samples. The mixtures were sonicated for 10 min at room temperature and then were poured onto the glass plates, where they were sandwiched by placing another glass plate on top. Sample thicknesses of around 0.5 mm were achieved by placing spacers in between the glass plates. Glass plates with the samples were then placed under the UV light for 4 min to cure the samples, where the plates were flipped after 1 min. The membranes were then removed from the glass plates

and checked for homogeneity, clarity, and bubbles. As shown in the previous work, theoretical molecular weight between cross-links, M_c, was calculated assuming 1:1 thiol:ene stoichiometry of the reactants used in a homogeneous, crystalline lattice-like structure having tri-functional junction points.[8] Table 2.1 shows the broad range of M_c achieved in this system, the values of which will be used in the results and discussion section to compare the volumetric and transport properties of this system as a function of their cross-link density.

2.3.3 Characterization

The bulk density of the film samples was calculated via the Archimedes principle, using an analytical balance and the values are shown in Table 2.1.

Changes in specific volume with temperature and pressure were measured using the Gnomix pressure-volume-temperature (PVT) dilatometer,[26] where mercury was used as the confining liquid in the sample cell for the experiments. Measurements were conducted in isothermal mode, where the pressure was ramped from 10 MPa to 140 MPa at different temperatures starting from 30° C to 150° C with a step increment of 5° C. The instrument measures changes in specific volume with an accuracy of ±0.0002 cc/g. The Gnomix software uses Tait extrapolation to calculate specific volume values at atmospheric pressure. Then using Simha-Somcynsky lattice hole theory, changes in fractional free volume with temperature and pressure were calculated.[27-28]

Positron Annihilation Lifetime Spectroscopy (PALS) analysis was used to probe the free volume directly. In this technique, foil wrapped positron source, 30 μCi ^{22}Na, is sandwiched between two polymer discs having dimensions of 1 cm diameter and 1 mm thickness. The sample source assembly is placed between two photomultiplier tubes

(PMT). PMTs are equipped with BaF_2 γ-radiation sensitive scintillators and are tuned in a way that one PMT senses γ-photons associated with positron birth, and the other PMT its annihilation. The lifetimes of positrons are then compiled using a multi-channel analyzer, with a time resolution of 290 ps.

Positron emitted from the source gets thermalized inside the material to form positronium. A positronium in which the spins of both the electron and the positron is in the same direction is called an ortho-positronium (o-Ps). Since o-Ps is easily polarizable it prefers to localize in the low electron density regions i.e. free volume holes. The o-Ps gets annihilated when it gets picked off by an electron of opposite spin from the material, and this is called a "pick-off" annihilation. Therefore, the lifetime of the o-Ps depends on the electron density of the material or the physical size of the hole. Tao developed a semi-empirical model which relates the radius of the free volume hole *R* in the material to the o-Ps lifetime τ_3,[29] which can be written in the form shown below:

$$\tau_3 = 0.5\left[1 - \frac{R}{R_0+R} + \frac{1}{2\pi}\sin\left(\frac{2\pi R}{R_0+R}\right)\right]^{-1} ns \quad (1)$$

Where R_0 = 0.1656 nm, is the empirically derived electron layer thickness.[29] Assuming a spherical hole, the average free volume hole size $<v_h>$ was then calculated from the radius, $< v_h > = \frac{4}{3}\pi R^3$.

PALS measurements were carried out under vacuum, for a temperature range from -40° C to 100° C with a step size of 5° C. At each temperature, spectrum was collected for an hour to obtain more than 10^6 incidences using Ortec Positron Lifetime System (Advanced Measurement Technology, Oak Ridge, TN), and the temperature sweep was performed three times to obtain the average and the standard deviation of free

volume hole sizes across temperatures. The PALS spectra were then fit and deconvoluted to obtain the lifetime of the long-lived o-Ps species, τ_3, using the PATFIT-88 software.[30]

Novocontrol GmbH Concept 80 Broadband Dielectric Spectrometer was used to collect the dielectric spectra of the networks. The spectra were collected over the frequency range of 0.1 Hz – 3 MHz at room temperature (23° C). The sample was placed between two stainless steel discs having a diameter of 2 cm. Prior to the measurement, the sample-electrode assembly was conditioned in a dry nitrogen environment for 24 hours.

The permeability of the networks for different gases was measured by a custom built constant volume variable pressure (manometric) device which is described elsewhere by our group.[9] The permeability data of the networks to the gases CO_2, H_2, O_2, N_2, and CH_4 was presented in the previous paper.[8] In this work, we additionally measured the permeability to SF_6 gas. Permeability, diffusivity, and solubility of membranes to all the above-mentioned gases were calculated as shown in our previous work.[8] Sample cell used for gas transport measurements were maintained at a constant temperature of 23° C, and a high vacuum was used to degas the samples for 24 hours prior to the measurements. For the measurements, the upstream pressure was maintained at ~3 atm, and the change in downstream pressure was monitored as a function of time. Downstream pressure vs time curves was plotted for all the samples and they showed a typical Fickian behavior. Slope of the steady-state data gives dp/dt, V_d is the downstream volume, l is the membrane thickness, p is the applied upstream pressure, A is the testing area, R is the universal gas constant and T is the temperature, and substituting all these values in eq 6 gave the permeability, P, of the membranes to the gases, as shown below:

$$P = \frac{V_d l}{pART}\frac{dp}{dt} \tag{2}$$

The extrapolation of the steady state slope to x-axis gives the time lag values, t_L, from which the diffusivity of the membranes, D, as follows:

$$D = \frac{l^2}{6t_L} \tag{3}$$

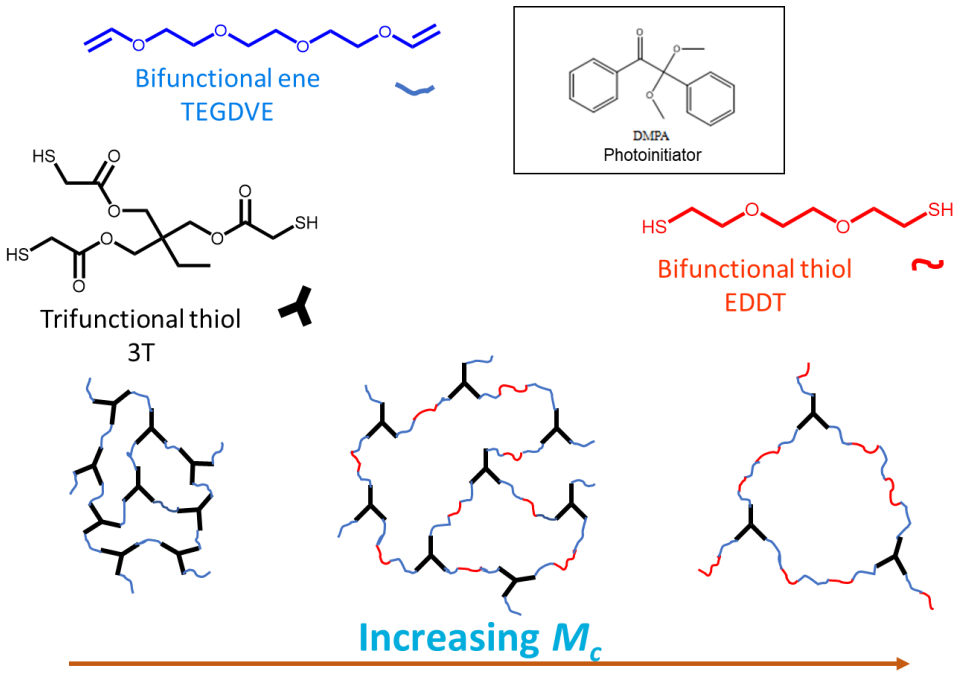

Figure 2.1 Chemicals used for the synthesis and schematic of networks

Table 2.1 Formulation for the networks [a]

	sample	parts	parts	parts	theoretical M_c	density
1	D1E00	0	67	100	467	1.205
2	D1E20	20	53	100	564	1.205
3	D1E40	40	40	100	724	1.19
4	D1E60	60	26.7	100	1040	1.185
5	D1E80	80	13.3	100	2010	1.173
6	D1E90	90	6.7	100	3930	1.165

[a] "parts" indicate relative molar quantities of each monomer.

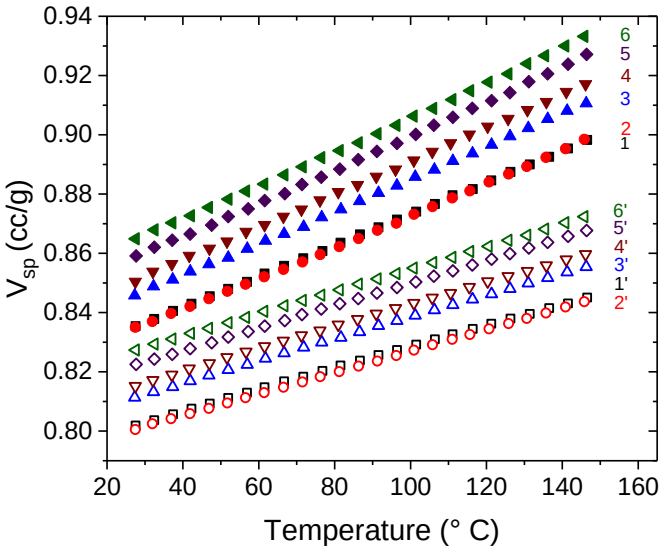

Figure 2.2 Specific Volume V_{sp} as a function of temperature.

Closed symbols P = 0.1 MPa, open symbols P = 140 MPa.

2.4 Results and discussion

2.4.1 PVT analysis

Figures 2.2 and 2.3 show thermal expansion and compression respectively of the networks obtained from PVT experiments. V_{sp} vs. T data shows that there were no transitions within the studied range of temperatures and pressures, as the networks have a

glass transition temperature of -42° C and lower as showed in the previous communication.[8] From the data, it was clear that V_{sp} increased gradually with increasing M_c. From the PVT data, parameters such coefficient of thermal expansivity α, compressibility β, and internal pressure P_i were calculated using the equations (4-6) and the values are reported in Table 2.2.

$$\alpha = \frac{1}{V}\left(\frac{\partial V}{\partial T}\right)_p \qquad (4)$$

$$\beta = -\frac{1}{V}\left(\frac{\partial V}{\partial p}\right)_T \qquad (5)$$

$$P_i = T\left(\frac{\alpha}{\beta}\right) - p \qquad (6)$$

The slope from the V_{sp} vs. T data are shown in Figure 2.2 was used to calculate α shown in Table 2.2. Vsp vs. P data are shown in Figure 2.3 was fit using a second order polynomial equation and the derivative of that was taken in order to obtain β shown in Table 2.2 using equation 5. Using α and β, internal pressure P_i was calculated using equation 6.

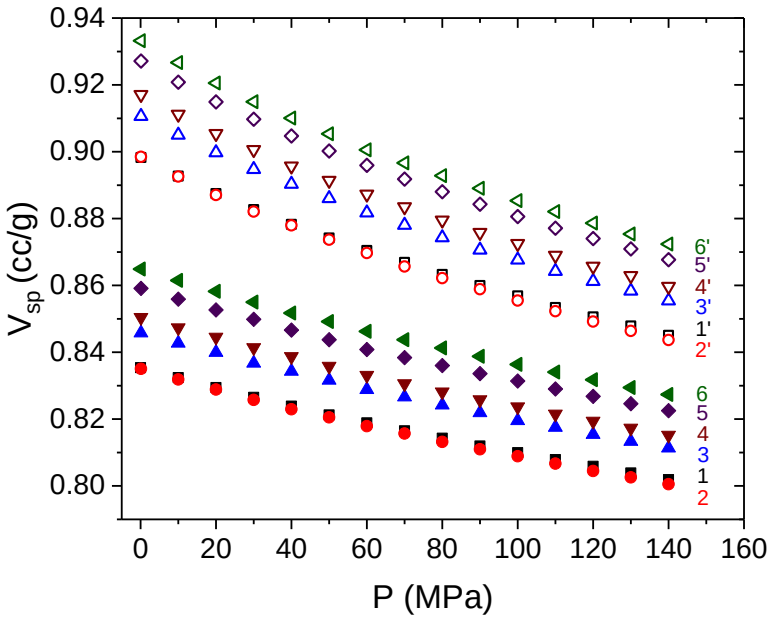

Figure 2.3 Specific volume V_{sp} as a function of pressure. Closed symbols T = 27.5° C, open symbols T = 146° C.

Table 2.2 Network parameters obtained from PVT experiments. α at 0.1 MPa, β and P_i at 27.5 °C and 0.1 MPa.

sample	M_c (g/mol)	α (° C $^{-1}$)	β (MPa^{-1})	P_i (MPa)
1	467	6.32E-04	3.58E-04	529
2	564	6.40E-04	3.69E-04	521
3	724	6.45E-04	3.58E-04	542
4	1040	6.56E-04	3.70E-04	532
5	2010	6.64E-04	3.82E-04	522
6	3930	6.65E-04	3.86E-04	518

In order to quantify free volume, PVT data was analyzed using Simha-Somcynsky equation-of-state (S-S eos) theory.[27, 31]The S-S eos model was used to fit the obtained PVT data of the networks. According to this model, a polymer chain is divided into *s* equal segments called s-mers, where each s-mer occupies a lattice cell. $sM_s = nM_{rep} =$

M_n, where M_s is the molar mass of the s-mer, M_{rep} is the molar mass of the monomer repeat unit, n is the degree of polymerization and M_n is the number average molar mass of the polymer chain. s-mers occupy a fraction of the lattice which is represented by y and the remaining vacant space is called the hole fraction (or fractional free volume), $h = 1-y$. The S-S theory assumes random mixing and utilizes the Flory-Huggins approach for calculating the configurational entropy. S-S eos constitutes of two coupled equations (eq 7 and 8) which was solved simultaneously.

$$(\tilde{P}\tilde{V})/\tilde{T} = \left[1 - y\left(2^{\frac{1}{2}}y\tilde{V}\right)^{-\frac{1}{3}}\right]^{-1} + y/\tilde{T}\left[2.002\left(y\tilde{V}\right)^{-4} - 2.409\left(y\tilde{V}\right)^{-2}\right] \quad (7)$$

$$3c\left[\left(2^{-\frac{1}{6}}y\left(1/y\tilde{V}\right)^{\frac{1}{3}} - 1/3\right)\Big/\left(1 - 2^{-\frac{1}{6}}y\left(1/y\tilde{V}\right)^{\frac{1}{3}}\right) - y\left(1/y\tilde{V}\right)^{2}\left(3.033\left(1/y\tilde{V}\right)^{2} - 2.409\right)/6\tilde{T}\right] + (1-s) - s\ln(1-y)/y = 0 \quad (8)$$

Where $\tilde{P} = P/P^*$, $\tilde{V} = V/V^*$, and $\tilde{T} = T/T^*$ are the reduced variables, and P^*, V^*, and T^* are the scaling parameters. The scaling parameters are defined as shown in equation 9, where R is the gas constant, zq is the number of interchain contacts for a lattice cell with a coordination number z, $3c$ is the external volume-dependent degrees of freedom, ϵ^* and v^* are Lennard-Jones interaction parameters: maximum attraction energy and segmental repulsion volume respectively. For long polymer chains $s \to \infty$, so it is typically assumed that $3c/s = 1$.

$$\left.\begin{array}{c} P^* = zq\epsilon^*/sv^* \\ T^* = zq\epsilon^*/Rc \\ V^* = v^*/M_s \end{array}\right\} (P^*V^*M_s)/T^* = Rc/s \Rightarrow R/3 \quad (9)$$

From r^2 values shown in Table 2.3, it can be said that the S-S eos model gave good fits to the PVT data. Previously, S-S eos model has been successfully applied for

numerous linear polymer melts, blends, and nanocomposites.[32-37] Rodgers reviewed six equations of state models by fitting them to the PVT data of 56 polymers available in the literature. He found that the SS eos was one of the two models, which fit the PVT data of polymers in equilibrium, for a wide range of temperatures and pressures, outstandingly well,[32] and thus it shows the validity of using S-S eos model for these PEG thiol-ene networks.

Table 2.3 shows the S-S eos fitting parameters for the PEG based thiol-ene networks. Interestingly, the change in cross-link density did not affect the size of the lattice cells, i.e., the lattice cell parameters: volume of a lattice cell v^* and molecular weight of a s-mer M_s (which occupies a lattice cell) remained almost constant as can be seen from Table 2.3. However, the fraction of unoccupied lattice cells (or fractional free volume) h changed linearly with the crosslink density (i.e. $1/M_c$) as shown in Table 2.3 and Figures 2.7. Analogous results have been previously shown in linear systems, where the changes in molecular weight of polystyrene did not have much of an effect on v^* and M_s,[38] but they had a significant effect on fractional free volume.[39] Thus, the S-S eos analysis of these PEG based thiol-ene networks clearly showed that the changing cross-link density only affected the free volume, in this lattice model of polymer networks.

Comparable S-S lattice cell parameters across the broad range of cross-link density further indicate the uniformity in chemical nature across the entire series. To get another estimate of the polarity of networks, permittivity was quantified using dielectric analysis. It is well known that the polarity or chemical nature of the material has a strong influence on permittivity.[40] Figure 2.4 clearly shows that changing cross-link density did not influence storage permittivity. Also, the internal pressure values of the networks were

constant across the series (Table 2). Internal pressure describes the changes in internal energy of the system in the event of a volume change, and it is a measure of cohesive energy or intermolecular interactions within a material. Constant Pi values further prove the similarity of chemical nature across the series. Figure 2.1 shows the building blocks used for the synthesis of the networks and Table 2.1 shows their molar amounts. The molar amounts of the ene component TEGDVE was kept constant across the series. To decrease cross-link density, the ratio of molar amounts of trifunctional thiol 3T to bifunctional thiol EDDT was decreased. Whereas, to maintain 1:1 thiol:ene stoichiometry, if 3T was decreased by two units, EDDT was increased by three units. 3T has three ester groups and a hydrocarbon tail, whereas EDDT is made up of two ether groups. Therefore, when cross-link density was decreased, for every ester group that was removed, an ether group was added. Ester group is comparatively more polar than the ether group.[41] But the decrease in cross-link density also led to a decrease in the molar amounts of non-polar hydrocarbon content (contribution from the hydrocarbon tail of 3T). Therefore, ester content and hydrocarbon content were decreased, whereas ether content was increased because of decreasing cross-link density. This compensation effect led to the uniformity of chemical nature across the entire series.

Table 2.3 Simha-Somcynsky EOS fit parameters

sample	M_c	P*(bar)	V*(cc/g)	T*(K)	M_s	v*(cc/mol)	ε*(kJ/mol)	h^a	r^2
D1E00	467	10418	0.83029	10845.2	34.74659	28.84974	3.005566	0.05257	0.9994536
D1E20	564	10230	0.827991	10737.7	35.13167	29.08871	2.975775	0.05407	0.9998156
D1E40	724	10281.7	0.838805	10696.9	34.37326	28.83246	2.964468	0.05458	0.9996527
D1E60	1040	10071.6	0.842383	10581.3	34.56366	29.11584	2.932431	0.05634	0.9995829
D1E80	2010	9983.75	0.848619	10489.6	34.31162	29.11749	2.907018	0.05783	0.9997821
D1E90	3930	9667.97	0.854985	10515	35.25366	30.14135	2.914057	0.05737	0.9998030

[a] h data estimated at 27.5° C and 0.1 MPa is shown in the table

Figure 2.5 shows the changes in fractional free volume with temperature and pressure for the highest cross-link density system and the lowest cross-link density system. The specific free volume V_f of the networks can be calculated as $V_f = h \times V_{sp}$. Figure 2.6 shows for different cross-link densities, how the specific free volume changed with the temperature. It can be seen that, increases in M_c led to free volume increases, which is in line with what was hypothesized for this system in the previous paper.[8] At 27.5° C and 0 MPa, V_f increased by 13%, when M_c was increased from 467 g/mol to 3930 g/mol, which shows the significant effect cross-link density has on free volume (which in turn would have a significant effect on transport and mechanical properties).

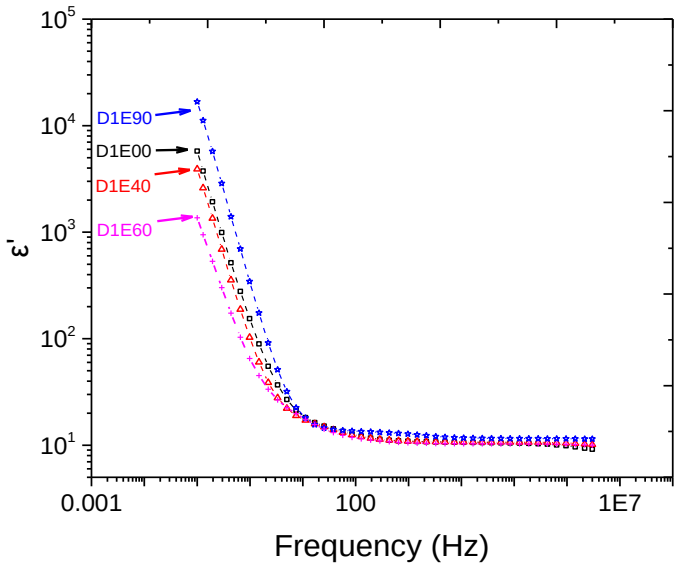

Figure 2.4 Dielectric storage ε' as a function of frequency measured at room temperature (23° C).

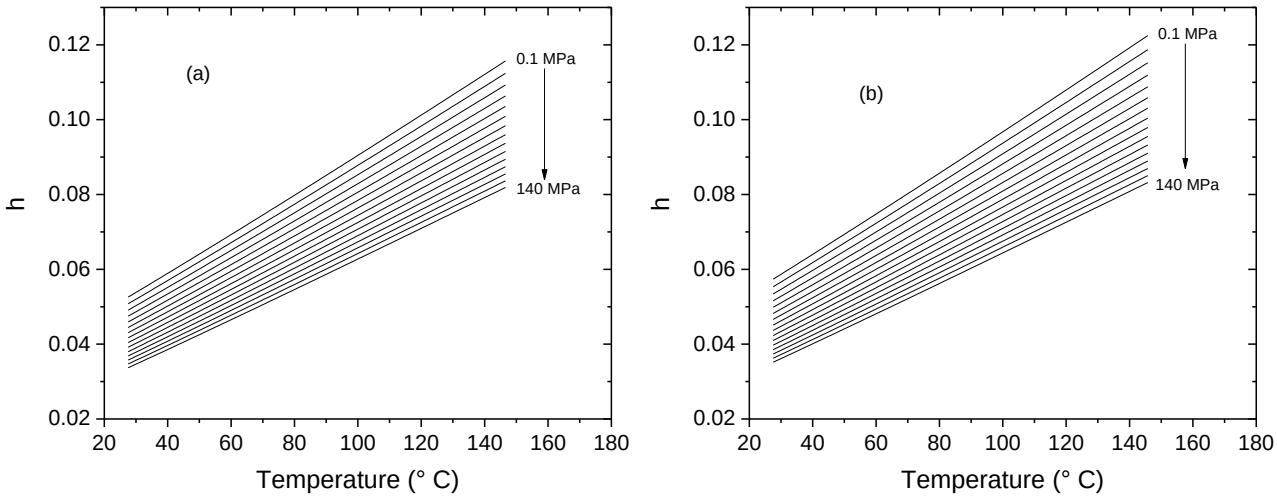

Figure 2.5 Fractional free volume vs. temperature at different pressures for (a) D1E00 and (b) D1E90.

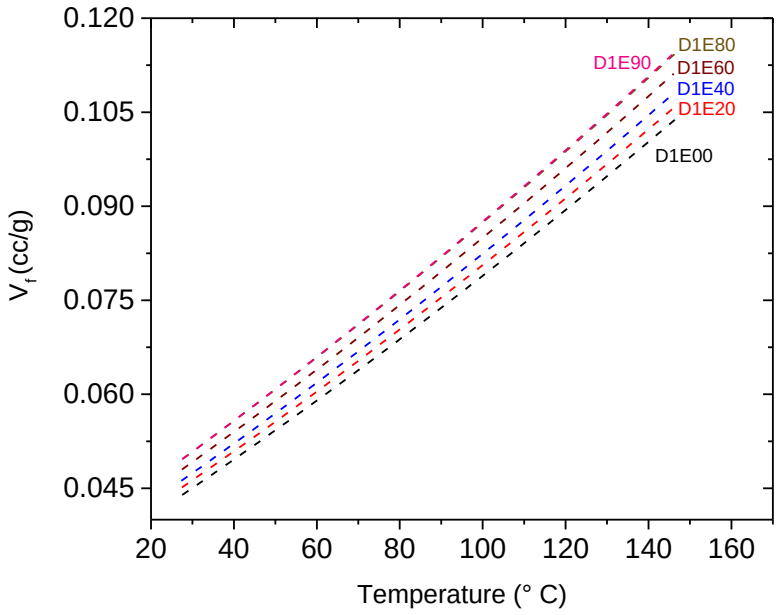

Figure 2.6 Specific free volume V_f as a function of temperature for all the networks.

Fox and Loshaek derived an equation[12] which relates the degree of cross-linking to the specific volume of a polymer. The premise behind that derivation is that, cross-linking involves replacement of van der Waals' bonds by shorter and more compact covalent bonds, which causes decreases in specific volume *v*. The equation is written as follows[12]

$$v(\rho, M) = v_0(\infty) + \alpha_\infty T + \frac{m(\Delta\alpha T + \Delta v_0)}{M} - [\Delta\alpha_x T + \Delta v_0(x)] m_x \rho \qquad (10)$$

Where, ρ is the number of cross-links per gram, M is the molecular weight of the polymer with no cross-links, $v_0(\infty)$, α_∞ is the specific volume at 0 K, thermal expansivity respectively of the polymer having infinite length, T is temperature, m is the molecular weight of the repeat unit of the chain, $\Delta\alpha = \alpha_l - \alpha_\infty$, $\Delta v_0 = v_0(l) - v_0(\infty)$, $v_0(l)$, α_l is the specific volume at 0 K, thermal expansivity respectively of the monomer.

$$\Delta\alpha_x = \alpha_x - \alpha_\infty; \alpha_x = \frac{dv(x)}{dT}; v(x) = \frac{V_x}{m_x}; \Delta v_0(x) = v_0(x) - v_0(\infty) \quad (11)$$

V_x is the volume shrinkage caused by the introduction of each cross-link, m_x is the weight of two atoms eliminated while forming a cross-link, and $v_0(x)$ is $v(x)$ at 0 K. The simplified form of equation 10 can be written as follows

$$v = v_{lp} - c_{lp}\rho \quad (12)$$

Where, v_{lp} is the specific volume of the linear polymer with no cross-links and $c_{lp}\rho$ is the reduction in specific volume caused by the introduction of cross-links.

In practical applications, cross-linking is introduced to the polymer by the addition of a cross-linking agent or a hardener, whose chemical nature, in most cases, is vastly different from that of the chain backbone. Fox and Loshaek further modified equation 10 to take the chemical nature change into account for the calculation of the specific volume of the cross-linked polymer. Their assumption was that the polymer networks can be considered as a copolymer, wherein the comonomer creates the cross-link points or junctions in the network. The modified form of specific volume equation of a polymer network can be written as follows.[12]

$$v(\rho) = v_0(c) + \alpha_c T - (\Delta\alpha_c T + \frac{\Delta V_0}{m_c})m_c\rho \quad (13)$$

Where, $v_0(c)$, α_c is the specific volume at 0 K, thermal expansivity respectively of the copolymer having no cross-links, which would depend on composition. $\Delta\alpha_c = \alpha_l - \alpha_c$, where α_l is the average thermal expansivity of the monomers (dependent on composition), ΔV_0 is the volume contraction caused by the reaction of a mole of the functional group in the cross-linking agent at 0 K. m_c is the average molecular weight of the monomers (dependent on composition). Therefore, if the chemical nature of the

monomers is vastly different, most parameters on the right side of the equation 13 can change with composition (which in this case is cross-link density). Therefore, if changes in cross-link density also induce changes in chemical nature, the system might deviate from linearity according to equation 13. Equation 13 can be written in simplified form as follows:

$$v = v_{cp} - c_{cp}\rho \tag{14}$$

Where, v_{cp} is the specific volume of the copolymer with no cross-links $c_{cp}\rho$ is the reduction is specific volume caused by the introduction of cross-links. Specific volume is the sum of occupied volume and free volume, $v = v_{occ} + v_f$. Therefore, the equation 14 can be written in the following form:

$$\frac{v_f}{v} = \frac{v_{vp} - v_{occ}}{v} - \frac{c_{cp}\rho}{v} \tag{15}$$

Where, v_f/v is the fractional free volume *h* of the material. Number of cross-links per gram is directly proportional to the reciprocal of molecular weight between cross-links, $1/M_c$. Therefore, equation 15 can be written as follows

$$h = h_0 - \frac{c}{M_c} \tag{16}$$

Equation 16 is similar to the equation used in previous works, where fractional free volume was studied as a function of cross-link density.[8, 17] Fractional free volume obtained from S-S analysis *h* can be plotted as a function of cross-link density (i.e. $1/M_c$) to check whether this system obeys the Fox and Loshaek model. The fractional free volume of the networks at 23°C was obtained by linear extrapolation of S-S eos fractional free volume-temperature data. Figure 2.6 shows that fractional free volume changed linearly with $1/M_c$. Over the entire range of temperature and pressure conditions,

this was the case and the linear fits gave r^2 values 0.83 or greater. At ambient conditions, i.e. 23° C and 0.1 MPa, the fractional free volume data fitted linearly to $1/M_c$, gave Fox Loshaek parameters h_0 = 0.0556 and c = 2.66508 g/mol and the r^2 for the fit was 0.96. Thus, it can be validated that Fox Loshaek theory can be applied to this system, as hypothesized in the previous paper.[8] Previously Morgan et al used ^{129}Xe NMR peak shift to qualitatively obtain fractional free volume change in poly(oxypropylene) networks having four different M_c values. Their data showed a reasonable fit to the Fox and Loshaek equation but the data also showed a deviation from linearity.[17] In the case of those networks, triiscocyante cross-linkers were used, which probably also resulted in chemical nature change, therefore the deviation from linearity. Whereas, in this PEG based thiol-ene system, changing M_c by even an order of magnitude did not result in changes in chemical nature, thereby the system showed the model Fox and Loshaek behavior.

The constants h_0 and c were obtained from the linear fits of equation 13 for the entire range of temperatures and pressures studied. The constants were then studied for their temperature and pressure dependence. h_0 and c show a linear dependence to temperature (Figure 2.8(a)) as expected, and the parent equation derived by Fox and Loshaek[12] (equation 10) shows the same. However, Fox and Loshaek did not derive an equation which has the effect of pressure in it. Our results showed that h_0 and c have a non-linear pressure dependence (Figure 2.8(b)) similar to that of the free volume pressure dependence of these PEG thiol-ene networks (Figure 2.8(c)) and other polymers as well.[42,43,44]

Table 2.4 Free volume parameters and gas diffusivities of the networks at 23 °C

sample	theoretical M_c (g/mol)	free volume parameters		gas diffusivity D ($cm^2\ s^{-1}$)					
		h	$<v_h>$ (Å^3)	H_2[a]	O_2[a]	N_2[a]	CO_2[a]	CH_4[a]	SF_6
D1E00	467	0.04962	172	3E-6	3.8E-7	2.4E-7	2.2E-7	1.6E-7	2.8E-9
D1E20	564	0.05113	175	3.2E-6	6E-7	4.7E-7	3.4E-7	2.5E-7	1.7E-8
D1E40	724	0.05171	182	5.3E-6	7.6E-7	5E-7	5.1E-7	3.5E-7	3.7E-8
D1E60	1040	0.05338	193	6.2E-6	8.7E-7	7E-7	5.3E-7	4.2E-7	6.2E-8
D1E80	2010	0.05472	208	6.4E-6	1.1E-6	8.2E-7	7.9E-7	5.9E-7	9.4E-8
D1E90	3930	0.05435	2010	6.1E-6	1.1E-6	7.2E-7	7.3E-7	5.5E-7	1.8E-7

[a] Gas diffusivity values reported in the previous paper, ref 1, p 3250.

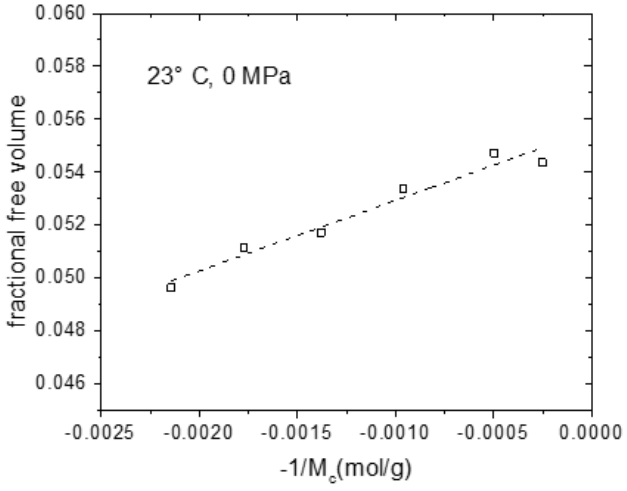

Figure 2.7 Hole fraction or fractional free volume (h) as a function of $1/M_c$.

Dashed lines indicate the Fox Loshaek fits to the data.

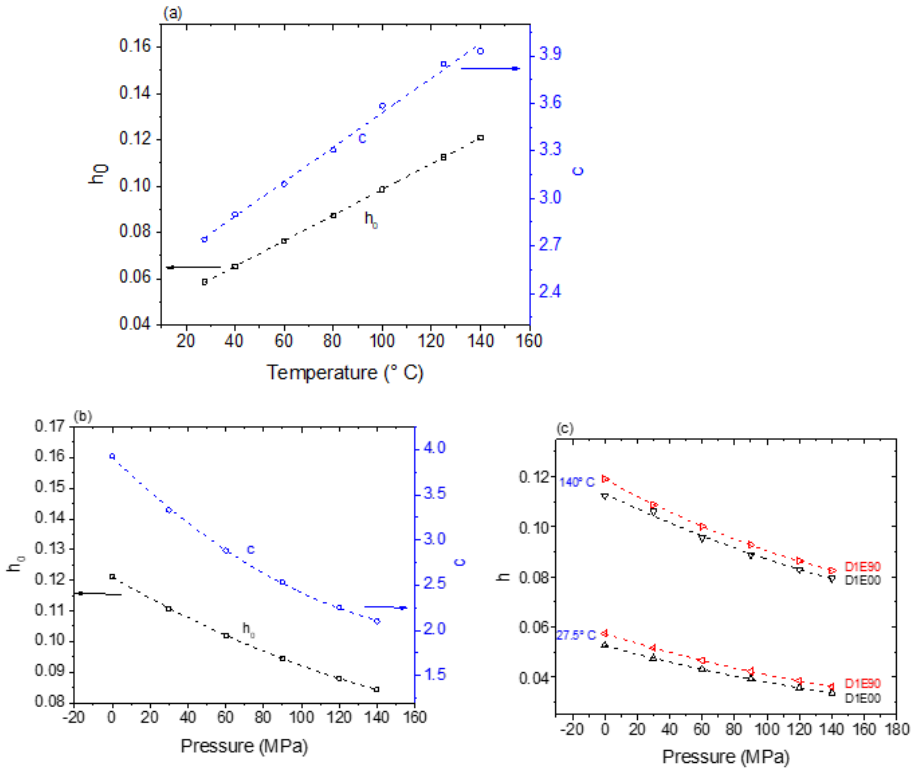

Figure 2.8 Fox Loshaek parameters h0 and c as a function of temperature (a) and pressure (b) respectively. (c) fractional free volume of the networks D1E00, D1E90 as a function of pressure.

Dashed lines indicate linear fits in figures 2.8 (a) and second order polynomial fits in figure 2.8(b) and (c).

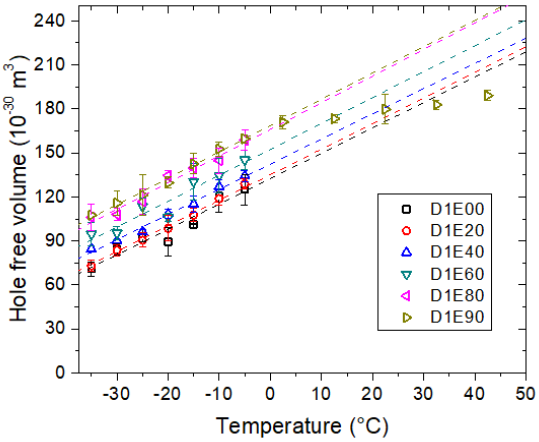

Figure 2.9 Average free volume hole size <vh> as a function of temperature for all the networks.

Dashed lines are the linear fits to the data from -35° C to -5° C. Error bars indicate one standard deviation.

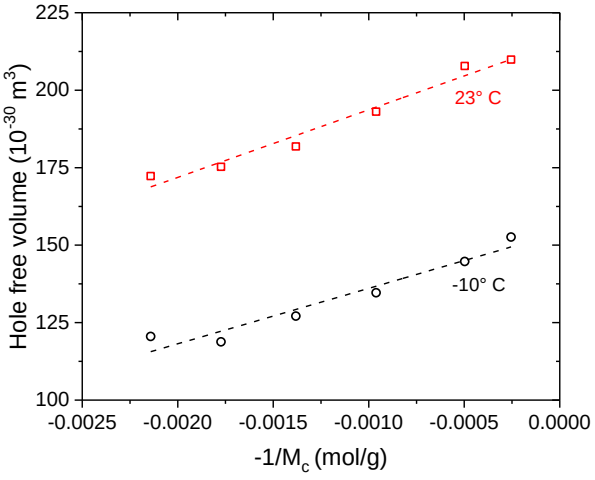

Figure 2.10 Free volume hole size $<v_h>$ (at 23° C and -10° C) as a function of $1/M_c$.

Dashed lines indicate the Fox Loshaek fits to the data.

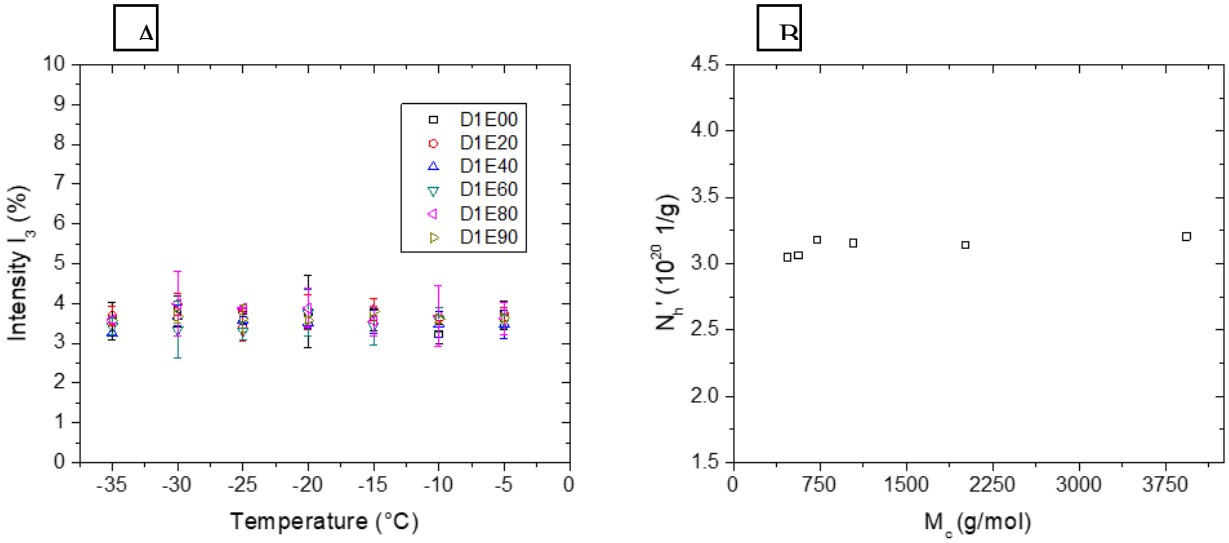

Figure 2.11 (a). Ortho positronium intensity I_3 (%) as a function of temperature for all the networks. (b). Concentration of free volume holes N_h' as a function of M_c. Error bars indicate one standard deviation.

2.4.2 PALS analysis:

The free volume quantity that can be directly probed using the PALS technique is the average free volume hole size $<v_h>$. Figure 2.9 shows the temperature dependence of $<v_h>$ from -35° C to 45° C. $<v_h>$ showed linear dependence with temperature till 0° C, after that it started leveling off (all the networks showed this behavior, but for clarity, the high temperature data for only D1E90 was included in Figure 2.9). As previously stated, the networks used in this study have T_g values -42° C or lower, therefore at 0° C, the networks are well above their T_gs. The explanations for this behavior at $T >> T_g$ that are available in the literature are: positronium bubble formation,[45] *o*-Ps lifetime is comparable to the relaxation time of the chains. [46-47] Therefore, when $T >> Tg$, o-Ps lifetime would not give a good measure of free volume hole size, which caused the leveling-off behavior that is shown in Figure 2.9. Assuming linear thermal expansion of free volume holes, extrapolated values of $<v_h>$ can be obtained at higher temperatures (i.e. ≥ 0° C). For linear fits, data points for $<v_h>$ from -35° C (well into rubbery regime) to -5° C (beyond this temperature positron bubble effect was observed in the networks) was used. Figure 2.9 and Table 2.3 shows that increases in M_c led to increases in $<v_h>$, as expected.

The specific free volume can be written as the product of average free volume hole size and the concentration of holes:

$$v_f = < v_h > \times N_h' \quad (17)$$

Where, N_h' is the number of free volume holes per gram of the material (concentration of free volume holes). Combining equations 14 and 17, the following expression can be written:

$$< v_h > = \frac{v_{cp} - v_{occ}}{N_h'} - \frac{C_{cp}\rho}{N_h'} \quad (18)$$

This equation can be further simplified and written as follows:

$$< v_h > = < v_h >_0 - \frac{c_2}{M_c} \quad (19)$$

Thus, free volume parameter computed using PALS technique, $<v_h>$, can be plotted as a function of $1/M_c$ to check the validity of the equation 19. Figure 2.10 shows that $<v_h>$ also changed linearly with $1/M_c$. At ambient temperature, i.e. 23° C, the average free volume hole size data fitted linearly to $1/M_c$, gave Fox Loshaek parameters $<v_h>_0$ = 215.5 Å³ and c_2 = 21821 Å³g/mol and the r^2 for the fit was 0.97. This result further proves that cross-link density alone was effecting free volume changes in this system. According to the equation 18, if both concentration of free volume holes and cross-link density were changing simultaneously, the system might deviate from linearity. The system did maintain linearity (Figure 2.10), which means that the concentration of free volume holes remained constant even though M_c was changed by almost an order of magnitude. Previous studies have shown that ortho-positronium intensity I_3 is proportional to the concentration of free volume holes.[42, 48] Figure 2.11(a) shows that I_3 does not have any dependence on M_c and temperature, which again proves that the concentration of free volume holes remains constant with changes in cross-link density. The concentration of the free volume holes N_h' can also be calculated by combining the PVT and PALS data using the formula $N_h' = \frac{E_r}{e_{hr}}$.[49] Where, E_r is the thermal expansivity of the networks and e_{hr} is the thermal expansivity of the free volume holes of the networks. Figure 2.11(b) further confims that degree of cross-linking had no significant effect on the concentration of free volume holes in this system.

Recently, Mansilla et al studied the effect of degree of cure on free volume in polybutadiene rubbers using PALS technique.[50] They claimed that in one of the systems, the degree of curing had no effect on the free volume hole size and whereas in the other system the free volume hole size increased with the degree of cure (i.e. the opposite trend). In that study, the PALS measurements were performed at room temperature, and those elastomers had a glass transition temperature of -100° C or lower.[50] Since the PALS measurements were performed at a temperature more than 120° C above the glass transition temperature, the networks were possibly in the bubbling regime. As previously discussed, when the samples are in the positron bubbling regime, accurate values of free volume hole sizes cannot be obtained from PALS, which is probably why different trends were observed in those systems. Whereas, Lin et al showed that crosslinking does not have any effect on free volume and gas transport in poly(ethylene glycol diacrylate) networks.[7] This was probably because of the inhomogeneity in the networks because traditional chain polymerization is not known to produce homogeneous networks. In those networks, cross-link density was varied by gradually reducing the prepolymer concentration in the solution, thereby gradually increasing the intramolecular cross-linking loops (or decreasing cross-link density) during free radical polymerization. The inhomogeneity of the network structure caused by the chain growth polymerization and intramolecular cross-linking loops most likely caused the non-dependence of free volume and gas transport on cross-linking. But most previous studies show a similar trend to what we see with these PEG thiol-ene networks (i.e. free volume increases as cross-link density decreases).[17-19, 51-52] However, in most of the systems chemical nature (or polarity) change could also have additionally affected the chain packing, and thereby the

free volume. In most systems, the concentration of highly polar cross-linking agents such as sulfur,[51] amines,[52] isocyanates[17] etc. are changed to vary the degree of cross-linking. Also, unreacted chain ends, heterogeneity in network structure caused by traditional polymerization methods would make it an arduous task to single out the effect of cross-linking "alone" on free volume. Whereas, in these PEG based networks, thiol-ene chemistry was employed and it is well established that this chemistry produces more uniform networks with better control over cross-link density.[23-24]. Furthermore, the similarity in chemical nature enabled in the creation of model networks to study the effect of cross-link density "alone" on free volume.

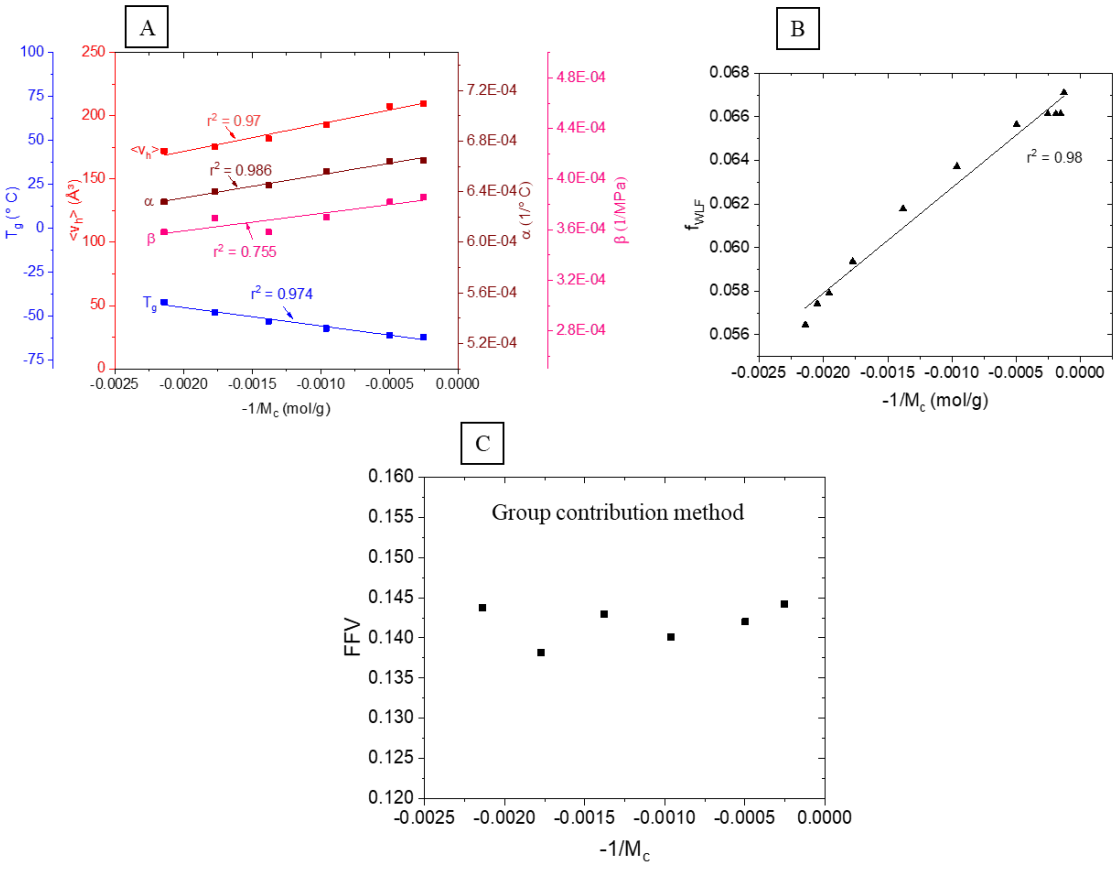

Figure 2.12 (a). Experimentally obtained free volume related parameters vs. $1/M_c$. (b) Fractional free volume obtained by WLF method plotted vs. $1/M_c$. (c) Fraction free volume obtained by group contribution method plotted as a function of $1/M_c$.

Figure 2.12(a) summarizes that all the experimentally free volume related parameters such as average free volume hole size $\langle v_h \rangle$, the coefficient of thermal expansivity α, compressibility β, and glass transition temperature T_g of these PEG thiol-ene networks has a linear dependence to $1/M_c$.

Fractional free volume can also be quantified from T_g using the following equation:[53]

$$f_{WLF} = f_g + \Delta\alpha(T - T_g) \qquad (20)$$

Where f_g is the fractional free volume of the material at T_g and $\Delta\alpha$ is the difference in thermal expansion coefficients above and below T_g. Using the universal constants value for f_g = 0.025 and $\Delta\alpha$ = 4.8 X 10^{-4} given by WLF, the f_{WLF} values were calculated for the PEG thiol-ene networks and they showed a linear dependence to $1/M_c$ (Figure 2.12 (b)), because T_g showed a linear dependence as well.

Fractional free volume is also commonly calculated via group contribution methods and is commonly used to compare free volume in polymer networks.[7, 54-55] In this method occupied volume is calculated via group contribution method[56]. The occupied volume can be subtracted from the specific volume of the material obtained from density measurements to obtain free volume, and thereby fractional free volume (FFV). FFV obtained via this method strangely showed no dependence on M_c. Change in density across the series is rather small, and because of the chemical similarity of the networks, occupied volume obtained from group contribution methods were similar, which explains why FFV did not show any dependence on M_c.

2.4.3 Diffusion-M_c model:

The previous sections showed that the effect of cross-link density on free volume obeys the Fox and Loshaek relationship. It is well known that increases in free volume lead to significant increases in gas diffusivity and the Cohen Turnbull equation[21, 57-62] relates the aforementioned parameters. The Cohen Turnbull relationship can be written as follows:

$$D = D_h e^{(\frac{-B_h}{h})} \quad (21)$$

Where D is gas diffusivity, h is the fractional free volume of the material. As previously discussed, the concentration of free volume holes remains almost constant with changes in cross-link density, therefore the Cohen Turnbull relationship can be modified to compare the effect of free volume hole size $<v_h>$ on gas diffusivity and the equation can be written as follows:

$$D = D_{vh} e^{(\frac{-B_{vh}}{<v_h>})} \quad (22)$$

D_h, D_{vh}, B_h, and B_{vh} are parameters which depend on penetrant gas.

Gas transport analysis of the networks for CO_2, H_2, O_2, N_2, and CH_4 was discussed in details in the previous paper[8] and in addition to that, in this work, transport analysis of a bigger gas molecule SF_6 was added. Using the CVVP instrument, the gas diffusivities of the networks were calculated using the equation 3 shown in the experimental section. Figure 2.13 shows that, when logarithms of gas diffusivities were plotted as a function of *1/h* or *1/*$<v_h>$ (extrapolated values of h and $<v_h>$ at 23°C were

used for the plots) linear relationships were obtained, which shows that the Cohen Turnbull equations 21 and 22 are valid for this system.

Since this PEG thiol-ene system obeys both the Fox Loshaek and the Cohen Turnbull equations, the diffusion-M_c model that was proposed in the previous paper[8] was validated. Combining equations 16 and 21, 19 and 22, the diffusion-M_c equations 23 and 24 respectively were derived.

$$D = D_h \exp\left(\frac{-B_h}{h_0 - \frac{c}{M_c}}\right) \quad (23)$$

$$D = D_{vh} \exp\left(\frac{-B_{vh}}{\langle v_h \rangle_0 - \frac{c_2}{M_c}}\right) \quad (24)$$

The above diffusion-M_c equations enable to correlate the effect of molecular weight between cross-links (or cross-link density) directly on gas diffusivities. Parameters D_h, B_h were obtained from the fits of equation 21 to the experimental data (shown in Table 2.4), h_0, c from equation 16, D_{vh}, B_{vh} from equation 22 (shown in Table 2.4), and $\langle vh \rangle_0$, c_2 from equation 19. Figure 2.14 shows the experimental gas diffusivities of the networks as a function of molecular weight between cross-links. Diffusion-M_c models based on both the free volume quantities, fractional free volume (Figure 2.14(a)) and average free volume hole size (Figure 2.14(b)) described the experimental data very well for all the gases and the r^2 values are shown in Table 2.5.

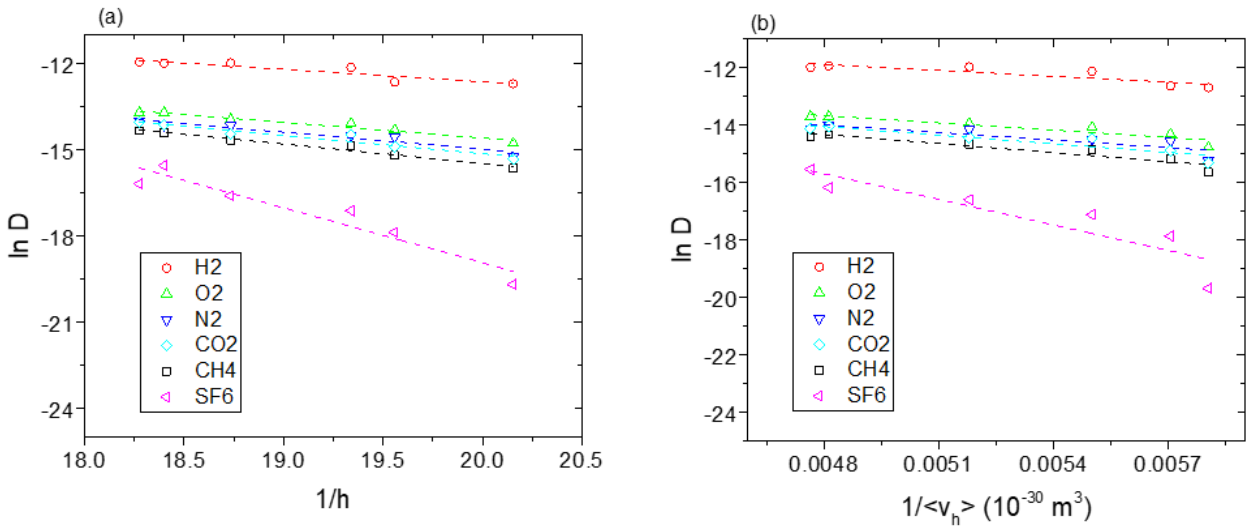

Figure 2.13 Logarithm of gas diffusivities as a function of *1/h* (a), *1/*$\langle v_h \rangle$ (b).

Dashed lines indicate linear fits based on eq 17 (a) and eq 18 (b).

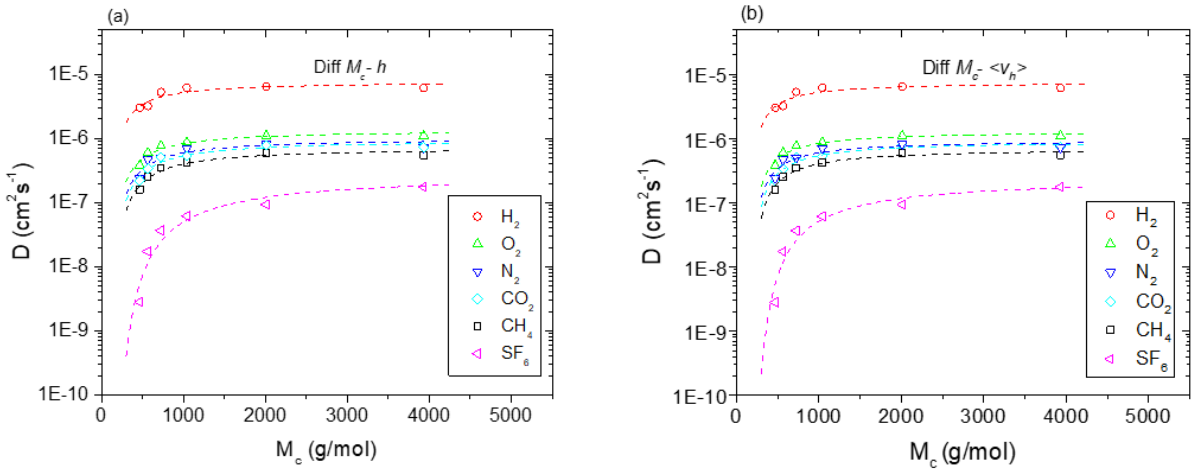

Figure 2.14 Gas diffusivities as a function of M_c.

Dashed lines are diffusivities calculated using eq 19 for (a) and eq 20 for (b).

Table 2.5 Cohen Turnbull fit parameters

Gas	Cohen Turnbull fit parameters using h (data in table 2.3 fit to eq 17)			Cohen Turnbull fit parameters using $<v_h>$ (data in table 2.3 fit to eq 18)		
	D_h	B_h	r^2	D_{vh}	B_{vh}	r^2
H_2	0.018076	0.43156	0.83032	0.000179	683.0424	0.77386
O_2	0.023536	0.54255	0.95281	6.527E-05	842.8186	0.85545
N_2	0.040841	0.58942	0.92433	5.424E-05	872.6351	0.75378
CO_2	0.090953	0.63744	0.93449	9.678E-05	1003.81	0.86218
CH_4	0.122819	0.669	0.97002	9.274E-05	1052.737	0.89365
SF_6	2.28×10^8	1.90886	0.90932	0.231504	2966.794	0.81724

Table 2.6 The coefficient of determination of gas diffusivities and M_c based on diffusion-M_c equations 19 and 20

Gas	r^2 based on eq 19 (h)	r^2 based on eq 20 ($<v_h>$)
H_2	0.7745	0.8002
O_2	0.9366	0.9546
N_2	0.7717	0.8264
CO_2	0.9008	0.9161
CH_4	0.9233	0.9399
SF_6	0.9468	0.9601

2.5 Conclusions

Free volume parameters were quantified both experimentally and using theoretical models in a PEG thiol-ene network series, where M_c was changed by an order of magnitude across the series. Fractional free volume obtained from Simha Somcynsky equation of state fitting of PVT data, average free volume hole size obtained from PALS analysis, fractional free volume obtained from WLF universal constants, changed linearly as a function of $1/M_c$, and thereby showing that this series of networks obey Fox Loshaek model. The model behavior of these networks was because of the similarity in chemical nature across the series. Similar permittivity, obtained from dielectric spectroscopy analysis, and internal pressure values, obtained from PVT data, across the series shed light on the similarity in chemical nature. Therefore, cross-link density or molecular weight between cross-links was the only material factor which was affecting free volume in this series. Because of this model behavior, the experimental gas diffusivities of the networks were modeled as a function of molecular weight between cross-links.

2.6 References

1. Paul, D. R.; Yampol'skii, Y. P., *Polymeric gas separation membranes*. CRC press: 1993.

2. Noble, R. D.; Stern, S. A., *Membrane separations technology: principles and applications*. Elsevier: 1995; Vol. 2.

3. Robeson, L. M., Polymer membranes for gas separation. *Current Opinion in Solid State and Materials Science* **1999,** *4* (6), 549-552.

4. Yang, H.; Xu, Z.; Fan, M.; Gupta, R.; Slimane, R. B.; Bland, A. E.; Wright, I., Progress in carbon dioxide separation and capture: A review. *Journal of Environmental Sciences* **2008,** *20* (1), 14-27.

5. D'Alessandro, D. M.; Smit, B.; Long, J. R., Carbon Dioxide Capture: Prospects for New Materials. *Angewandte Chemie International Edition* **2010,** *49* (35), 6058-6082.

6. Kenarsari, S. D.; Yang, D.; Jiang, G.; Zhang, S.; Wang, J.; Russell, A. G.; Wei, Q.; Fan, M., Review of recent advances in carbon dioxide separation and capture. *RSC Advances* **2013,** *3* (45), 22739-22773.

7. Lin, H.; Kai, T.; Freeman, B. D.; Kalakkunnath, S.; Kalika, D. S., The Effect of Cross-Linking on Gas Permeability in Cross-Linked Poly(Ethylene Glycol Diacrylate). *Macromolecules* **2005,** *38* (20), 8381-8393.

8. Kwisnek, L.; Goetz, J.; Meyers, K. P.; Heinz, S. R.; Wiggins, J. S.; Nazarenko, S., PEG Containing Thiol–Ene Network Membranes for CO2 Separation: Effect of Cross-Linking on Thermal, Mechanical, and Gas Transport Properties. *Macromolecules* **2014,** *47* (10), 3243-3253.

9. Kwisnek, L.; Heinz, S.; Wiggins, J. S.; Nazarenko, S., Multifunctional thiols as additives in UV-cured PEG-diacrylate membranes for CO2 separation. *Journal of Membrane Science* **2011,** *369* (1–2), 429-436.

10. Du, N.; Park, H. B.; Robertson, G. P.; Dal-Cin, M. M.; Visser, T.; Scoles, L.; Guiver, M. D., Polymer nanosieve membranes for CO2-capture applications. *Nature materials* **2011,** *10* (5), 372.

11. Yave, W.; Car, A.; Funari, S. S.; Nunes, S. P.; Peinemann, K.-V., CO2-Philic Polymer Membrane with Extremely High Separation Performance. *Macromolecules* **2010,** *43* (1), 326-333.

12. Fox, T. G.; Loshaek, S., Influence of molecular weight and degree of crosslinking on the specific volume and glass temperature of polymers. *Journal of Polymer Science* **1955,** *15* (80), 371-390.

13. Barrer, R. M.; Skirrow, G., Transport and equilibrium phenomena in gas–elastomer systems. I. Kinetic phenomena. *Journal of Polymer Science* **1948,** *3* (4), 549-563.

14. Barrer, R. M.; Skirrow, G., Transport and equilibrium phenomena in gas–elastomer systems. II. Equilibrium phenomena. *Journal of Polymer Science* **1948,** *3* (4), 564-575.

15. Bixler, H. J.; Michaels, A. S.; Salame, M., Gas transmission in irradiated polyethylene. *Journal of Polymer Science Part A: General Papers* **1963,** *1* (3), 895-919.

16. Andrady, A. L.; Sefcik, M. D., Transport of hydrogen and carbon monoxide in highly crosslinked poly(propylene glycol) networks. *Journal of Polymer Science: Polymer Physics Edition* **1984,** *22* (2), 237-243.

17. Morgan, D. R.; Stejskal, E. O.; Andrady, A. L., 129Xe NMR Investigation of the Free Volume in Dendritic and Cross-Linked Polymers. *Macromolecules* **1999,** *32* (6), 1897-1903.

18. Consolati, G.; Kansy, J.; Pegoraro, M.; Quasso, F.; Zanderighi, L., Positron annihilation study of free volume in cross-linked amorphous polyurethanes through the glass transition temperature. *Polymer* **1998,** *39* (15), 3491-3498.

19. Dlubek, G.; Stejny, J.; Alam, M. A., Effect of Cross-Linking on the Free-Volume Properties of Diethylene Glycol Bis(allyl carbonate) Polymer Networks: A Positron Annihilation Lifetime Study. *Macromolecules* **1998,** *31* (14), 4574-4580.

20. Barrer, R. M.; Barrie, J. A.; Wong, P. S. L., The diffusion and solution of gases in highly crosslinked copolymers. *Polymer* **1968,** *9*, 609-627.

21. Lin, H.; Wagner, E. V.; Swinnea, J. S.; Freeman, B. D.; Pas, S. J.; Hill, A. J.; Kalakkunnath, S.; Kalika, D. S., Transport and structural characteristics of crosslinked poly(ethylene oxide) rubbers. *Journal of Membrane Science* **2006,** *276* (1–2), 145-161.

22. Raharjo, R. D.; Lin, H.; Sanders, D. F.; Freeman, B. D.; Kalakkunnath, S.; Kalika, D. S., Relation between network structure and gas transport in crosslinked poly(propylene glycol diacrylate). *Journal of Membrane Science* **2006,** *283* (1–2), 253-265.

23. Hoyle, C. E.; Lee, T. Y.; Roper, T., Thiol–enes: chemistry of the past with promise for the future. *Journal of Polymer Science Part A: Polymer Chemistry* **2004,** *42* (21), 5301-5338.

24. Hoyle, C. E.; Lowe, A. B.; Bowman, C. N., Thiol-click chemistry: a multifaceted toolbox for small molecule and polymer synthesis. *Chemical Society Reviews* **2010,** *39* (4), 1355-1387.

25. Hoyle, C. E.; Bowman, C. N., Thiol–Ene Click Chemistry. *Angewandte Chemie International Edition* **2010,** *49* (9), 1540-1573.

26. Walsh, D.; Zoller, P., *Standard pressure volume temperature data for polymers*. CRC Press: 1995.

27. Simha, R.; Somcynsky, T., On the Statistical Thermodynamics of Spherical and Chain Molecule Fluids. *Macromolecules* **1969,** *2* (4), 342-350.

28. Utracki, L. A.; Simha, R., Analytical Representation of Solutions to Lattice-Hole Theory. *Macromolecular Theory and Simulations* **2001,** *10* (1), 17-24.

29. Tao, S. J., Positronium Annihilation in Molecular Substances. *The Journal of Chemical Physics* **1972,** *56* (11), 5499-5510.

30. Kirkegaard, P.; Eldrup, M.; Mogensen, O. E.; Pedersen, N. J., Program system for analysing positron lifetime spectra and angular correlation curves. *Computer Physics Communications* **1981,** *23* (3), 307-335.

31. Simha, R.; Wilson, P. S., Thermal Expansion of Amorphous Polymers at Atmospheric Pressure. II. Theoretical Considerations. *Macromolecules* **1973,** *6* (6), 908-914.

32. Rodgers, P. A., Pressure–volume–temperature relationships for polymeric liquids: A review of equations of state and their characteristic parameters for 56 polymers. *Journal of Applied Polymer Science* **1993,** *48* (6), 1061-1080.

33. Utracki, L. A.; Simha, R.; Garcia-Rejon, A., Pressure−Volume−Temperature Dependence of Poly-ε-caprolactam/Clay Nanocomposites. *Macromolecules* **2003,** *36* (6), 2114-2121.

34. Utracki, L. A.; Simha, R., Pressure−Volume−Temperature Dependence of Polypropylene/Organoclay Nanocomposites. *Macromolecules* **2004,** *37* (26), 10123-10133.

35. Utracki, L. A., Equations of state for polyamide-6 and its nanocomposites. II. Effects of clay. *Journal of Polymer Science Part B: Polymer Physics* **2009,** *47* (10), 966-980.

36. Utracki, L. A., Equations of state for polyamide-6 and its nanocomposites. 1. Fundamentals and the matrix. *Journal of Polymer Science Part B: Polymer Physics* **2009,** *47* (3), 299-313.

37. Utracki, L. A., Compressibility and thermal expansion coefficients of nanocomposites with amorphous and crystalline polymer matrix. *European Polymer Journal* **2009,** *45* (7), 1891-1903.

38. Utracki, L. A., Pressure–volume–temperature dependencies of polystyrenes. *Polymer* **2005,** *46* (25), 11548-11556.

39. Yu, Z.; Yahsi, U.; McGervey, J. D.; Jamieson, A. M.; Simha, R., Molecular weight-dependence of free volume in polystyrene studied by positron annihilation measurements. *Journal of Polymer Science Part B: Polymer Physics* **1994,** *32* (16), 2637-2644.

40. Baker, W.; Yager, W., The relation of dielectric properties to structure of crystalline polymers. II. Linear polyamides. *Journal of the American Chemical Society* **1942,** *64* (9), 2171-2177.

41. Kamlet, M. J.; Abboud, J. L.; Taft, R., The solvatochromic comparison method. 6. The. pi.* scale of solvent polarities. *Journal of the American Chemical Society* **1977,** *99* (18), 6027-6038.

42. Wang, Y. Y.; Nakanishi, H.; Jean, Y. C.; Sandreczki, T. C., Positron annihilation in amine-cured epoxy polymers—pressure dependence. *Journal of Polymer Science Part B: Polymer Physics* **1990,** *28* (9), 1431-1441.

43. Deng, Q.; Sundar, C. S.; Jean, Y. C., Pressure dependence of free-volume hole properties in an epoxy polymer. *The Journal of Physical Chemistry* **1992,** *96* (1), 492-495.

44. Dlubek, G.; Wawryszczuk, J.; Pionteck, J.; Goworek, T.; Kaspar, H.; Lochhaas, K. H., High-Pressure Dependence of the Free Volume in Fluoroelastomers from Positron Lifetime and PVT Experiments. *Macromolecules* **2005,** *38* (2), 429-437.

45. Mikhin, K. V.; Stepanov, S. V.; Byakov, V. M., Formation of the Ps bubble in liquid media. *Radiation Physics and Chemistry* **2003,** *68* (3–4), 415-417.

46. Bartos, J.; Sausa, O.; Kristiak, J.; Blochowicz, T.; Rössler, E., Free-volume microstructure of glycerol and its supercooled liquid-state dynamics. *Journal of Physics: Condensed Matter* **2001,** *13* (50), 11473.

47. Bamford, D.; Dlubek, G.; Reiche, A.; Alam, M.; Meyer, W.; Galvosas, P.; Rittig, F., The local free volume, glass transition, and ionic conductivity in a polymer electrolyte: A positron lifetime study. *Polymer* **2001,** *1*, 5.

48. Eldrup, M.; Mogensen, O.; Trumpy, G., Positron Lifetimes in Pure and Doped Ice and in Water. *The Journal of Chemical Physics* **1972,** *57* (1), 495-504.

49. Dlubek, G.; Bondarenko, V.; Pionteck, J.; Supej, M.; Wutzler, A.; Krause-Rehberg, R., Free volume in two differently plasticized poly(vinyl chloride)s: a positron lifetime and PVT study. *Polymer* **2003,** *44* (6), 1921-1926.

50. Mansilla, M. A.; Rodríguez Garraza, A. L.; Silva, L.; Salgueiro, W.; Macchi, C.; Marzocca, A. J.; Somoza, A., Evolution of the free volume and glass transition temperature with the degree of cure of polybutadiene rubbers. *Polymer Testing* **2013,** *32* (4), 686-690.

51. Srithawatpong, R.; Peng, Z.; Olson, B.; Jamieson, A.; Simha, R.; McGervey, J.; Maier, T.; Halasa, A.; Ishida, H., Positron annihilation lifetime studies of changes in free volume on cross-linking cis-polyisoprene, high-vinyl polybutadiene, and their miscible blends. *Journal of Polymer Science Part B Polymer Physics* **1999,** *37* (19), 2754-2770.

52. Jean, Y. C.; Sandreczki, T. C.; Ames, D. P., Positronium annihilation in amine-cured epoxy polymers. *Journal of Polymer Science Part B: Polymer Physics* **1986,** *24* (6), 1247-1258.

53. Williams, M.; Landel, R.; Ferry, J., Mechanical properties of substances of high molecular weight. 19. The temperature dependence of relaxation mechanisms in amorphous polymers and other glass-forming liquids. *Journal of the American Chemical Society* **1955,** *77* (14), 3701-3707.

54. Kusuma, V. A.; Freeman, B. D.; Borns, M. A.; Kalika, D. S., Influence of chemical structure of short chain pendant groups on gas transport properties of cross-

linked poly(ethylene oxide) copolymers. *Journal of Membrane Science* **2009,** *327* (1), 195-207.

55. Kusuma, V. A.; Freeman, B. D.; Smith, S. L.; Heilman, A. L.; Kalika, D. S., Influence of TRIS-based co-monomer on structure and gas transport properties of cross-linked poly(ethylene oxide). *Journal of Membrane Science* **2010,** *359* (1), 25-36.

56. Van Krevelen, D. W.; Te Nijenhuis, K., *Properties of polymers: their correlation with chemical structure; their numerical estimation and prediction from additive group contributions*. Elsevier: 2009.

57. Cohen, M. H.; Turnbull, D., Molecular Transport in Liquids and Glasses. *The Journal of Chemical Physics* **1959,** *31* (5), 1164-1169.

58. Park, J. Y.; Paul, D. R., Correlation and prediction of gas permeability in glassy polymer membrane materials via a modified free volume based group contribution method. *Journal of Membrane Science* **1997,** *125* (1), 23-39.

59. Haraya, K.; Hwang, S.-T., Permeation of oxygen, argon and nitrogen through polymer membranes. *Journal of Membrane Science* **1992,** *71* (1), 13-27.

60. Tanaka, K.; Okano, M.; Toshino, H.; Kita, H.; Okamoto, K.-I., Effect of methyl substituents on permeability and permselectivity of gases in polyimides prepared from methyl-substituted phenylenediamines. *Journal of Polymer Science Part B: Polymer Physics* **1992,** *30* (8), 907-914.

61. Nagel, C.; Günther-Schade, K.; Fritsch, D.; Strunskus, T.; Faupel, F., Free Volume and Transport Properties in Highly Selective Polymer Membranes. *Macromolecules* **2002,** *35* (6), 2071-2077.

62. Sanders, D. F.; Smith, Z. P.; Guo, R.; Robeson, L. M.; McGrath, J. E.; Paul, D. R.; Freeman, B. D., Energy-efficient polymeric gas separation membranes for a sustainable future: A review. *Polymer* **2013,** *54* (18), 4729-4761.

2.7 Supplementary informtion

Table 2.7 PVT data of network 1 - D1E00

T (℃)	Pressure (MPa)														
	0.1	10	20	30	40	50	60	70	80	90	100	110	120	130	140
27.5	0.8354	0.8324	0.8295	0.8265	0.8239	0.8213	0.8189	0.8165	0.8143	0.8119	0.8100	0.8079	0.8059	0.8039	0.8019
32.5	0.8379	0.8348	0.8318	0.8289	0.8263	0.8236	0.8209	0.8184	0.8161	0.8141	0.8119	0.8099	0.8078	0.8056	0.8037
37.4	0.8406	0.8373	0.8341	0.8308	0.8284	0.8255	0.8231	0.8208	0.8184	0.8160	0.8139	0.8119	0.8096	0.8076	0.8057
42.3	0.8430	0.8397	0.8366	0.8335	0.8304	0.8280	0.8253	0.8225	0.8204	0.8180	0.8160	0.8138	0.8116	0.8096	0.8076
47.1	0.8455	0.8421	0.8389	0.8359	0.8328	0.8302	0.8274	0.8250	0.8224	0.8201	0.8178	0.8157	0.8136	0.8116	0.8093
51.9	0.8480	0.8446	0.8414	0.8381	0.8352	0.8323	0.8295	0.8269	0.8245	0.8221	0.8198	0.8176	0.8154	0.8132	0.8112
56.9	0.8504	0.8469	0.8437	0.8403	0.8373	0.8344	0.8318	0.8290	0.8264	0.8241	0.8219	0.8196	0.8173	0.8151	0.8130
61.5	0.8532	0.8495	0.8461	0.8428	0.8395	0.8368	0.8338	0.8311	0.8285	0.8260	0.8237	0.8215	0.8192	0.8169	0.8148
66.7	0.8558	0.8521	0.8485	0.8452	0.8417	0.8389	0.8361	0.8333	0.8306	0.8281	0.8257	0.8234	0.8212	0.8189	0.8168
71.7	0.8583	0.8545	0.8511	0.8474	0.8443	0.8411	0.8381	0.8354	0.8326	0.8301	0.8277	0.8254	0.8230	0.8209	0.8184
76.8	0.8608	0.8570	0.8534	0.8497	0.8465	0.8433	0.8402	0.8374	0.8347	0.8322	0.8296	0.8272	0.8248	0.8225	0.8203
81.6	0.8636	0.8596	0.8557	0.8520	0.8486	0.8455	0.8425	0.8397	0.8368	0.8342	0.8316	0.8291	0.8267	0.8244	0.8221
86.7	0.8664	0.8622	0.8580	0.8544	0.8509	0.8478	0.8446	0.8416	0.8388	0.8359	0.8335	0.8310	0.8286	0.8261	0.8238
91.6	0.8688	0.8646	0.8605	0.8567	0.8533	0.8498	0.8470	0.8438	0.8409	0.8380	0.8356	0.8327	0.8303	0.8281	0.8257
96.4	0.8714	0.8671	0.8631	0.8592	0.8554	0.8520	0.8490	0.8459	0.8428	0.8399	0.8373	0.8346	0.8322	0.8298	0.8274
101.5	0.8741	0.8697	0.8655	0.8615	0.8579	0.8544	0.8510	0.8479	0.8449	0.8420	0.8392	0.8366	0.8342	0.8315	0.8292
106.4	0.8767	0.8721	0.8678	0.8637	0.8600	0.8566	0.8532	0.8501	0.8470	0.8440	0.8411	0.8385	0.8359	0.8334	0.8310
111.1	0.8796	0.8748	0.8702	0.8662	0.8624	0.8588	0.8554	0.8520	0.8491	0.8459	0.8432	0.8404	0.8377	0.8351	0.8327
116.4	0.8817	0.8771	0.8728	0.8684	0.8644	0.8609	0.8573	0.8541	0.8510	0.8480	0.8450	0.8423	0.8395	0.8370	0.8345
121.3	0.8846	0.8797	0.8752	0.8709	0.8668	0.8631	0.8597	0.8563	0.8531	0.8500	0.8470	0.8441	0.8415	0.8388	0.8362
126.3	0.8875	0.8824	0.8776	0.8733	0.8693	0.8655	0.8620	0.8585	0.8551	0.8520	0.8490	0.8461	0.8433	0.8405	0.8380
131.4	0.8900	0.8849	0.8800	0.8756	0.8714	0.8676	0.8638	0.8605	0.8570	0.8539	0.8509	0.8479	0.8450	0.8424	0.8396
136.5	0.8926	0.8874	0.8824	0.8779	0.8739	0.8700	0.8660	0.8625	0.8592	0.8560	0.8529	0.8499	0.8471	0.8442	0.8415
141.5	0.8954	0.8901	0.8849	0.8803	0.8760	0.8721	0.8684	0.8646	0.8611	0.8580	0.8547	0.8515	0.8487	0.8460	0.8431
146.6	0.8983	0.8927	0.8875	0.8827	0.8783	0.8742	0.8705	0.8669	0.8633	0.8600	0.8569	0.8534	0.8506	0.8479	0.8451

Table 2.8 PVT data of network 2 - D1E20

T (℃)	Pressure (MPa)														
	0.1	10	20	30	40	50	60	70	80	90	100	110	120	130	140
27.5	0.8351	0.8319	0.8288	0.8258	0.8229	0.8205	0.8179	0.8157	0.8132	0.8110	0.8089	0.8067	0.8045	0.8026	0.8005
32.0	0.8370	0.8339	0.8308	0.8278	0.8251	0.8226	0.8201	0.8176	0.8151	0.8130	0.8107	0.8085	0.8065	0.8045	0.8025
36.9	0.8397	0.8364	0.8331	0.8301	0.8274	0.8246	0.8219	0.8196	0.8172	0.8148	0.8127	0.8105	0.8081	0.8062	0.8042
41.9	0.8421	0.8387	0.8355	0.8325	0.8294	0.8266	0.8242	0.8215	0.8192	0.8168	0.8145	0.8122	0.8101	0.8080	0.8059
46.8	0.8447	0.8412	0.8378	0.8347	0.8318	0.8288	0.8262	0.8236	0.8210	0.8187	0.8165	0.8141	0.8118	0.8098	0.8077
51.7	0.8472	0.8436	0.8402	0.8368	0.8337	0.8310	0.8281	0.8255	0.8230	0.8206	0.8183	0.8161	0.8137	0.8115	0.8095
56.5	0.8496	0.8459	0.8424	0.8392	0.8361	0.8331	0.8302	0.8275	0.8249	0.8225	0.8201	0.8179	0.8156	0.8134	0.8113
61.4	0.8521	0.8484	0.8448	0.8415	0.8380	0.8353	0.8324	0.8296	0.8270	0.8245	0.8218	0.8197	0.8176	0.8153	0.8130
66.5	0.8546	0.8509	0.8473	0.8439	0.8406	0.8373	0.8345	0.8318	0.8290	0.8265	0.8240	0.8215	0.8193	0.8171	0.8148
71.5	0.8571	0.8532	0.8495	0.8460	0.8429	0.8395	0.8366	0.8338	0.8310	0.8283	0.8258	0.8234	0.8210	0.8188	0.8166
76.2	0.8596	0.8556	0.8520	0.8484	0.8450	0.8417	0.8387	0.8358	0.8330	0.8304	0.8278	0.8253	0.8229	0.8206	0.8184
81.2	0.8623	0.8583	0.8543	0.8508	0.8473	0.8441	0.8409	0.8378	0.8351	0.8322	0.8298	0.8273	0.8248	0.8224	0.8200
86.3	0.8650	0.8608	0.8566	0.8531	0.8496	0.8463	0.8430	0.8401	0.8371	0.8344	0.8315	0.8292	0.8266	0.8242	0.8219
91.3	0.8678	0.8634	0.8593	0.8557	0.8519	0.8486	0.8451	0.8423	0.8393	0.8364	0.8336	0.8311	0.8286	0.8260	0.8236
96.2	0.8702	0.8659	0.8618	0.8579	0.8541	0.8507	0.8474	0.8444	0.8413	0.8384	0.8355	0.8329	0.8305	0.8279	0.8255
100.9	0.8732	0.8687	0.8644	0.8605	0.8566	0.8532	0.8498	0.8465	0.8433	0.8405	0.8376	0.8350	0.8324	0.8298	0.8273
105.8	0.8758	0.8712	0.8669	0.8628	0.8589	0.8554	0.8520	0.8488	0.8454	0.8425	0.8398	0.8370	0.8343	0.8317	0.8291
111.0	0.8787	0.8739	0.8693	0.8651	0.8614	0.8576	0.8542	0.8509	0.8476	0.8445	0.8416	0.8388	0.8361	0.8334	0.8310
115.6	0.8811	0.8763	0.8717	0.8675	0.8636	0.8599	0.8562	0.8527	0.8495	0.8464	0.8437	0.8407	0.8380	0.8352	0.8326
120.7	0.8841	0.8791	0.8743	0.8700	0.8658	0.8622	0.8584	0.8550	0.8518	0.8485	0.8455	0.8425	0.8399	0.8371	0.8345
125.8	0.8868	0.8816	0.8768	0.8724	0.8685	0.8645	0.8607	0.8573	0.8538	0.8507	0.8474	0.8445	0.8417	0.8389	0.8363
130.6	0.8893	0.8842	0.8794	0.8748	0.8704	0.8667	0.8629	0.8592	0.8558	0.8525	0.8495	0.8464	0.8435	0.8409	0.8380
135.7	0.8924	0.8870	0.8818	0.8773	0.8729	0.8690	0.8652	0.8614	0.8581	0.8549	0.8516	0.8485	0.8455	0.8426	0.8398
140.8	0.8953	0.8898	0.8843	0.8798	0.8754	0.8713	0.8674	0.8636	0.8601	0.8565	0.8536	0.8504	0.8475	0.8445	0.8419
145.8	0.8985	0.8926	0.8871	0.8821	0.8780	0.8737	0.8697	0.8657	0.8622	0.8589	0.8555	0.8523	0.8492	0.8464	0.8437

Table 2.9 PVT data of network 3 - D1E40

T (℃)	Pressure (MPa)														
	0.1	10	20	30	40	50	60	70	80	90	100	110	120	130	140
27.3	0.8458	0.8427	0.8400	0.8368	0.8343	0.8317	0.8288	0.8266	0.8242	0.8219	0.8195	0.8175	0.8154	0.8133	0.8113
32.3	0.8488	0.8455	0.8422	0.8392	0.8363	0.8337	0.8310	0.8283	0.8262	0.8239	0.8216	0.8195	0.8171	0.8152	0.8132
37.3	0.8511	0.8478	0.8446	0.8414	0.8386	0.8356	0.8332	0.8308	0.8281	0.8257	0.8235	0.8214	0.8192	0.8170	0.8149
42.0	0.8538	0.8504	0.8471	0.8440	0.8409	0.8381	0.8353	0.8327	0.8302	0.8278	0.8258	0.8233	0.8211	0.8189	0.8169
46.8	0.8563	0.8528	0.8495	0.8463	0.8430	0.8402	0.8375	0.8349	0.8322	0.8300	0.8276	0.8253	0.8231	0.8209	0.8188
51.9	0.8585	0.8551	0.8518	0.8485	0.8454	0.8425	0.8397	0.8370	0.8342	0.8317	0.8297	0.8273	0.8250	0.8227	0.8207
57.0	0.8615	0.8578	0.8543	0.8508	0.8478	0.8446	0.8419	0.8390	0.8364	0.8339	0.8316	0.8294	0.8270	0.8247	0.8224
61.8	0.8642	0.8604	0.8569	0.8532	0.8500	0.8470	0.8441	0.8411	0.8384	0.8361	0.8336	0.8311	0.8290	0.8266	0.8245
66.7	0.8665	0.8627	0.8592	0.8558	0.8522	0.8493	0.8462	0.8435	0.8406	0.8381	0.8357	0.8332	0.8309	0.8285	0.8263
71.8	0.8689	0.8652	0.8617	0.8583	0.8547	0.8514	0.8485	0.8456	0.8429	0.8401	0.8377	0.8351	0.8327	0.8304	0.8282
76.6	0.8721	0.8680	0.8642	0.8606	0.8570	0.8537	0.8506	0.8477	0.8448	0.8423	0.8396	0.8371	0.8346	0.8323	0.8299
81.6	0.8748	0.8706	0.8665	0.8628	0.8594	0.8560	0.8527	0.8498	0.8470	0.8439	0.8413	0.8390	0.8366	0.8341	0.8316
86.6	0.8776	0.8733	0.8690	0.8654	0.8616	0.8580	0.8549	0.8520	0.8492	0.8462	0.8435	0.8410	0.8385	0.8359	0.8335
91.6	0.8804	0.8759	0.8719	0.8677	0.8640	0.8606	0.8575	0.8542	0.8511	0.8483	0.8457	0.8429	0.8404	0.8379	0.8356
96.4	0.8828	0.8784	0.8742	0.8703	0.8664	0.8627	0.8595	0.8562	0.8533	0.8502	0.8475	0.8449	0.8422	0.8398	0.8373
101.3	0.8858	0.8811	0.8767	0.8728	0.8687	0.8650	0.8618	0.8585	0.8554	0.8523	0.8495	0.8467	0.8442	0.8416	0.8390
106.3	0.8882	0.8836	0.8792	0.8749	0.8713	0.8673	0.8638	0.8606	0.8574	0.8543	0.8513	0.8487	0.8459	0.8435	0.8409
111.1	0.8912	0.8863	0.8819	0.8775	0.8735	0.8697	0.8661	0.8627	0.8594	0.8565	0.8533	0.8506	0.8479	0.8452	0.8426
116.3	0.8937	0.8888	0.8842	0.8797	0.8757	0.8719	0.8683	0.8648	0.8615	0.8584	0.8552	0.8525	0.8498	0.8471	0.8445
121.3	0.8966	0.8915	0.8867	0.8821	0.8781	0.8744	0.8704	0.8671	0.8635	0.8604	0.8574	0.8544	0.8516	0.8489	0.8462
126.2	0.8995	0.8942	0.8893	0.8848	0.8806	0.8765	0.8727	0.8689	0.8656	0.8625	0.8594	0.8563	0.8535	0.8508	0.8481
131.0	0.9022	0.8968	0.8919	0.8872	0.8830	0.8790	0.8750	0.8713	0.8676	0.8645	0.8615	0.8583	0.8555	0.8524	0.8499
136.2	0.9053	0.8997	0.8947	0.8897	0.8853	0.8814	0.8775	0.8735	0.8701	0.8667	0.8635	0.8603	0.8573	0.8545	0.8517
141.3	0.9081	0.9024	0.8971	0.8923	0.8877	0.8835	0.8796	0.8758	0.8722	0.8687	0.8654	0.8622	0.8593	0.8563	0.8536
146.3	0.9106	0.9050	0.8997	0.8947	0.8903	0.8860	0.8817	0.8780	0.8743	0.8706	0.8676	0.8642	0.8612	0.8583	0.8554

Table 2.10 PVT data of network 4 - D1E60

T (℃)	Pressure (MPa)														
	0.1	10	20	30	40	50	60	70	80	90	100	110	120	130	140
27.5	0.8504	0.8473	0.8445	0.8414	0.8387	0.8358	0.8331	0.8306	0.8281	0.8258	0.8237	0.8215	0.8194	0.8173	0.8152
32.1	0.8538	0.8504	0.8472	0.8438	0.8409	0.8382	0.8356	0.8330	0.8304	0.8281	0.8257	0.8235	0.8213	0.8192	0.8172
37.1	0.8564	0.8529	0.8495	0.8463	0.8433	0.8404	0.8379	0.8351	0.8326	0.8303	0.8278	0.8255	0.8234	0.8212	0.8190
41.7	0.8592	0.8556	0.8522	0.8488	0.8458	0.8428	0.8398	0.8375	0.8349	0.8322	0.8299	0.8276	0.8253	0.8232	0.8211
47.0	0.8616	0.8580	0.8545	0.8511	0.8480	0.8450	0.8421	0.8396	0.8370	0.8345	0.8320	0.8296	0.8273	0.8251	0.8229
51.6	0.8640	0.8605	0.8570	0.8537	0.8504	0.8472	0.8444	0.8416	0.8389	0.8363	0.8340	0.8316	0.8294	0.8270	0.8249
56.6	0.8673	0.8633	0.8595	0.8559	0.8527	0.8496	0.8466	0.8438	0.8410	0.8384	0.8360	0.8336	0.8312	0.8289	0.8268
61.5	0.8696	0.8657	0.8621	0.8582	0.8550	0.8519	0.8487	0.8459	0.8432	0.8403	0.8378	0.8355	0.8332	0.8309	0.8286
66.5	0.8724	0.8683	0.8646	0.8610	0.8573	0.8540	0.8512	0.8481	0.8452	0.8424	0.8398	0.8373	0.8350	0.8328	0.8305
71.2	0.8748	0.8708	0.8672	0.8634	0.8596	0.8564	0.8532	0.8503	0.8474	0.8448	0.8419	0.8392	0.8370	0.8346	0.8323
76.1	0.8779	0.8736	0.8697	0.8656	0.8621	0.8586	0.8555	0.8524	0.8494	0.8467	0.8439	0.8413	0.8389	0.8364	0.8339
81.0	0.8807	0.8762	0.8719	0.8680	0.8644	0.8609	0.8577	0.8546	0.8515	0.8487	0.8459	0.8432	0.8408	0.8383	0.8359
86.0	0.8831	0.8787	0.8744	0.8704	0.8667	0.8634	0.8597	0.8567	0.8535	0.8508	0.8480	0.8453	0.8428	0.8403	0.8378
91.0	0.8859	0.8813	0.8770	0.8731	0.8691	0.8656	0.8622	0.8591	0.8558	0.8528	0.8500	0.8471	0.8446	0.8420	0.8396
96.1	0.8883	0.8838	0.8797	0.8755	0.8715	0.8679	0.8644	0.8610	0.8580	0.8549	0.8520	0.8493	0.8466	0.8439	0.8414
100.9	0.8914	0.8867	0.8821	0.8779	0.8740	0.8702	0.8666	0.8633	0.8600	0.8571	0.8539	0.8510	0.8484	0.8457	0.8432
105.7	0.8943	0.8894	0.8847	0.8803	0.8763	0.8724	0.8691	0.8654	0.8622	0.8590	0.8561	0.8531	0.8503	0.8475	0.8450
110.5	0.8972	0.8921	0.8873	0.8828	0.8787	0.8749	0.8713	0.8676	0.8641	0.8609	0.8580	0.8551	0.8521	0.8495	0.8466
115.5	0.9001	0.8948	0.8898	0.8851	0.8810	0.8772	0.8733	0.8698	0.8662	0.8631	0.8599	0.8570	0.8539	0.8512	0.8486
120.3	0.9028	0.8974	0.8922	0.8877	0.8835	0.8795	0.8758	0.8719	0.8686	0.8651	0.8621	0.8590	0.8561	0.8532	0.8505
125.7	0.9054	0.9000	0.8950	0.8902	0.8860	0.8819	0.8779	0.8743	0.8708	0.8673	0.8641	0.8610	0.8578	0.8550	0.8522
130.8	0.9084	0.9028	0.8972	0.8928	0.8884	0.8842	0.8803	0.8765	0.8730	0.8693	0.8661	0.8629	0.8599	0.8569	0.8540
135.8	0.9111	0.9055	0.9003	0.8953	0.8908	0.8866	0.8825	0.8788	0.8751	0.8718	0.8681	0.8650	0.8619	0.8589	0.8559
141.0	0.9145	0.9085	0.9029	0.8978	0.8933	0.8891	0.8852	0.8811	0.8774	0.8739	0.8706	0.8672	0.8639	0.8609	0.8579
146.1	0.9171	0.9112	0.9054	0.9006	0.8957	0.8914	0.8873	0.8835	0.8795	0.8758	0.8725	0.8690	0.8657	0.8629	0.8597

Table 2.11 PVT data of network 5 - D1E80

T (℃)	Pressure (MPa)														
	0.1	10	20	30	40	50	60	70	80	90	100	110	120	130	140
27.7	0.8591	0.8559	0.8527	0.8498	0.8467	0.8437	0.8408	0.8384	0.8360	0.8336	0.8314	0.8290	0.8268	0.8246	0.8225
32.5	0.8620	0.8585	0.8553	0.8519	0.8488	0.8460	0.8430	0.8406	0.8381	0.8355	0.8332	0.8307	0.8286	0.8263	0.8243
37.2	0.8644	0.8608	0.8572	0.8539	0.8509	0.8480	0.8451	0.8424	0.8397	0.8374	0.8350	0.8328	0.8305	0.8282	0.8259
41.9	0.8665	0.8631	0.8598	0.8565	0.8531	0.8504	0.8476	0.8445	0.8418	0.8398	0.8371	0.8346	0.8323	0.8300	0.8278
47.6	0.8695	0.8658	0.8621	0.8589	0.8556	0.8524	0.8493	0.8470	0.8442	0.8414	0.8390	0.8367	0.8341	0.8319	0.8298
51.9	0.8724	0.8685	0.8648	0.8611	0.8580	0.8549	0.8516	0.8489	0.8462	0.8437	0.8412	0.8385	0.8362	0.8339	0.8317
57.2	0.8750	0.8710	0.8673	0.8638	0.8603	0.8572	0.8542	0.8510	0.8481	0.8457	0.8432	0.8406	0.8381	0.8359	0.8336
61.6	0.8778	0.8736	0.8696	0.8660	0.8627	0.8594	0.8561	0.8534	0.8505	0.8477	0.8453	0.8427	0.8402	0.8377	0.8354
66.8	0.8801	0.8760	0.8721	0.8683	0.8649	0.8614	0.8586	0.8555	0.8526	0.8498	0.8472	0.8447	0.8422	0.8397	0.8373
71.4	0.8832	0.8789	0.8750	0.8704	0.8672	0.8640	0.8606	0.8576	0.8547	0.8519	0.8490	0.8466	0.8442	0.8416	0.8393
76.5	0.8857	0.8814	0.8771	0.8733	0.8696	0.8662	0.8631	0.8597	0.8569	0.8541	0.8510	0.8486	0.8459	0.8435	0.8412
81.3	0.8884	0.8841	0.8801	0.8759	0.8722	0.8685	0.8651	0.8619	0.8591	0.8562	0.8533	0.8508	0.8480	0.8454	0.8430
86.2	0.8916	0.8869	0.8826	0.8783	0.8746	0.8710	0.8675	0.8643	0.8614	0.8583	0.8551	0.8526	0.8500	0.8474	0.8447
91.1	0.8944	0.8896	0.8850	0.8808	0.8768	0.8735	0.8699	0.8664	0.8631	0.8602	0.8572	0.8546	0.8520	0.8492	0.8466
96.4	0.8971	0.8923	0.8879	0.8833	0.8793	0.8755	0.8722	0.8686	0.8656	0.8621	0.8592	0.8563	0.8537	0.8511	0.8485
101.4	0.9001	0.8951	0.8905	0.8859	0.8818	0.8778	0.8743	0.8708	0.8676	0.8646	0.8615	0.8583	0.8557	0.8530	0.8503
106.1	0.9032	0.8980	0.8931	0.8885	0.8844	0.8807	0.8766	0.8731	0.8697	0.8666	0.8634	0.8607	0.8577	0.8550	0.8523
111.1	0.9059	0.9006	0.8956	0.8912	0.8869	0.8828	0.8791	0.8755	0.8719	0.8687	0.8653	0.8626	0.8596	0.8568	0.8541
116.3	0.9089	0.9035	0.8983	0.8937	0.8891	0.8851	0.8812	0.8777	0.8743	0.8709	0.8675	0.8646	0.8617	0.8587	0.8561
121.4	0.9115	0.9061	0.9012	0.8964	0.8919	0.8877	0.8839	0.8800	0.8762	0.8731	0.8697	0.8667	0.8636	0.8608	0.8580
126.2	0.9142	0.9088	0.9036	0.8989	0.8946	0.8902	0.8860	0.8825	0.8788	0.8752	0.8719	0.8687	0.8658	0.8628	0.8599
131.2	0.9179	0.9120	0.9064	0.9016	0.8970	0.8926	0.8884	0.8845	0.8810	0.8775	0.8742	0.8706	0.8677	0.8647	0.8618
136.1	0.9206	0.9148	0.9094	0.9042	0.8994	0.8952	0.8912	0.8869	0.8832	0.8796	0.8764	0.8729	0.8698	0.8665	0.8637
141.5	0.9238	0.9178	0.9120	0.9069	0.9022	0.8975	0.8933	0.8893	0.8856	0.8819	0.8784	0.8749	0.8719	0.8686	0.8657
146.4	0.9271	0.9208	0.9149	0.9097	0.9047	0.9002	0.8959	0.8918	0.8880	0.8843	0.8806	0.8771	0.8740	0.8709	0.8677

Table 2.12 PVT data of network 6 - D1E90

T (℃)	Pressure (MPa)														
	0.1	10	20	30	40	50	60	70	80	90	100	110	120	130	140
27.5	0.8649	0.8615	0.8582	0.8550	0.8517	0.8492	0.8463	0.8438	0.8413	0.8388	0.8364	0.8341	0.8318	0.8295	0.8274
32.5	0.8679	0.8643	0.8609	0.8576	0.8543	0.8513	0.8486	0.8459	0.8434	0.8409	0.8384	0.8360	0.8336	0.8315	0.8294
37.2	0.8703	0.8666	0.8631	0.8599	0.8566	0.8535	0.8507	0.8479	0.8455	0.8430	0.8404	0.8379	0.8357	0.8333	0.8311
42.1	0.8727	0.8691	0.8656	0.8621	0.8589	0.8558	0.8527	0.8499	0.8473	0.8449	0.8423	0.8399	0.8374	0.8351	0.8330
46.8	0.8755	0.8717	0.8679	0.8646	0.8613	0.8580	0.8550	0.8522	0.8495	0.8468	0.8443	0.8419	0.8393	0.8371	0.8347
52.0	0.8783	0.8744	0.8705	0.8669	0.8635	0.8603	0.8572	0.8543	0.8514	0.8487	0.8463	0.8438	0.8414	0.8390	0.8366
56.6	0.8810	0.8769	0.8730	0.8693	0.8658	0.8626	0.8593	0.8565	0.8535	0.8508	0.8483	0.8458	0.8432	0.8409	0.8384
61.4	0.8834	0.8794	0.8755	0.8717	0.8679	0.8647	0.8614	0.8585	0.8556	0.8530	0.8503	0.8476	0.8453	0.8428	0.8404
66.7	0.8865	0.8823	0.8783	0.8744	0.8707	0.8672	0.8640	0.8610	0.8580	0.8551	0.8524	0.8497	0.8471	0.8447	0.8423
71.5	0.8892	0.8848	0.8808	0.8768	0.8730	0.8695	0.8662	0.8632	0.8601	0.8572	0.8544	0.8517	0.8490	0.8464	0.8441
76.4	0.8923	0.8877	0.8834	0.8791	0.8754	0.8719	0.8685	0.8653	0.8621	0.8593	0.8563	0.8536	0.8511	0.8484	0.8459
81.3	0.8947	0.8901	0.8859	0.8817	0.8778	0.8741	0.8708	0.8675	0.8642	0.8612	0.8584	0.8556	0.8529	0.8503	0.8477
86.3	0.8973	0.8927	0.8883	0.8841	0.8802	0.8765	0.8729	0.8697	0.8664	0.8632	0.8604	0.8576	0.8549	0.8521	0.8496
91.3	0.9003	0.8955	0.8909	0.8865	0.8826	0.8789	0.8751	0.8718	0.8686	0.8655	0.8625	0.8596	0.8568	0.8540	0.8513
96.3	0.9032	0.8982	0.8935	0.8893	0.8850	0.8810	0.8776	0.8740	0.8707	0.8672	0.8642	0.8615	0.8585	0.8558	0.8531
100.8	0.9063	0.9010	0.8961	0.8915	0.8872	0.8835	0.8798	0.8761	0.8729	0.8694	0.8663	0.8635	0.8605	0.8577	0.8550
105.9	0.9089	0.9037	0.8987	0.8942	0.8898	0.8859	0.8819	0.8783	0.8749	0.8715	0.8684	0.8656	0.8625	0.8596	0.8569
111.0	0.9119	0.9065	0.9014	0.8967	0.8921	0.8880	0.8843	0.8804	0.8771	0.8738	0.8703	0.8670	0.8642	0.8616	0.8586
115.7	0.9149	0.9093	0.9040	0.8992	0.8948	0.8906	0.8867	0.8828	0.8793	0.8758	0.8727	0.8694	0.8663	0.8634	0.8606
120.5	0.9178	0.9121	0.9067	0.9020	0.8973	0.8932	0.8889	0.8850	0.8814	0.8780	0.8747	0.8715	0.8683	0.8654	0.8623
125.8	0.9206	0.9148	0.9093	0.9044	0.8997	0.8954	0.8913	0.8873	0.8836	0.8801	0.8767	0.8734	0.8703	0.8672	0.8644
130.7	0.9240	0.9179	0.9122	0.9069	0.9021	0.8978	0.8937	0.8896	0.8857	0.8823	0.8789	0.8753	0.8724	0.8691	0.8661
135.4	0.9267	0.9206	0.9150	0.9095	0.9048	0.9004	0.8962	0.8921	0.8884	0.8844	0.8810	0.8777	0.8745	0.8712	0.8682
140.8	0.9300	0.9237	0.9180	0.9124	0.9075	0.9027	0.8987	0.8945	0.8905	0.8869	0.8830	0.8798	0.8766	0.8733	0.8703
145.8	0.9332	0.9267	0.9206	0.9150	0.9101	0.9054	0.9006	0.8967	0.8928	0.8891	0.8854	0.8821	0.8787	0.8754	0.8724

CHAPTER III - EFFECT OF PERFLUORINATED DANGLING MOIETIES ON FREE VOLUME, OXYGEN AND WATER VAPOR TRANSPORT PROPERTIES OF THIOL-ENE ELASTOMERIC NETWORKS

3.1 Abstract

Perfluorinated thiol-ene elastomers were prepared using a two-step synthesis. In the first step, a tetrafunctional thiol was reacted with a perfluorinated acrylate, via Thio Michael addition to obtain trifunctional thiol containing perfluorinated dangling moiety. In the second step, this modified trifunctional thiol was reacted with a trifunctional ene to produce thiol-ene network containing perfluorinated dangling moiety. This strategy was used to produce a series of perfluorinated thiol-ene elastomers, where the length of the perfluorinated dangling moiety in the network was changed by altering the length of perfluorinated acrylate for the first step. Thiol monomer modifications were confirmed using ^{1}H NMR analysis. Real time FTIR analysis showed that perfluorination and the length of perfluorination did not impact the fast reaction kinetics of thiol-ene chemistry, and near full conversions were obtained in all the cases. DSC and DMA analysis showed that length of the dangling moiety did not have any effect on T_g and cross-link density of the networks. Free volume analysis using PALS showed that average hole size increased as a function of the length of the perfluorinated dangling moiety, and was quadrupled when compared to an unmodified network. The oxygen permeability of the networks increased exponentially as a function of the length of the dangling moiety. Comparison of oxygen diffusivity to free volume sizes showed deviations from Cohen Turnbull model. The static nature of free volume pockets around perfluorinated moieties and percolation at higher free volume sizes, described using 2D lattice like model, was used to explain

the deviation from Cohen Turnbull model. Water vapor permeability of the networks was unaffected by the length of perfluorinated dangling moieties, and this was explained as a trade-off between diffusivity and solubility.

3.2 Introduction

Perfluorinated polymers exhibit excellent properties such as hydrophobicity, chemical resistance, and thermal resistance among many others.[1-2] Furthermore, the strong C-F bond enhances the oxidation and hydrolytic resistance of these polymers.[3] Hence these materials find applications as membranes, seals, o-rings etc. that are used in harsh chemical conditions. But the homopolymers such as polytetrafluoroethylene, polyvinylidene fluoride (PVDF) are highly crystalline and are difficult to melt or solvent process. Therefore, a generation of perfluorinated co/ter polymers where generated, where disorder (brought by the second or third monomer) reduces or gets rid of high crystallinity,[1, 4] and these polymers are typically amorphous and elastomeric. Typically, fluoroalkenes are copolymerized using free radical polymerization under high temperature and pressure, or emulsion conditions to obtain most of the commercially available fluoroelastomers, and the synthetic processes involved are rather complex.[2] These commercial fluoroelastomers are typically cured using peroxide cross-linking. Therefore, any alternative chemistries or processes that can ease the synthesis of perfluorinated materials will be highly beneficial.

Addition of small concentrations of perfluorinated monomer in epoxy[5], acrylic[6] systems have been reported previously. Also, perfluorinated prepolymers have been incorporated in polyurethane[7], acrylate chemistries[8]. Unfortunately, the above methods can result in phase separation or surface aggregation of perfluorinated moieties.

Therefore, novel methods that are easily processible and can produce homogeneous networks containing perfluorinated moieties are highly sought after, for coating and membrane applications.

Our lab previously demonstrated UV synthesis of perfluorinated elastomers using acrylate chemistry, which showed interesting side-chain liquid crystalline behavior, which can be used as a thermal stimulus for controlling gas permeability.[9] Similar chemistry was used by Yao et al to produce fluorogels that showed excellent chemical resistance and anti-fouling properties.[10] But compared to acrylate chemistry, thiol-ene chemistry offers advantages such as network uniformity, low oxygen inhibition, and low shrinkage stress.[11-13] The reaction between thiol and ene functional groups present in the monomers produces uniform networks where cross-link density, and thereby glass transition temperature, modulus, transport properties etc. can be precisely controlled.[14] Our group has previously shown a two-step synthesis by which networks containing different dangling moieties can be prepared.[15-16] In the first step, a tetrafunctional thiol is reacted with a monofunctional acrylate, via thio Michael addition, such that it produces a trifunctional thiol monomer containing a dangling moiety. In the second step, the modified monomer is reacted with ene monomers to produce modified thiol-ene networks. By varying the type of acrylate chosen, intermolecular interactions between the chains was altered, thereby an easy approach to alter/tune chain rigidity, free volume, and transport properties was demonstrated. In the preceding communication, using the aforementioned approach, the effect of length of hydrophobic alkylated dangling moieties on network properties were studied.[16] It was shown that the fast reaction kinetics of thiol-ene chemistry along with this 2-step approach, locks in the covalently bonded

hydrophobic moieties within the polar thiol-ene backbone. By changing the length of alkylated dangling moieties, oxygen permeability of the thiol-ene networks could be tuned in the range of 2 orders of magnitude. In the present study, the main goal was to incorporate more hydrophobic perfluorinated dangling moieties into the thiol-ene networks, and to study their free volume and transport characteristics, and compare them with alkylated networks.

3.3 Experimental

3.3.1 Materials

Thiol monomers pentaerythritol tetrakis(3-mercaptopropionate) (4T) and trimethylolpropane tris(3-mercaptopropionate) (3T) were provided by Bruno Bock Thiochemicals. Ene monomer 1,3,5-Triallyl-1,3,5-triazine-2,4,6(1H,3H,5H)-trione (TTT), photoinitiator 2,2-Dimethoxy-2-phenylacetophenone (DMPA), and nucleophilic catalyst, di-n-butyl amine (DBA), were obtained from Sigma-Aldrich. Perfluoroacrylates 2,2,2 trifluoro ethyl acrylate (f2) and 1H,1H heptafluoro butyl acrylate (f4) were obtained from Synquest Laboratories (Alachua, FL). Whereas, 2-perfluorobutyl ethyl acrylate (f6), 2-perfluorohexyl ethyl acrylate (f8), and 2-perfluorooctyl ethyl acrylate (f10) were obtained from Fluoryx Labs (Carson City, NV). All the chemicals were used as received. Figure 3.1 shows the chemical structures of all the aforementioned molecules.

3.3.2 Synthesis of Perfluorinated Thiol Monomers

Perfluorinated thiol monomers were prepared using Thio-Michael addition reaction. Schematic of the reaction is shown in step 1 of Figure 3.2. Equimolar amounts of four functional thiol 4T and perfluorinated acrylate (fX) were used in this reaction. 4T was solubilized in excess acetone and was added to a round bottom flask. DBA catalyst

was then added to the solution to catalyze the reaction. Perfluorinated acrylate, dissolved in acetone, was then added drop-wise, using a separatory funnel, to the round bottom flask. The solution was sealed, kept stirring and the reaction was allowed to proceed overnight. The resulting product (4T-fX) will be a distribution of structures, but on average will be a trifunctional thiol containing perfluorinated moiety similar to the one shown in the product of reaction in step 1 of Figure 3.2.[16] The same reaction procedure was used to prepare all the five perfluorinated thiol monomers by using five different perfluorinated acrylates (f2, f4, f6, f8, and f10). Acetone was removed from perfluorinated monomers by Rotovap at 40 °C. The modified monomers were then subjected to vacuum to remove any residual acetone.

3.3.3 Synthesis of Perfluorinated Thiol-Ene Elastomers

Step 2 of Figure 3.2 shows the schematic for perfluorinated network synthesis. Perfluorinated thiol monomer (4T-fX) and trifunctional thiol TTT monomer were taken in a vial such that the mixture maintained 1:1 thiol:ene stoichiometry. 1 wt% DMPA photoinitiator was added to the mixture. The mixture was first mixed using a vortexer, following which it was sonicated for 15 minutes. The monomers readily dissolved into each other with the exception of 4T-f10 monomer. 4T-f10 and TTT mixture was stirred and heated at 40 °C until a clear solution was obtained. The monomer mixture was then poured on to a clean glass plate and was sandwiched by placing another glass plate on top, and the thickness of the product film was controlled by placing spacers having thickness ~0.3 mm in the corners between the plates. The glass plates assembly was then exposed to UV light (UVA400 UV, Cure-Tek curing systems- intensity 76 mW/cm^2) for 4 minutes, where the assembly was flipped after 1-minute exposure. The resulting

perfluorinated thiol-ene elastomer film was then carefully removed from the glass plates. The control networks (4T-TTT and 3T-TTT), without any perfluorinated moieties, was synthesized where 4T or 3T and TTT were used as the monomers.

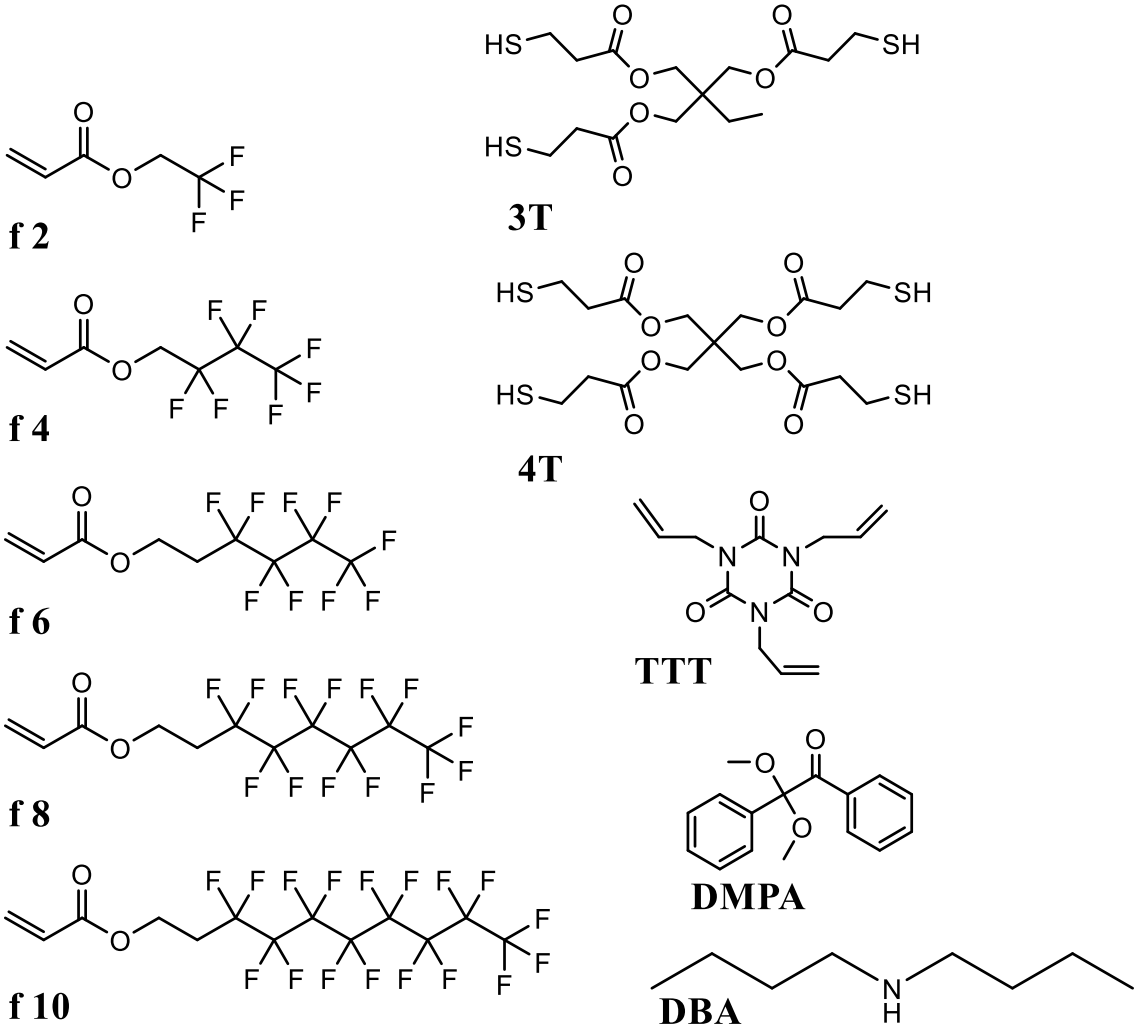

Figure 3.1 Chemical structures of perfluorinated acrylates (f2, f4, f6, f8, f10), thiol (3T, 4T), ene (TTT) monomers, photo-initiator (DMPA) and nucleophilic catalyst (DBA).

3.3.4 Characterization of Modified Monomers and Network Conversion

Perfluorinated thiol monomers were characterized by ^{1}H NMR using a Varian Mercury 200 MHz NMR spectrometer, where acetone-d_6 was used as the solvent. Network conversion (i.e., crosslinking) reaction was studied using Thermo Fisher

Scientific Nicolet 8700 real time FT-IR spectrometer - light intensity of 20 mW/cm^2 at 365 nm irradiance. A mixture containing stoichiometric quantities of monomers having 1 wt% DMPA was made. A drop was taken from that mixture and was placed between two KBr plates, and was then subjected to FTIR analysis. The change in areas under thiol peak (2570 cm^{-1}) and ene peak (3080 cm^{-1}) were monitored as a function of irradiance time in order to study network conversion.

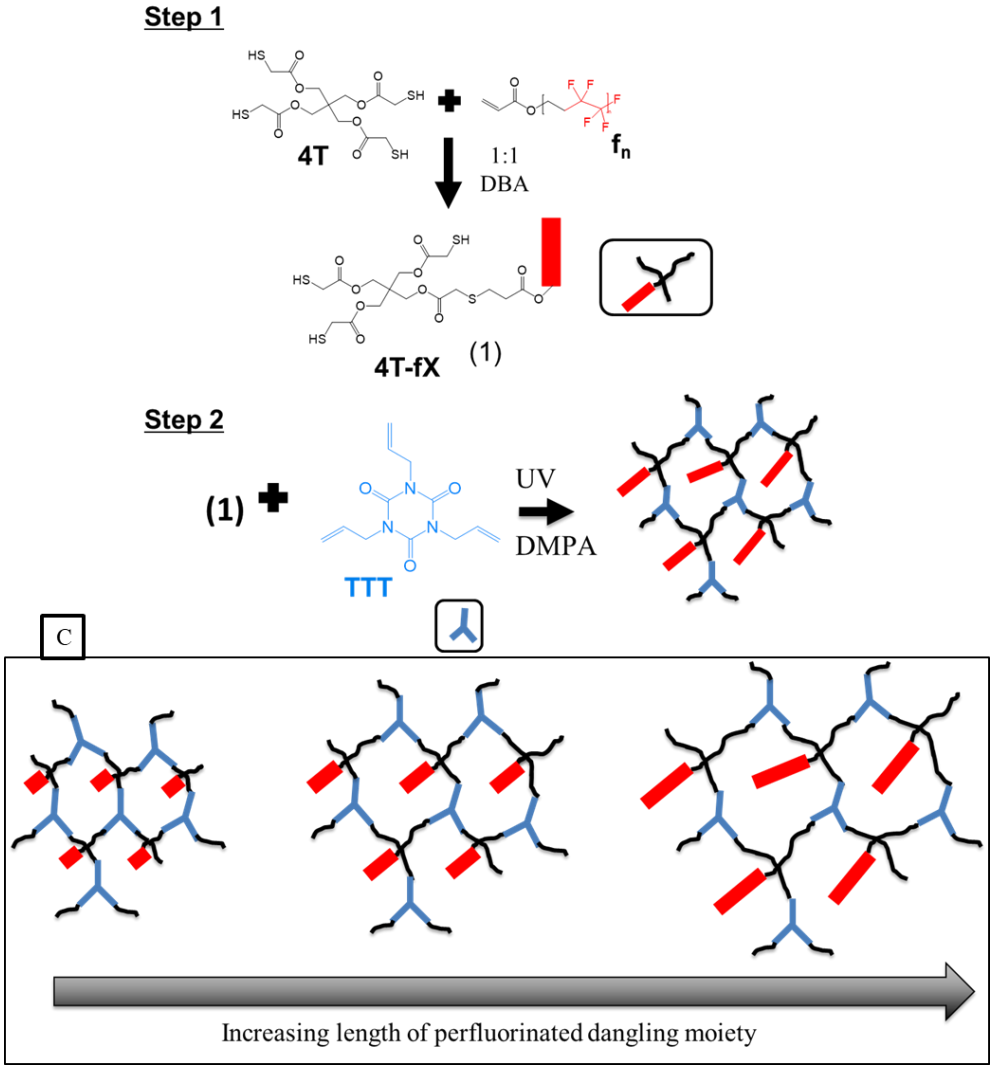

Figure 3.2 Schematic of 2-step perfluorinated thiol-ene elastomer synthesis. (c) Schematic of the family of networks produced in this study

Thermal analysis of the networks was performed using a differential scanning calorimetry - TA Q2000. Heat-cool-heat program was employed, i.e., 35 °C to 100 °C at a ramp rate of 10 °C/min, 100 °C to -70°C at 5 °C/min, and -70 °C to 100 °C at 10 °C/min. TA data analysis software was used to process the data. Glass transition temperature of the networks was determined from the second heat curves.

Dynamic mechanical thermal analysis (DMTA) was performed using Rheometric Scientific DMTAV instrument. The measurements were done at a frequency of 1 Hz, strain rate of 0.05%, and a temperature range of -50 °C to 200 °C at a ramp rate of 5 °C/min.

Water contact angle of the networks were measured using Rame-Hart model 200-00 standard goniometer. DI water droplets having diameter of ~5 mm were placed on a clean film and the contact angle was recorded using Rame-hart DROPimage Standard software.

Water sorption characteristics of the networks were studied using a TA Instruments Q5000 Sorption Analyzer. Discs having diameter of 6.3 mm and thickness of ~0.3 mm were punched out from the films. The disc was placed in a quartz pan and was subjected to drying at 60 °C and 0% RH, following the water sorption characteristics were studied at 20 °C and 95% RH.

Average free volume hole size, $<v_h>$, of the networks were measured using positron annihilation lifetime spectroscopy (PALS). Discs having diameter of 1 cm were punched out from the films. Discs were stacked to make thickness of 1 mm. Positron source, 30 μCi ^{22}Na, enclosed in an Al foil was sandwiched between two stacked discs. The sample source assembly was then placed between two photomultiplier tubes (PMT).

PMTs contain BaF_2 γ-radiation sensitive scintillators and are tuned such that one PMT can detect γ quanta associated with the birth signal and the other PMT with its annihilation. A multichannel analyzer compiled the positron lifetimes, i.e. the time difference between the birth and death signals of the positrons, with a time resolution of 290 ps.

Table 3.1 Fluorine content and glass transition temperature of the networks

Sample identity	**Thiol component**	**Fluorine content (wt%)**	**T_g (° C) DSC**
4T-TTT	4T	0	30
3T-TTT	3T	0	22.1
f2	4T-f2	6.4	12.9
f4	4T-f4	13.4	13.6
f6	4T-f6	16.2	11.7
f8	4T-f8	21.4	13.5
f10	4T-f10	25.7	13.4

Positrons thermalize in the sample and can form positronium species with secondary electrons. The longer lived ortho positronium (o-Ps) species, in which both electron and positron spins in the same direction, localizes within the less electron dense regions, i.e., free volume holes within the sample. o-Ps gets annihilated when it gets picked-off by an electron having opposite spin and this is called pick-off annihilation. Therefore, the lifetime of o-Ps depends on electron scarcity within the sample or the physical size of the free volume hole in which o-Ps localizes. Using semi-empirical

equation (eq. 1) derived by Tao, o-Ps lifetime τ_3 was related to free volume hole radius R.[17]

$$\tau_3 = 0.5\left[1 - \frac{R}{R_0+R} + \frac{1}{2\pi}\sin\left(\frac{2\pi R}{R_0+R}\right)\right]^{-1} ns \qquad (1)$$

Where R_0 = 0.1656 nm is the empirically derived electron layer thickness.[17] If it is assumed that the free volume holes are spherical, then average free volume hole size, $< v_h > = \frac{4}{3}\pi R^3$.

Each PALS spectrum was collected for 1 hour to get at least 1 million incidences using Ortec Positron Lifetime System (Advanced Measurement Technology, Oak Ridge, TN). For each sample, seven spectrums were collected at ambient conditions (i.e., 23 °C and 45% RH). Spectrums were fit and o-Ps lifetimes τ_3 were obtained using PATFIT-88 software to obtain $<v_h>$ values.[18]

Oxygen permeation of the networks were studied using custom-built constant volume variable pressure (CVVP) instrument described elsewhere by our group.[19] Networks were degassed for at least 12 hours prior to permeation experiments. In the upstream oxygen gas was purged at a pressure of ~3 atm. Increase in pressure in the downstream was recorded as a function of time. Oxygen permeability *P* of the networks were calculated from the steady state slope of downstream pressure vs. time (*dp/dt*) using equation 2.

$$P = \frac{V_d l}{pART}\left(\frac{dp}{dt}\right) \qquad (2)$$

Where, V_d is the downstream volume, *l* is the film thickness, *p* is the applied upstream pressure, *A* is the area under test, *R* is the universal gas constant, and *T* is temperature. The extrapolation of steady state slope to x-axis gives the time lag values (t_L), from which

the oxygen diffusivity of the networks were calculated using equation 3. Oxygen solubility *S* can be calculated from $P = D \times S$.

$$D = \frac{l^2}{6t_L} \qquad (3)$$

Water vapor permeability of the networks was measured using desiccant and wet cup test methods as described by ASTM E 96-95. In this method an open mouth cup containing desiccant or water was covered by the test sample. The edges of the sample film were sealed to the edges of the cup. The assembly was then placed in a 57% relative humidity chamber, where the 57% relative humidity was controlled by having saturated sodium bromide solution. The mass of the cup test assembly was then recorded at periodic intervals, from which the water vapor transmission rate (WVTR) was calculated as follows.

$$WVTR = \frac{change\ in\ mass\ of\ the\ cup}{time \times A} \qquad (4)$$

Where, *A* is the cup mouth area. The sample was allowed to equilibrate for one day, after which the mass readings were taken at different time intervals for over a period of 10 days. Change in mass of the cup assembly showed linear trend, when it was plotted as a function of time, and from that slope, *change in mass of the cup/time* was obtained. Water vapor permeability (WVP) was then calculated as follows:

$$WVP = WVTR\left(\frac{l}{\Delta p}\right) \qquad (5)$$

Where, *l* is the sample thickness and *∆p* is the water vapor pressure difference across the film, which can be calculated based on the relative humidity difference across the film.

3.4 Results and discussion

^{1}H NMR was used to confirm the completion of the reaction (step 1) shown in Figure 3.2. Figure 3.3(a) shows the ^{1}H NMR spectra of unreacted acrylate which shows the acrylate double bond shifts at 6 ppm. Following the thio-Michael reaction, the modified monomers (i.e., 4T-fX) were analyzed using ^{1}H NMR and Figure 3.3(a) shows the disappearance of acrylate peaks which confirmed that the perfluorinated thiol monomers were produced.

Figure 3.3(b) and (c) shows the thiol and ene conversions of f2 and f10 networks respectively. It can be seen that the perfluorination of thiol monomers did not impact the network formation. UV exposure resulted in >90% conversion within few seconds of irradiation, demonstrating that perfluorination and long perfluorinated dangling moieties did not impact the fast reaction kinetics of thiol-ene chemistry. These network conversion results were consistent with the previous results published by our lab on alkylated thiol-ene networks.[16]

Even the network (f10) containing fluorine content as high as 27% (Table 3.1), was a clear film, i.e, no visible phase separation was seen. Previously, work on acrylic networks showed that when more than 0.8% (w/w) perfluorinated monomers were used, the resulting films were opaque because of phase separation of perfluorinated acrylates.[20] Whereas in the present study, perfluorinated moieties are covalently bonded (or locked) to the thiol monomer (i.e., 4T) post thio-Michael reaction. During the film formation (or curing), the fast reaction kinetics[11-12] of thiol-ene chemistry (Figure 3.3(b) and (c)) prevents the phase separation of perfluorianted moieties, and therefore the perfluorinated moieties are locked in to the network, and hence homogeneous networks were obtained

even at a high fluorine content of 27 wt%. Figure 3.2(c) shows the schematic of perfluorinated networks produced in this series.

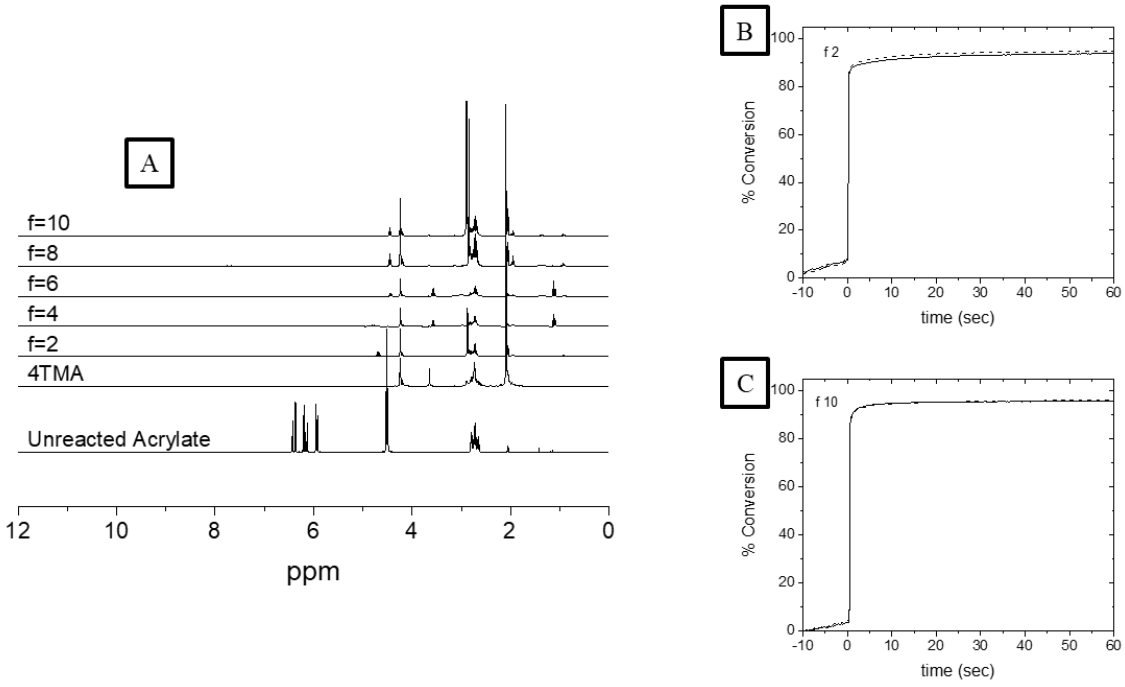

Figure 3.3 (a) NMR spectra of unreacted acrylate (bottom spectrum) and 4T modified with acrylates (top 5 and the number indicates the type of perfluorinated acrylate). (b) Thiol and ene conversion of 4T-f2 and TTT reaction obtained from real time FTIR analysis. (c) Thiol and ene conversion of 4T-f10 and TTT. Dashed lines represent thiol conversion and solid lines indicate ene conversion in figures b and c.

Figure 3.4 compares the schematic of perfluorinated networks with the alkylated networks that were reported by our group previously.[16] The network architecture is similar except for the alkylated dangling moieties, the present networks consist of perfluorinated dangling moieties.

Figure 3.5(a) and Table 3.1 compares the T_g of the perfluorinated networks. Henceforth, network properties are mainly plotted as a function of the length of the dangling moiety. For e.g. 2 is the count of carbon atoms (count does not include the carbon atoms in the acrylate group) in the f2 dangling acrylate, 4 for f4, and 6 for f6 and

so on. The length of the dangling moiety did not affect the T_g of the networks, and therefore it can be concluded that T_g was dictated by the network scaffold. Compared to the alkylated networks, perfluorinated networks' T_gs were higher by 5 °C or greater (Figure 3.5(a)). This is probably because perfluorinated dangling moieties pose more restriction to the mobility of the backbone than the alkylated networks.

Figure 3.5(b) compares the storage modulus of perfluorinated networks obtained from DMA analysis. There was no significant difference in the rubbery modulus (i.e., Storage modulus at T_g + 40 °C) of the networks. This shows that the presence or length of dangling moiety did not influence the cross-link density. Because rubbery modulus is a measure of cross-link density of the networks. Also, the rubbery modulus of perfluorinated networks were comparable to the rubbery modulus of alkylated networks[16]. The presence of single glass transitions (Figure 3.5 (b) and (c)) further indicates that perfluorination of thiol-ene networks did not result in any phase separation.

Figure 3.6 shows the oxygen transport properties of perfluorinated networks compared with alkylated networks. Increasing the size of perfluorinated dangling moiety led to an exponential increase in oxygen permeability of the networks (Figure 3.6(a) and Table 3.2). The network containing longest perfluorinated dangling chains (f10) showed oxygen permeability value which was two orders of magnitude greater than that of the unmodified network (4T-TTT). Perfluorination of the networks yielded much greater improvements in oxygen permeability than alkylation. For e.g. when dangling chain length was 10, the perfluorinated network (f10) showed oxygen permeability value which was an order of magnitude greater than thiol-ene network having alkylated dangling moiety of the same length (Figure 3.6(a)). In order to get a deeper understanding of the

effect of dangling moieties on oxygen transport, oxygen permeability values were decoupled to obtain oxygen diffusivity and oxygen solubility values as outlined in the experimental section.

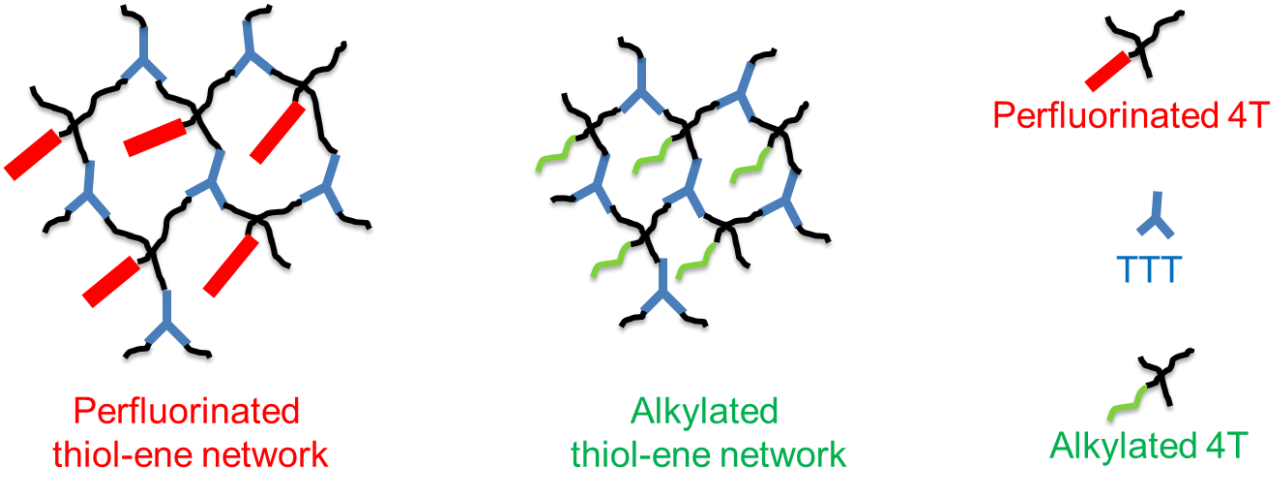

Figure 3.4 Schematic of perfluorinated and alkylated thiol-ene networks

Figure 3.6(b) shows that the exponential increase in oxygen permeability of the networks can be attributed mainly to the oxygen diffusivity, i.e., oxygen diffusivity (of f10) also showed about two orders of magnitude increase compared to the unmodified network. Increasing the length of perfluorinated moiety also caused slight increases in the oxygen solubility of the networks. When compared to alkylated networks, the length of the dangling chain had a much more pronounced effect on both oxygen diffusivity and solubility. Transport properties are often correlated to the free volume in the material, and hence we compared the average free volume hole size $<v_h>$ of the networks, obtained from PALS analysis, to oxygen diffusivity of the networks.

Figure 3.7(a) and Table 3.2 shows that $<v_h>$, of the networks, increases as a function of the length of the perfluorinated dangling moiety. Perfluorinated network f10 showed a $<v_h>$ value four times greater than that of the unmodified network. Whereas,

alkylation with 16 chain length dangling moieties only resulted in 100% increase in $<v_h>$.[16] Therefore, the enormous improvements in oxygen transport properties of perflourinated networks, as expected, is because of the high amounts of free volume in them.

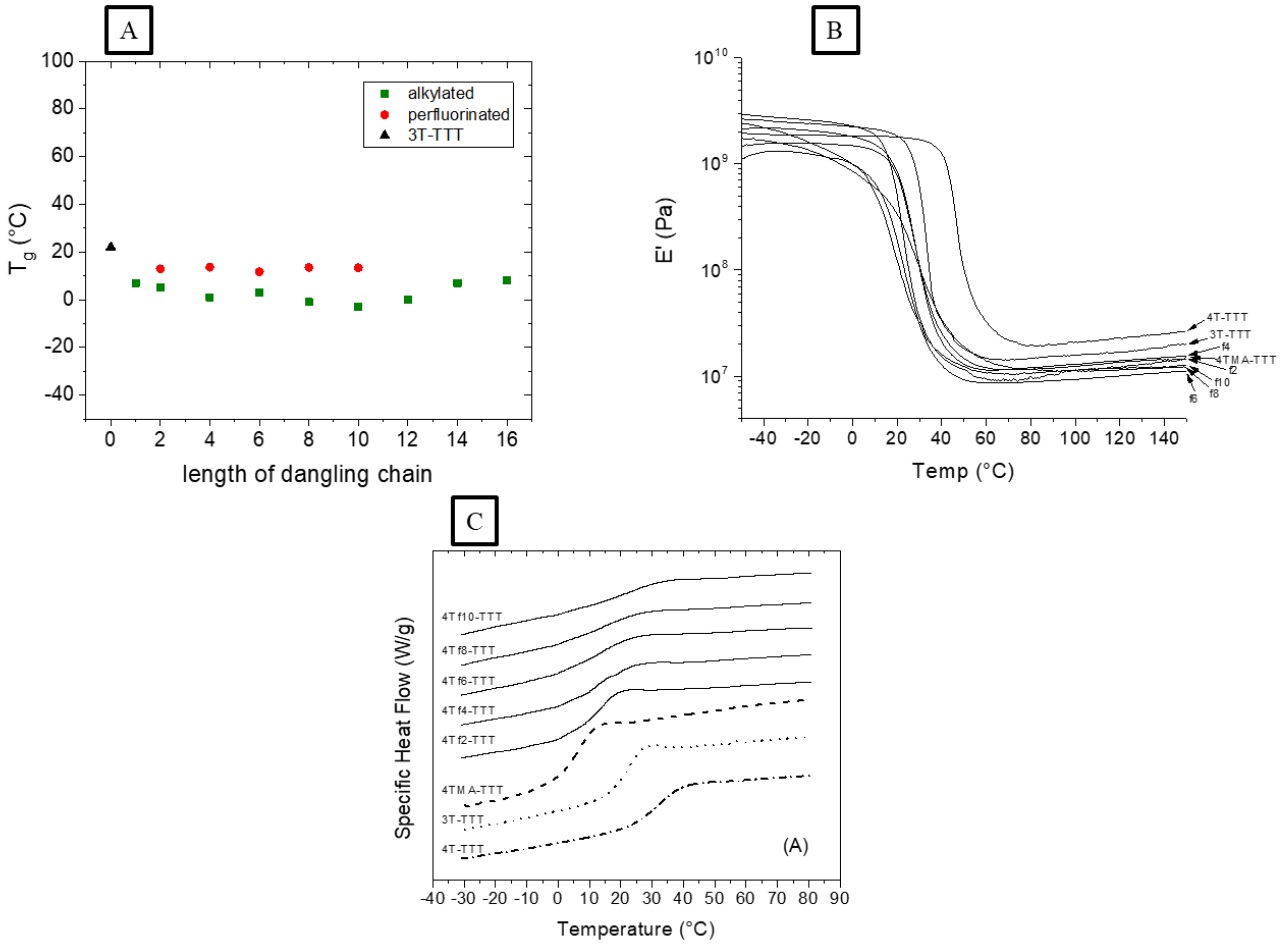

Figure 3.5 (a) Glass transition temperatures (DSC) of perfluorinated, alkylated[16] networks plotted as a function of length of dangling chain. (b) Storage modulus of networks obtained from DMA analysis. (c) Specific heat flow vs. temperature of networks obtained from DSC experiments.

Some of the factors which can increase free volume in elastomers are, increasing the concentration of chain ends[21-24] and decreasing cross-link density[14, 21, 25-27]. Whereas in this series, the number of chain ends per cross-link junction is the same (Figure 3.2(c)),

though the length of the dangling moiety is changed. Also, DMA analysis showed that the cross-link density, as expected, remained constant across the series. Therefore, it can be said that perfluorinated dangling moiety and its length were only responsible for the increase in free volume and oxygen transport properties.

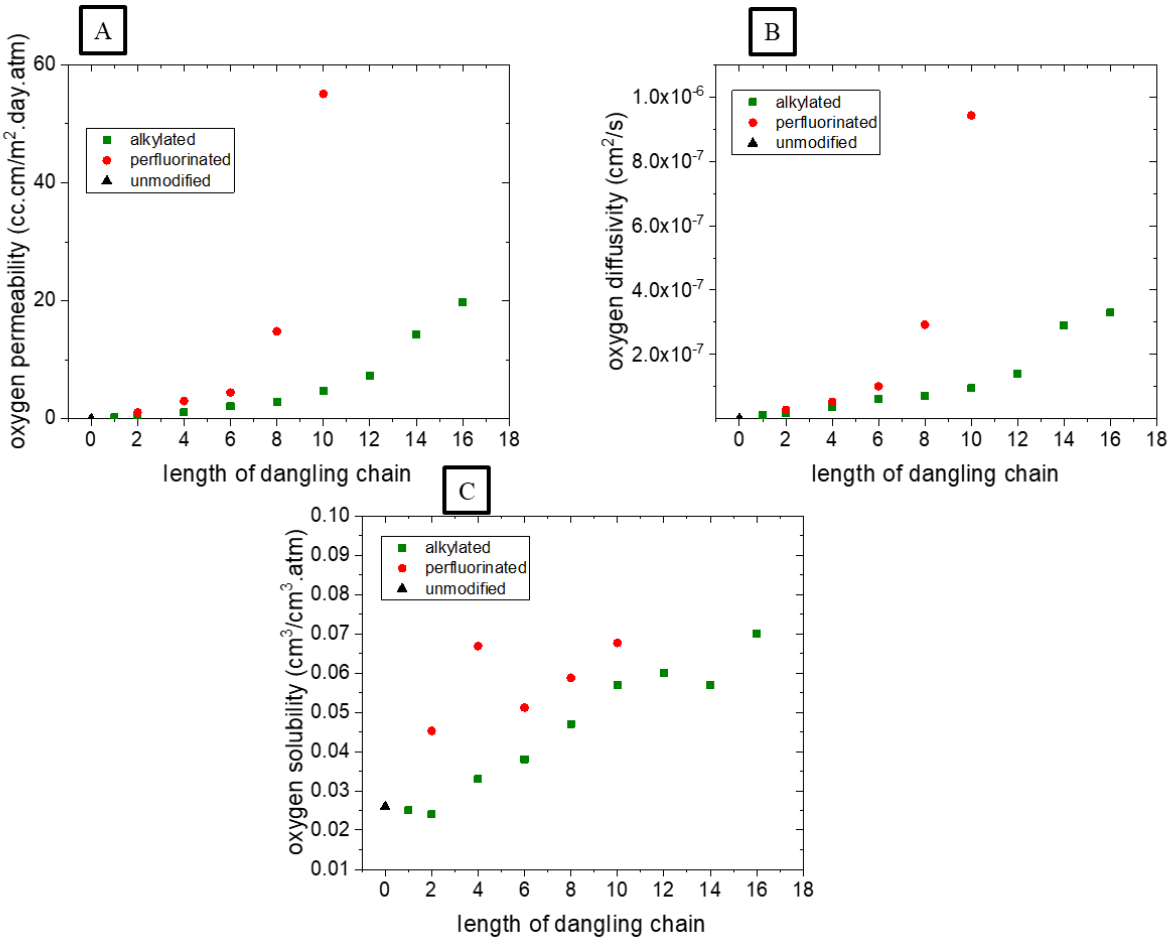

Figure 3.6 (a) Oxygen permeability, (b) oxygen diffusivity, and (c) oxygen solubility of perfluorinated and alkylated[16] networks plotted as a function of length of dangling chain.

Table 3.2 Oxygen transport parameters and free volume hole size $<v_h>$ of networks

Sample	Oxygen tranport parameters			$<v_h>$ (Å^3)
	Permeability (cc.cm/m^2.day.atm)	Diffusivity (cm^2/s)	Solubility (cc/cc.atm)	
4T-TTT	0.04	1.7E-09	0.03	63
f2	1.1	2.8E-08	0.05	96

f4	3	5.3E-08	0.07	164
f6	4.5	1.0E-07	0.05	210
f8	14.8	2.9E-07	0.06	265
f10	55	9.4E-07	0.07	276

In the previous work on alkylated networks, it was hypothesized that rigid and hydrophobic alkylated dangling moieties reduce the intermolecular interactions that are present in the backbone, and these moieties act as spacers resulting in free volume increase.[16] Similar hypothesis have previously been reported for linear polymers.[28-29] Also, we recently reported on hybrid epoxy-amine networks where free volume was significantly increased by hydrophobic POSS moieties covalently bonded to epoxy amine networks.[30] Whereas, the effect from perfluorinated moieties is much more pronounced than all the aforementioned cases because of the more rigid and more hydrophobic nature of perfluorinated moieties. It can be hypothesized that, as the size of the perfluorinated dangling moiety is increased, the sizes of free volume pockets around it increases, because of the repulsive forces between hydrophobic perfluorinated moieties and polar backbone. Previously, Guizard et al showed improvements in permeation properties of silicone elastomers with the incorporation of perfluorinated moieties. But in their chemistry, along with increasing perfluorination concentration, they also simultaneously decreased cross-link density, therefore the effect of perfluorination alone on free volume cannot be understood.[31] Whereas, in our study, as we discussed earlier, cross-link density and chain end concentration, i.e., other factors that could also influence free volume, were constant. Therefore, it can be said that enormous increments of free volume were only because of the incorporation of perfluorinated moieties.

Gas diffusivity *D* of the material can be quantitatively related to free volume by Cohen Turnbull relationship,[23, 32-37] which can be written as shown in equation 6.

$$D = D_{vh} e^{\left(\frac{-B_{vh}}{<v_h>}\right)} \qquad (6)$$

Where D_{vh} and B_{vh} are parameters which depend on penetrant gas.

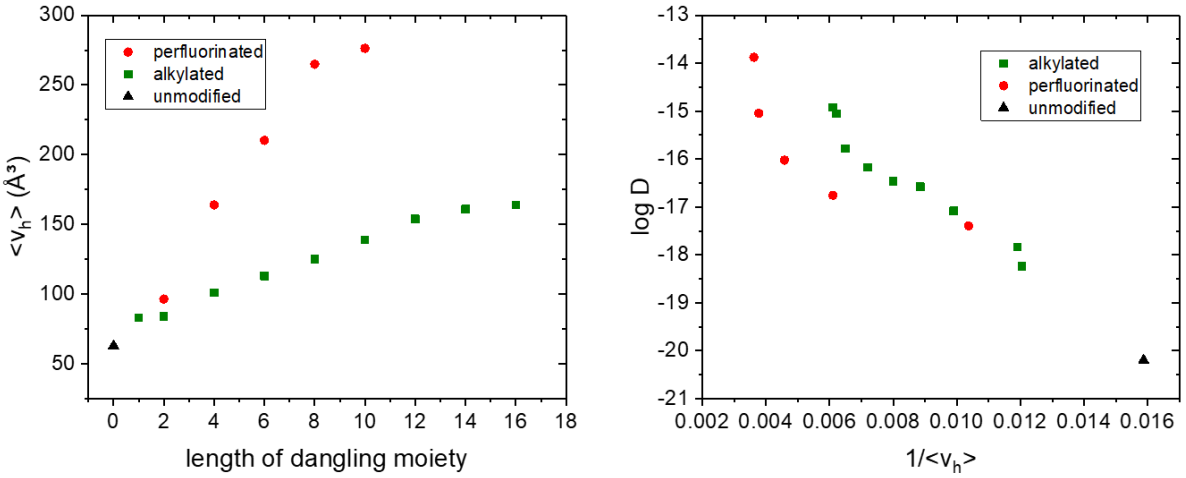

Figure 3.7 (a) Free volume hole size $<v_h>$ of perfluornated networks compared with alkylated[16] networks. (b) Logarithm of oxygen gas diffusivity of perfluorinated and alkylated[16] networks plotted as function of $1/<v_h>$.

Logarithm of gas diffusivity should change linearly as a function of $1/<v_h>$ according to equation 6, and it is well known that elastomers do obey this relationship.[23] Figure 3.7(b) shows that both perfluorinated and alkylated networks show deviation from Cohen Turnbull relationship, but the deviation is more pronounced in perfluorinated networks. At lower free volume (i.e. higher $1/<v_h>$), the networks have lower gas diffusivities than what their $<v_h>$ value suggests, i.e. they are showing negative deviation from Cohen Turnbull model. Again, this deviation is more pronounced for perfluorinated networks as can be seen from Figure 3.7(b). During oxygen transport through a material,

the oxygen molecules occupy free volume holes and jump or hop between free volume holes towards the region of lower oxygen partial pressure. In the case of elastomers (T_g < room temperature), the higher segmental motions of the chains make the free volume holes dynamic and are redistributed, which aids in transport.[34] Whereas, in the case of glasses (T_g > room temperature), the free volumes holes are frozen-in or static, and the diffusion happens by penetrant molecules hoping between different static free volume holes due to thermal rearrangement of chains aided by sub-T_g relaxations.[34, 38] Therefore, Haraya observed that when the logarithm of gas diffusivity is plotted as a function of the inverse of free volume, rubbery polymers show a larger slope when compared to glassy polymers, i.e. changes in free volume have a more significant effect in elastomers than in glasses.[34] It can be assumed that, in case of these perfluorinated or alkylated networks, the free volume pockets around these hydrophobic moieties are static in nature, i.e., though these networks are elastomeric, the free volume pockets around hydrophobic moieties cannot be redistributed through the network. Hence, the oxygen diffusivity of these networks (up to dangling chain length of 6, i.e., lower two data points for perfluorinated and lower four data points for alkylated in Figure 3.7(b)) show lower values than what they are supposed to give according to Cohen Turnbull equation. Tanaka et al observed this under prediction or downward deviation from Cohen Turnbull model in glassy polymers.[39-40]

After dangling chain length of 6, there is an upswing in oxygen diffusivity, (i.e., third data point from below for perfluorinated and fourth data point from below for alkylated). This upswing can be assumed as a transition where the free volume pockets start to percolate. Once the free volume pockets started to percolate, oxygen diffusivity

values started to increase tremendously when free volume was increased (by changing the length of dangling moiety). This can explain the deviation from the Cohen Turnbull model for top three and top four data points for perfluorinated and alkylated networks respectively. Percolation of free volume pockets has been previously used to explain the tremendous increase in diffusivity values seen in highly glassy polymers.[41-43] In order to understand this free volume percolation phenomenon, an idealized lattice-like two dimensional model was created assuming all trans configurations as shown in Figure 3.8. The distance between alternating junction points containing perfluorinated dangling moiety is compared to the length of the perfluorinated dangling moiety. For networks f2 and f4 the length of perfluorinated moieties are way smaller than the distance between the alternating junction points. Therefore, the free volume pockets around perfluorinated dangling moieties which are static cannot aid in diffusion significantly. For network f6, the length of dangling moiety approaches the distance between alternating junction points if an ideal 2D lattice like model is assumed. This indicates that beyond f6, the perfluorinated dangling moieties will be close enough for the free volume pockets around them to start merging or percolating, which results in higher than expected oxygen diffusivity values for networks f6, f8 and f10.

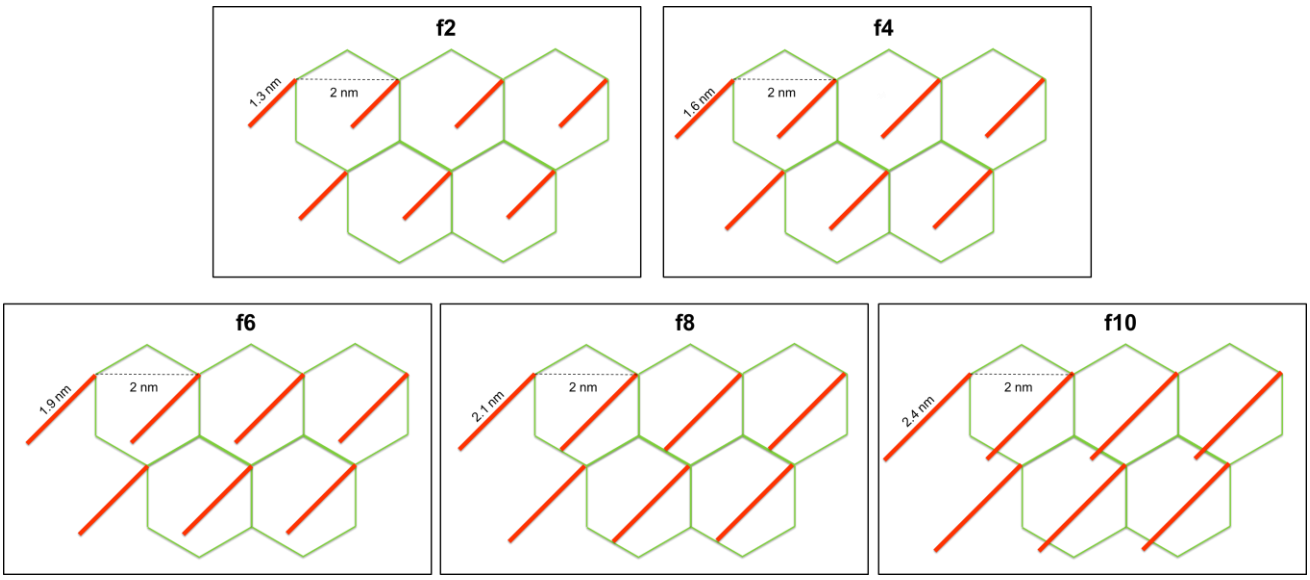

Figure 3.8 Idealized two-dimensional lattice like model of the perfluorinated thiol-ene networks. The distance between alternating junctions containing perfluorinated moiety is compared to the length of perfluorinated dangling moieties.

Interestingly, the length of dangling moiety did not have any effect on water vapor permeability (Figure 3.9(a)). This can be explained by the compromise between increases in water vapor diffusivity compensated by decreases in water vapor solubility. As discussed earlier, increasing the length of perfluorinated dangling moiety led to increases in free volume, and Figure 3.9(b) shows improvements in water vapor diffusion rates (i.e, the initial part of the curve) as a function of the length of dangling moiety because of the enhancements in free volume. But increasing the amount of hydrophobic perfluorinated moieties led to decreases in the amount of water sorbed by the networks, i.e. water vapor solubility of the networks decreased as a function of the length of the dangling moiety. Thus, the water vapor diffusivity increase was compensated by water vapor solubility decrease, and therefore their product, i.e., water vapor permeability remained constant across the series of networks. This increase in hydrophobicity or reduction in water vapor solubility is further explained by the gradual increase in water

contact angle as a function of the length of perfluorinated dangling moiety incorporated into the network (Figure 3.9(c)). But most importantly, these hydrophobic networks (water contact angle > 100°) can still let water vapor permeate through them at high rates. Water vapor permeability of these hydrophobic networks are in the range of 4000 Barrers, i.e., these perfluorinated elastomers are breathable but would not swell when exposed to water.

3.5 Conclusions

Novel perfluorinated thiol-ene elastomers were synthesized using easy 2-step UV synthesis. Fluorine content and the network properties were altered by changing the length of perfluorinated dangling moieties within these networks. The length of dangling moieties did not have any effect on the T_g of the networks, and T_g was mainly controlled by the network scaffold. The fast reaction kinetics of thiol-ene chemistry locked in the perfluorinated moieties within the network scaffold and prevented phase separation, and the repulsive interaction between the hydrophobic perfluorinated moieties and polar backbone resulted in creation of huge free volume pockets within the networks, and PALS analysis showed that the sizes of these free volume holes increased with increasing length of perfluorinated dangling moiety. As expected, perfluorinated dangling moieties created more free volume in the networks than the alkylated dangling moieties. Because of this free volume effect, the networks showed an exponential increase in oxygen permeability values as a function of the length of perfluorinated dangling chain. Oxygen diffusivity values of the networks did not obey Cohen Turnbull model. Static free volume and percolation of free volume as hole sizes increased, was used to explain the deviation, and a 2D lattice like model was used to explain this behavior. Perfluorinated chain length

did not show any effect on water vapor transport properties, because the increase in diffusivity (due to free volume) was compensated by the decrease in solubility, which was explained using water sorption analysis.

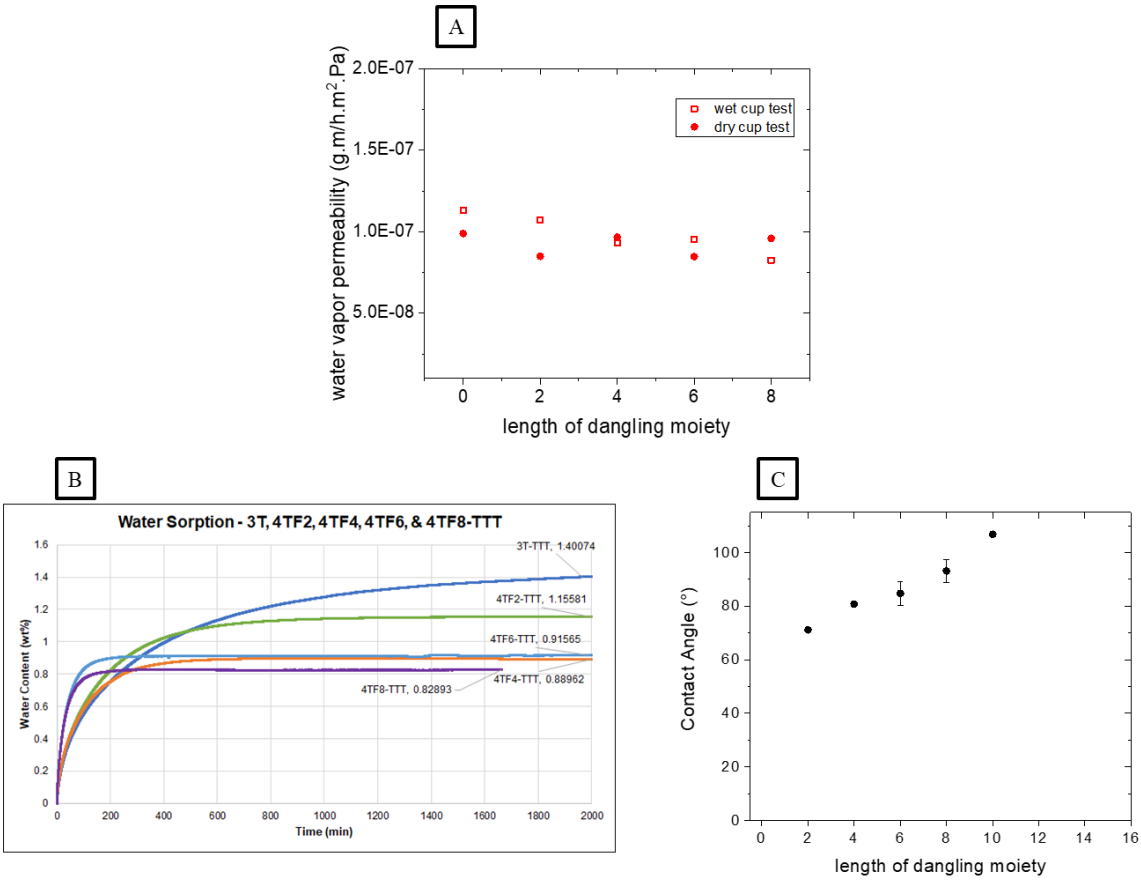

Figure 3.9 (a) Water vapor permeability of the perfluorinated networks plotted as a function of length of dangling moiety. (b) Water sorption characteristics of the networks obtained from DVS analysis. (c) Water contact angle of the networks plotted vs. length of dangling moiety

3.6 References

1. Uschold, R. E., Fluoroelastomers: Today's Technology and Tomorrow's Polymers. *Polymer Journal* **1985,** *17*, 253.

2. Améduri, B.; Boutevin, B.; Kostov, G., Fluoroelastomers: synthesis, properties and applications. *Progress in Polymer Science* **2001,** *26* (1), 105-187.

3. Smart, B.; Patai, S.; Rapporport, Z., The Chemistry of Functional Groups, Suppl. D. *The Chemistry of Halides, Pseudohalides and Azides.(Eds.: Patai, S* **1983**, 603-655.

4. Logothetis, A. L., Chemistry of fluorocarbon elastomers. *Progress in Polymer Science* **1989,** *14* (2), 251-296.

5. Sangermano, M.; Bongiovanni, R.; Malucelli, G.; Priola, A.; Pollicino, A.; Recca, A., Fluorinated epoxides as surface modifying agents of UV-curable systems. *Journal of Applied Polymer Science* **2003,** *89* (6), 1524-1529.

6. Bongiovanni, R.; Malucelli, G.; Pollicino, A.; Priola, A., Properties of films obtained by UV-curing 4,4'-hexafluoroisopropylidenediphenoldihydroxyethylether diacrylate and its mixtures with the hydrogenated homologue. *Journal of Applied Polymer Science* **1997,** *63* (8), 979-983.

7. Hwang, H.-D.; Kim, H.-J., UV-curable low surface energy fluorinated polycarbonate-based polyurethane dispersion. *Journal of Colloid and Interface Science* **2011,** *362* (2), 274-284.

8. Priola, A.; Bongiovanni, R.; Malucelli, G.; Pollicino, A.; Tonelli, C.; Simeone, G., UV-curable systems containing perfluoropolyether structures: Synthesis and characterisation. *Macromolecular Chemistry and Physics* **1997,** *198* (6), 1893-1907.

9. Goetz, J.; Nazarenko, S., Thermotropic, side-chain ordered polymeric coatings: gas permeability switching via a thermal stimulus. *Journal of Coatings Technology and Research* **2014,** *11* (2), 123-129.

10. Yao, X.; Dunn, S. S.; Kim, P.; Duffy, M.; Alvarenga, J.; Aizenberg, J., Fluorogel Elastomers with Tunable Transparency, Elasticity, Shape-Memory, and Antifouling Properties. *Angewandte Chemie International Edition* **2014,** *53* (17), 4418-4422.

11. Hoyle, C. E.; Bowman, C. N., Thiol–Ene Click Chemistry. *Angewandte Chemie International Edition* **2010,** *49* (9), 1540-1573.

12. Hoyle, C. E.; Lee, T. Y.; Roper, T., Thiol–enes: Chemistry of the past with promise for the future. *Journal of Polymer Science Part A: Polymer Chemistry* **2004,** *42* (21), 5301-5338.

13. Hoyle, C. E.; Lowe, A. B.; Bowman, C. N., Thiol-click chemistry: a multifaceted toolbox for small molecule and polymer synthesis. *Chemical Society Reviews* **2010,** *39* (4), 1355-1387.

14. Kwisnek, L.; Goetz, J.; Meyers, K. P.; Heinz, S. R.; Wiggins, J. S.; Nazarenko, S., PEG Containing Thiol–Ene Network Membranes for CO2 Separation: Effect of Cross-Linking on Thermal, Mechanical, and Gas Transport Properties. *Macromolecules* **2014,** *47* (10), 3243-3253.

15. Kwisnek, L.; Nazarenko, S.; Hoyle, C. E., Oxygen Transport Properties of Thiol−Ene Networks. *Macromolecules* **2009,** *42* (18), 7031-7041.

16. Kwisnek, L.; Kaushik, M.; Hoyle, C. E.; Nazarenko, S., Free Volume, Transport, and Physical Properties of n-Alkyl Derivatized Thiol−Ene Networks: Chain Length Effect. *Macromolecules* **2010,** *43* (8), 3859-3867.

17. Tao, S. J., Positronium Annihilation in Molecular Substances. *The Journal of Chemical Physics* **1972,** *56* (11), 5499-5510.

18. Kirkegaard, P.; Eldrup, M.; Mogensen, O. E.; Pedersen, N. J., Program system for analysing positron lifetime spectra and angular correlation curves. *Computer Physics Communications* **1981,** *23* (3), 307-335.

19. Kwisnek, L.; Heinz, S.; Wiggins, J. S.; Nazarenko, S., Multifunctional thiols as additives in UV-cured PEG-diacrylate membranes for CO2 separation. *Journal of Membrane Science* **2011,** *369* (1–2), 429-436.

20. Ameduri, B.; Bongiovanni, R.; Lombardi, V.; Pollicino, A.; Priola, A.; Recca, A., Effect of the structural parameters of a series of fluoromonoacrylates on the surface properties of cured films. *Journal of Polymer Science Part A: Polymer Chemistry* **2001,** *39* (24), 4227-4235.

21. Fox, T. G.; Loshaek, S., Influence of molecular weight and degree of crosslinking on the specific volume and glass temperature of polymers. *Journal of Polymer Science* **1955,** *15* (80), 371-390.

22. Lin, H.; Kai, T.; Freeman, B. D.; Kalakkunnath, S.; Kalika, D. S., The Effect of Cross-Linking on Gas Permeability in Cross-Linked Poly(Ethylene Glycol Diacrylate). *Macromolecules* **2005,** *38* (20), 8381-8393.

23. Lin, H.; Wagner, E. V.; Swinnea, J. S.; Freeman, B. D.; Pas, S. J.; Hill, A. J.; Kalakkunnath, S.; Kalika, D. S., Transport and structural characteristics of crosslinked poly(ethylene oxide) rubbers. *Journal of Membrane Science* **2006,** *276* (1–2), 145-161.

24. Raharjo, R. D.; Lin, H.; Sanders, D. F.; Freeman, B. D.; Kalakkunnath, S.; Kalika, D. S., Relation between network structure and gas transport in crosslinked

poly(propylene glycol diacrylate). *Journal of Membrane Science* **2006,** *283* (1–2), 253-265.

25. Morgan, D. R.; Stejskal, E. O.; Andrady, A. L., 129Xe NMR Investigation of the Free Volume in Dendritic and Cross-Linked Polymers. *Macromolecules* **1999,** *32* (6), 1897-1903.

26. Consolati, G.; Kansy, J.; Pegoraro, M.; Quasso, F.; Zanderighi, L., Positron annihilation study of free volume in cross-linked amorphous polyurethanes through the glass transition temperature. *Polymer* **1998,** *39* (15), 3491-3498.

27. Dlubek, G.; Stejny, J.; Alam, M. A., Effect of Cross-Linking on the Free-Volume Properties of Diethylene Glycol Bis(allyl carbonate) Polymer Networks: A Positron Annihilation Lifetime Study. *Macromolecules* **1998,** *31* (14), 4574-4580.

28. Qiao, X.; Wang, X.; Mo, Z., The effects of different alkyl substitution on the structures and properties of poly(3-alkylthiophenes). *Synthetic Metals* **2001,** *118* (1), 89-95.

29. Hsu, W. P.; Levon, K.; Ho, K. S.; Myerson, A. S.; Kwei, T. K., Side-chain order in poly(3-alkylthiophenes). *Macromolecules* **1993,** *26* (6), 1318-1323.

30. Sharma, A. K.; Sloan, R.; Ramakrishnan, R.; Nazarenko, S. I.; Wiggins, J. S., Structure-property relationships in epoxy hybrid networks based on high mass fraction pendant POSS incorporated at molecular level. *Polymer* **2018,** *139*, 201-212.

31. Guizard, C.; Boutevin, B.; Guida, F.; Ratsimihety, A.; Amblard, P.; Lasserre, J. C.; Naiglin, S., VOC vapour transport properties of new membranes based on cross-linked fluorinated elastomers. *Separation and Purification Technology* **2001,** *22-23*, 23-30.

32. Cohen, M. H.; Turnbull, D., Molecular Transport in Liquids and Glasses. *The Journal of Chemical Physics* **1959,** *31* (5), 1164-1169.

33. Park, J. Y.; Paul, D. R., Correlation and prediction of gas permeability in glassy polymer membrane materials via a modified free volume based group contribution method. *Journal of Membrane Science* **1997,** *125* (1), 23-39.

34. Haraya, K.; Hwang, S.-T., Permeation of oxygen, argon and nitrogen through polymer membranes. *Journal of Membrane Science* **1992,** *71* (1), 13-27.

35. Tanaka, K.; Okano, M.; Toshino, H.; Kita, H.; Okamoto, K.-I., Effect of methyl substituents on permeability and permselectivity of gases in polyimides prepared from methyl-substituted phenylenediamines. *Journal of Polymer Science Part B: Polymer Physics* **1992,** *30* (8), 907-914.

36. Nagel, C.; Günther-Schade, K.; Fritsch, D.; Strunskus, T.; Faupel, F., Free Volume and Transport Properties in Highly Selective Polymer Membranes. *Macromolecules* **2002,** *35* (6), 2071-2077.

37. Sanders, D. F.; Smith, Z. P.; Guo, R.; Robeson, L. M.; McGrath, J. E.; Paul, D. R.; Freeman, B. D., Energy-efficient polymeric gas separation membranes for a sustainable future: A review. *Polymer* **2013,** *54* (18), 4729-4761.

38. Hiltner, A.; Liu, R.; Hu, Y.; Baer, E., Oxygen transport as a solid-state structure probe for polymeric materials: A review. *Journal of Polymer Science Part B: Polymer Physics* **2005,** *43* (9), 1047-1063.

39. Tanaka, K.; Kawai, T.; Kita, H.; Okamoto, K.-i.; Ito, Y., Correlation between Gas Diffusion Coefficient and Positron Annihilation Lifetime in Polymers with Rigid Polymer Chains. *Macromolecules* **2000,** *33* (15), 5513-5517.

40. Tanaka, K.; Kita, H.; Okano, M.; Okamoto, K.-i., Permeability and permselectivity of gases in fluorinated and non-fluorinated polyimides. *Polymer* **1992,** *33* (3), 585-592.

41. Thornton, A. W.; Nairn, K. M.; Hill, A. J.; Hill, J. M., New relation between diffusion and free volume: I. Predicting gas diffusion. *Journal of Membrane Science* **2009,** *338* (1), 29-37.

42. Greenfield, M. L.; Theodorou, D. N., Geometric analysis of diffusion pathways in glassy and melt atactic polypropylene. *Macromolecules* **1993,** *26* (20), 5461-5472.

43. Hedstrom, J. A.; Toney, M. F.; Huang, E.; Kim, H.-C.; Volksen, W.; Magbitang, T.; Miller, R. D., Pore morphologies in disordered nanoporous thin films. *Langmuir* **2004,** *20* (5), 1535-1538.

CHAPTER IV – PREPARATION OF HYBRID THIOL-ENE ELASTOMERIC NETWORKS CONTAINING PEG AND PERFLUORINATED MOIETIES

4.1 Abstract

Thiol-ene networks containing perfluorinated and poly(ethylene glycol) (PEG) dangling moieties were synthesized using a 2-step synthetic procedure. Modified trifunctional thiol crosslinkers (4T-PEG, 4T-f6) containing PEG and perfluorinated dangling moieties respectively were prepared using Thio-Michael addition reaction, where a four-functional thiol (4T) was reacted with a functional acrylate (PEG and perfluorinated). Hybrid networks were then prepared by varying the ratio of 4T-PEG:4T-f6 and UV crosslinking them with a tri-functional ene (TTT), while maintaining 1:1 thiol:ene stoichiometry, which resulted in a series of networks having varying amounts of PEG and fluorine contents in them. Increasing the PEG content resulted in decreases in glass transition temperature due to the more flexible nature of PEG dangling moieties. PALS analysis showed that with increasing PEG content, the average free volume hole size within the networks decreased. This is because increasing the ratio of PEG:fluorine content resulted in a contraction of the networks brought about by increased attractive interactions. Increasing the PEG content, resulted in increases in water vapor permeability of the networks due to increases in hydrogen bonding interactions. Gas transport analysis showed that with increasing PEG content, CO_2 solubility increased because of the Lewis acid-base interactions between CO_2 and PEG moieties. Addition of PEG increased both CO_2 permeability and selectivity, over N_2, of the networks.

4.2 Introduction

Polymer membranes for gas separation is a fast-growing industry. Within that, CO_2 gas separation is one of the most targeted sectors. CO_2 separation is commercially very relevant because it is required for natural gas purification, power plant flue gas capture, hydrogen purification etc.[1-5] Presence of ether or amide groups in membranes can improve its CO_2 solubility because of the Lewis acid - Lewis base type interaction between these functional groups and CO_2.[6-8] Therefore, designing amorphous membranes containing ether or amide groups can improve CO_2 gas separation performance.[9-16] Previously, our group showed that thiol-ene chemistry can be utilized to synthesize a family of PEG-containing thiol-ene networks of varying cross-link densities. These PEG containing thiol-ene membranes showed good CO_2 gas selectivity performance.[16] Recent studies in our group have also identified the amount of PEG required in membranes for CO_2 solubility saturation. In addition to selectivity, another important performance criterion, required for membranes, is high permeability. Kwisnek et al from our group showed that using thiol-ene chemistry, networks containing long alkyl dangling moieties can be synthesized, where the fast reaction kinetics of thiol-ene chemistry[17-18] "locks-in" the incompatible moieties, thereby preventing phase separation.[19] Using a similar strategy, in the previous chapter, we discussed the synthesis and properties of thiol-ene networks containing long perfluorinated moieties. The repulsive interaction between the long perfluorinated dangling chains and the backbone resulted in networks with very high free volume hole size and permeability. In the present work, the goal was to create hybrid thiol-ene networks containing dangling PEG and perfluorinated moieties and to study

how the concentration of these moieties affects chain mobility, free volume, and transport properties.

4.3 Experimental

4.3.1 Materials

Thiol monomer pentaerythritol tetrakis(3-mercaptopropionate) (4T) was provided by Bruno Bock Thiochemicals. Ene monomer 1,3,5-Triallyl-1,3,5-triazine-2,4,6(1H,3H,5H)-trione (TTT), photoinitiator 2,2-Dimethoxy-2-phenylacetophenone (DMPA), nucleophilic catalyst di-n-butyl amine (DBA), and poly(ethylene glycol) methyl ether acrylate (PEG-Ac) were obtained from Sigma-Aldrich. 2-perfluorobutyl ethyl acrylate (f6) was obtained from Fluoryx Labs (Carson City, NV). All the chemicals were used as received. Figure 4.1 shows the chemical structures of all the aforementioned molecules.

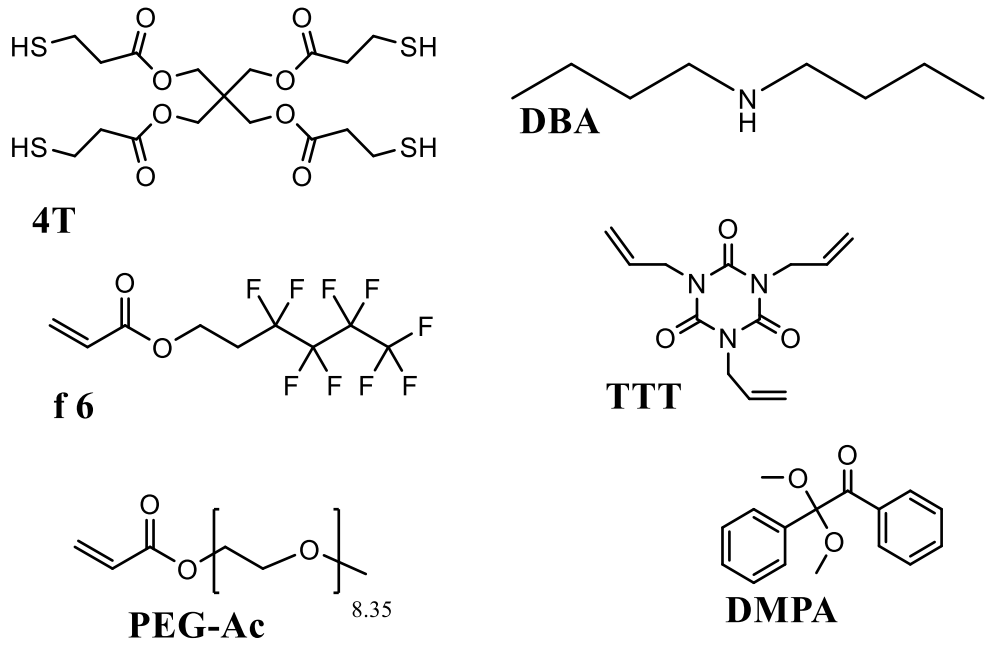

Figure 4.1 Chemical structures of perfluorinated acrylate (f6), PEG acrylate (PEG-Ac) thiol (4T), ene (TTT) monomers, photo-initiator (DMPA) and nucleophilic catalyst (DBA).

4.3.2 Synthesis of perfluorinated and PEG modified thiol monomers

4T-f6 and 4T-PEG monomers shown in Figure 4.2 were synthesized using thio-Michael reaction. The quantities of reactants are taken such that only thiol moiety of 4T in average gets reacted to the acrylate to produce a trifunctional thiol monomer containing PEG or perfluorinated dangling moiety (Figure 4.2). The synthetic procedure is explained in detail in Chapter 3. Prepared 4T-PEG modified monomer was analyzed using ^{1}H NMR to confirm the modification. The procedure of this analysis is explained in detail in Chapter 3.

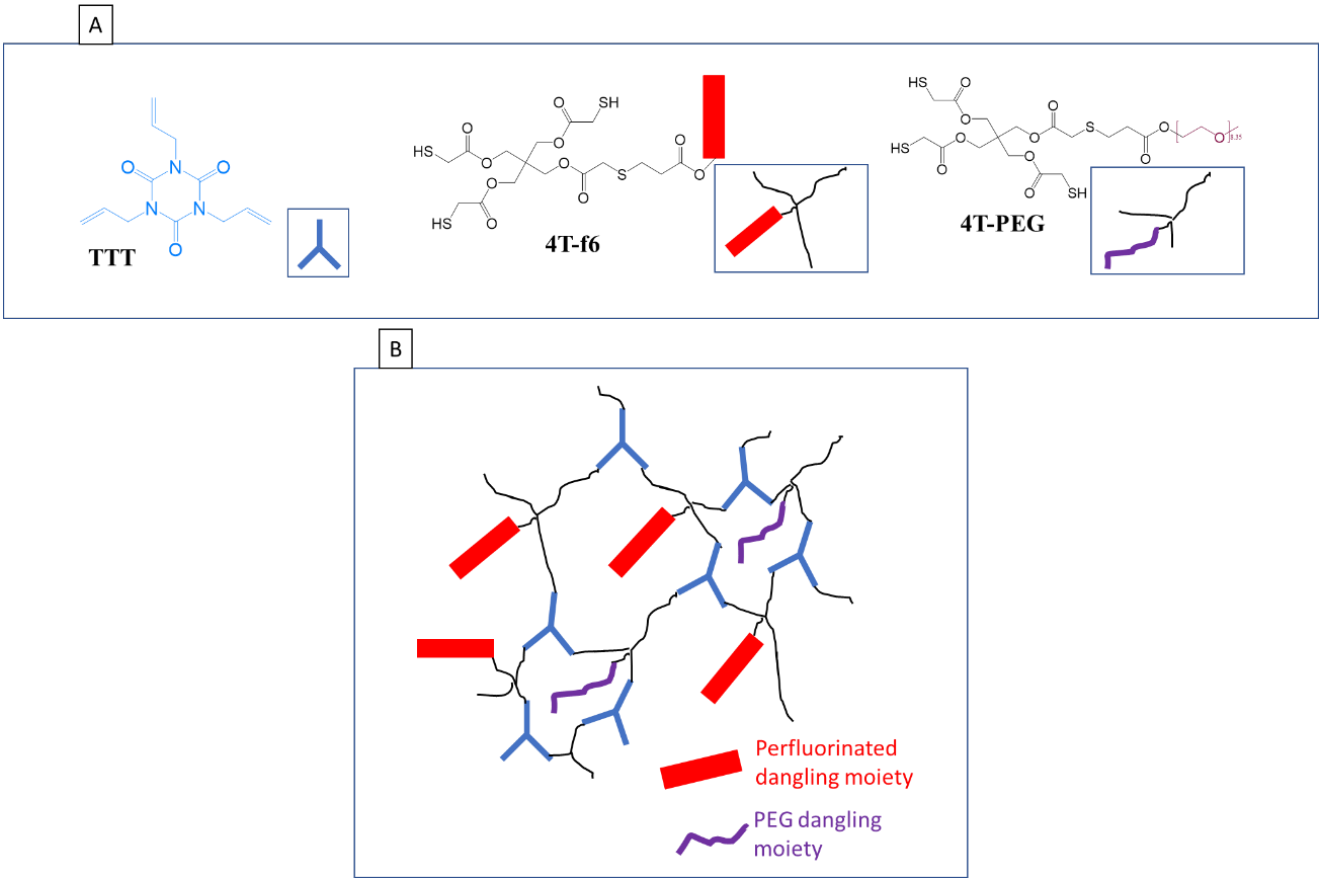

Figure 4.2 (a) Network components. (b) Schematic of a hybrid PEG and perfluorinated thiol-ene network.

4.3.3 Synthesis of Hybrid Thiol-Ene Elastomers

Appropriate amounts of 4T-f6 and 4T-PEG modified monomers were reacted with TTT while maintaining 1:1 thiol:ene stoichiometry, to obtain network films. Even though perfluorinated and PEG moiety were very different in their chemical nature, since they were covalently bonded to a common entity, i.e. 4T (Figure 4.2(a)), the modified monomers 4T-f6 and 4T-PEG readily dissolved into each other. Five networks were synthesized having varying amounts of PEG and perfluorinated contents using the synthetic procedure outlined in Chapter 3. Table 3.1 shows the list of networks synthesized and Figure 4.2(b) shows a schematic of the network.

Table 4.1 List of hybrid thiol-ene networks and their PEG and fluorine contents

Sample	PEG content (wt%)	Fluorine content (wt%)
PEG00	0	16.19
PEG08	8.44	11.76
PEG16	16.363	7.61
PEG24	23.824	3.69
PEG30	29.486	0.72

Thermal analysis of the networks was performed using a differential scanning calorimetry - TA Q2000. Heat-cool-heat program was employed, i.e., 35 °C to 100 °C at a ramp rate of 10 °C/min, 100 °C to -70°C at 5 °C/min, and -70 °C to 100 °C at 10 °C/min. TA data analysis software was used to process the data. Glass transition temperature of the networks was determined from the second heat curves.

Average free volume hole size, $<v_h>$, of the networks were measured using positron annihilation lifetime spectroscopy (PALS). Discs having a diameter of 1 cm

were punched out from the films. Discs were stacked to make the thickness of 1 mm. Positron source, 30 μCi ^{22}Na, enclosed in an Al foil was sandwiched between two stacked discs. A detailed description regarding PALS experimental procedure can be obtained from Chapter 3.

Each PALS spectrum was collected for 1 hour to get at least 1 million incidences using Ortec Positron Lifetime System (Advanced Measurement Technology, Oak Ridge, TN). For each sample, seven spectrums were collected at ambient conditions (i.e., 23 °C and 45% RH). Spectrums were fit and o-Ps lifetimes τ_3 were obtained using PATFIT-88 software to obtain $<v_h>$ values.[20]

Water vapor permeability of the networks was measured using wet cup test method as described by ASTM E 96-95. In this method, an open mouth cup containing water was covered by the test sample. The edges of the sample film were sealed to the edges of the cup. The assembly was then placed in a 57% relative humidity chamber, where the 57% relative humidity was controlled by having saturated sodium bromide solution. Further details regarding experimental procedure and analysis can be obtained from Chapter 3.

Gas permeation of the networks was studied using custom-built constant volume variable pressure (CVVP) instrument described elsewhere by our group.[15] Networks were degassed for at least 12 hours prior to permeation experiments. In the upstream, gas was purged at a pressure of ~3 atm. Increase in pressure in the downstream was recorded as a function of time. Permeability *P* of the networks were calculated from the steady-state slope of downstream pressure vs. time (*dp/dt*) using equation 2.

$$P = \frac{V_d l}{pART}\left(\frac{dp}{dt}\right) \qquad (2)$$

Where V_d is the downstream volume, l is the film thickness, p is the applied upstream pressure, A is the area under test, R is the universal gas constant, and T is temperature. The extrapolation of steady-state slope to x-axis gives the time lag values (t_L), from which the gas diffusivity of the networks was calculated using equation 3. Gas solubility S can be calculated from $P = D \times S$.

$$D = \frac{l^2}{6t_L} \qquad (3)$$

4.4 Results and discussion

4T-PEG monomer modification was confirmed by the ^{1}H NMR analysis. Figure 4.2(a) shows the disappearance of acrylate shifts at 6 ppm to confirm monomer modification.[19, 21]

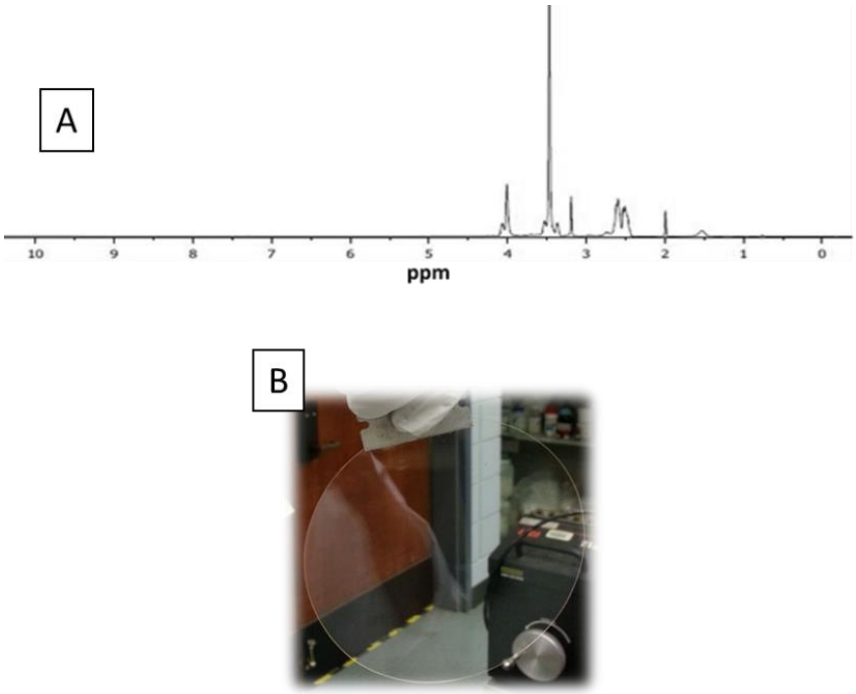

Figure 4.3 (a) ^{1}H NMR spectra of 4T-PEG modified monomer. (b) Picture of a transparent hybrid PEG and perfluorinated thiol-ene network film.

The hybrid thiol-ene networks obtained through this 2-step strategy yielded clear and transparent films and Figure 4.2(b) shows an example of a film produced through this method. This means, no visible phase separation was seen, even though two incompatible entities such as PEG and perfluorinated moieties were varied within the system. This again demonstrates the benefits of this 2-step approach and the fast reaction kinetics of thiol-ene chemistry.[18-19, 21-22] Since PEG and perfluorinated moieties are covalently bonded to the thiol monomer 4T (through the first step), during the thiol-ene curing (i.e., the second step), the fast reaction kinetics of thiol-ene chemistry prevents the phase separation, and locks-in PEG and perfluorinated dangling moieties within the network scaffold.

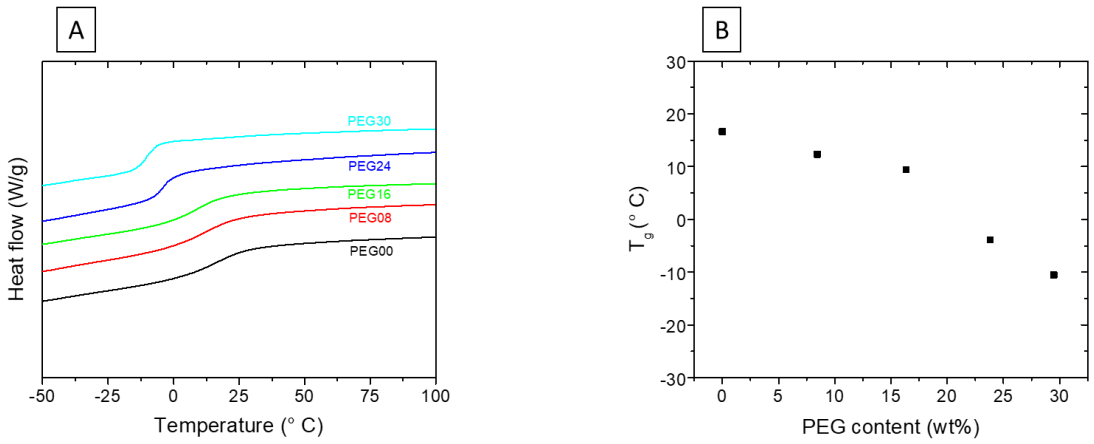

Figure 4.4 (a) Second heat thermograms of the hybrid networks obtained from DSC analysis (endo up). (b) Glass transition temperature of the hybrid networks plotted vs. PEG content

DSC results further proved the homogeneity of the networks, as only a single glass transition temperature was seen (Figure 4.4(a)) for all networks. Also, no endothermic peaks were seen, i.e., amorphous networks were obtained. The absence of

endothermic peaks also indicates that thiol-ene curing reactions resulted in close to 100% conversion.

Figure 4.4(b) shows a gradual decrease in T_g of the networks as PEG concentration was increased (or as fluorine concentration was decreased). It is well known that the flexible nature of PEG moieties can plasticize the material,[23] and this led to a gradual decrease in T_g of the networks as PEG concentration was increased. Addition of 30 wt% PEG resulted in a T_g decrease of ~25 °C.

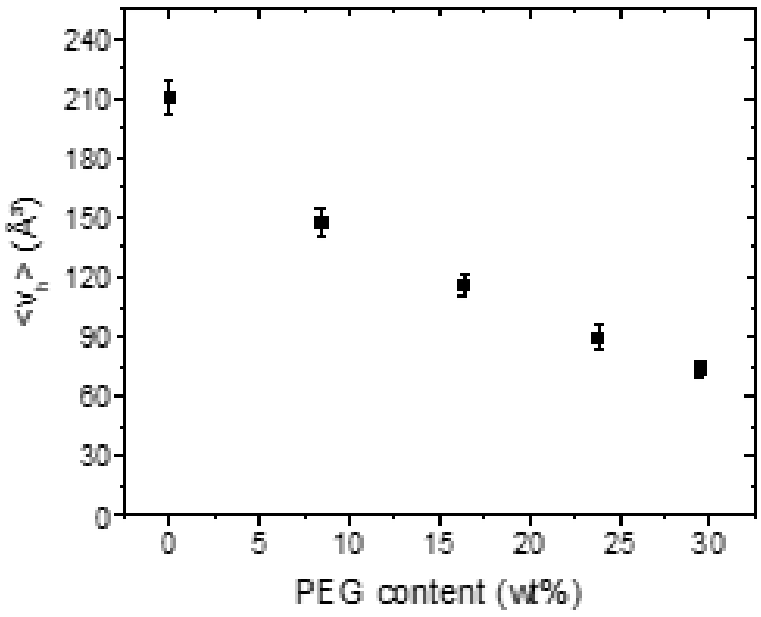

Figure 4.5 Average free volume hole size of the networks $<v_h>$ plotted as a function of PEG content.

In the previous chapter, the effect of perfluorinated moieties to create high amounts of free volume was discussed in detail. The repulsive interaction between perfluorinated dangling moieties and polar backbone is the reason why high free volume networks were created. Whereas, in this study as perfluorinated dangling moieties are gradually replaced with PEG moieties, $<v_h>$ measured from PALS analysis decreased as

shown in Figure 4.5. Unlike perfluorinated moieties, PEG moieties can have attractive polar interactions with the polar moieties in the thiol-ene backbone, which will reduce the average free volume hole size of the networks as shown in the schematic of Figure 4.2(b).

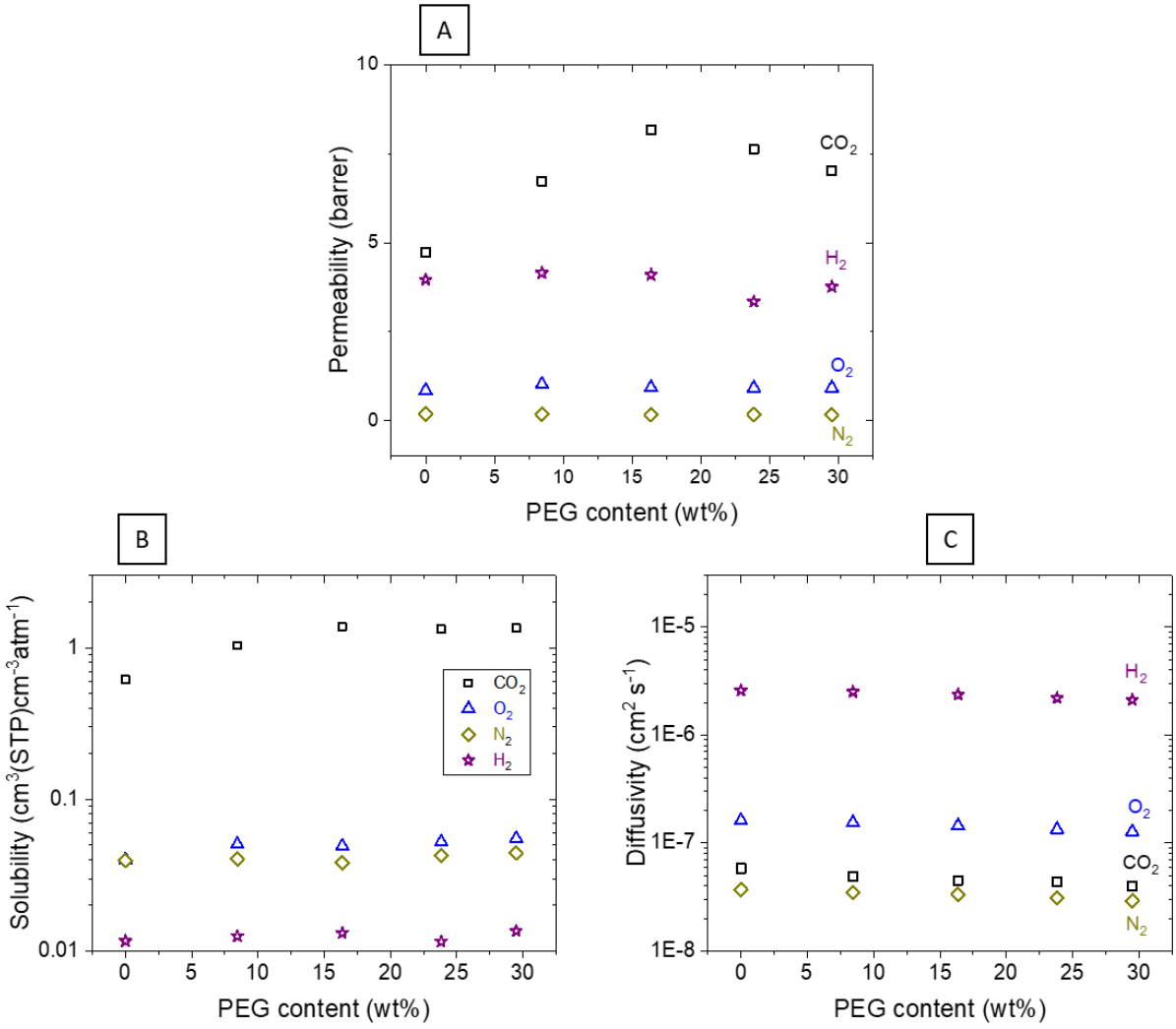

Figure 4.6 (a) Gas permeability, (b) Gas solubility, and (c) Gas diffusivity of the networks as a function of PEG content

Figure 4.6(a) shows that PEG concentration only influenced CO_2 permeability. For all other gases, PEG concentration did not have any significant effect on gas permeability. For CO_2, the permeability increased till 15 w% PEG, and after that CO_2

permeability leveled off. To get a deeper understanding, decoupled values, i.e., diffusivity and solubility are plotted as a function of PEG concentration.

Network modification did not affect gas solubility, except for CO_2 solubility (Figure 4.6(b)). Gas solubility scaled as a function of its critical temperature, i.e., CO_2 gas owing to its higher critical temperature has high solubility. Also, favorable interactions between gas molecules and network moieties can result in increase of gas solubility, and it is known that Lewis acid-base type interactions exist between CO_2 and PEG.[7-8] Therefore, as PEG concentration was increased, CO_2 solubility of the hybrid networks increased, and the effect leveled off beyond 15 wt% CO_2 (Figure 4.6(b)).

Whereas, surprisingly, PEG concentration did not have any effect on gas diffusivity (Figure 4.6(c)). Figure 4.5 shows that when PEG content in the network was about 30% wt%, $<v_h>$ of the networks decreased by 4 times compared to a network containing no PEG, i.e., only perfluorinated dangling moieties. It is well known that gas diffusivity depends on free volume in the material.[24-30] If that is the case, gas diffusivity should have shown a clear decreasing trend with increasing PEG concentration. But in chapter 3, we discussed the static nature of free volume around perfluorinated moieties which results in a negative deviation from Cohen Turnbull model[24], i.e., lower values of gas diffusivity than what its free volume suggests. Also, Figure 4.4 shows a clear decrease in T_g of the networks with increasing PEG concentration. That is, as the PEG concentration is increased, chain mobility of the networks increases, which will aid in the redistribution of free volume, which in turn would aid gas diffusivity.[31] Therefore, it can be said that the decreases in free volume were compromised by the increases in chain mobility, which thereby resulted in no effect of PEG concentration on gas diffusivity.

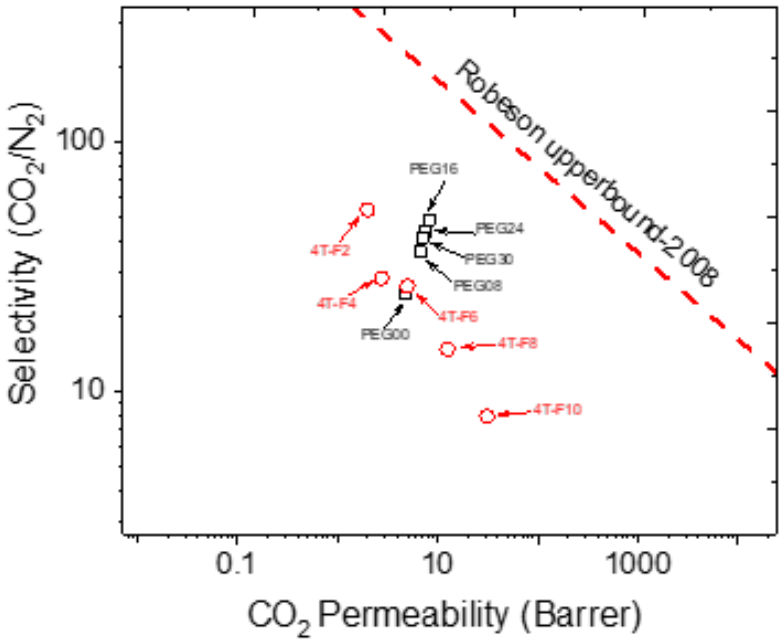

Figure 4.7 Robeson plot for CO_2/N_2 gas pair.[32] Data points for hybrid PEG perfluorinated thiol-ene networks are compared with that of perfluorinated thiol-ene networks.

Selectivity for CO_2 with respect to N_2, α, was calculated for each network using equation 4.

$$\alpha = P_{CO2}/P_{N2} \qquad (4)$$

where P_{CO2} is CO_2 permeability and P_{N2} is N_2 permeability. Selectivity values were plotted as a function of CO_2 permeability in Figure 4.7. It can be seen that for this series, as PEG concentration was increased, both permeability and selectivity for CO_2 increased because PEG concentration did not have any effect on N_2 permeability. Therefore, the networks were moving toward the Robeson upper bound. All PEG containing networks in this series had a CO2 selectivity value greater than 30, which can make them suitable for CO_2 separation membrane applications.[3]

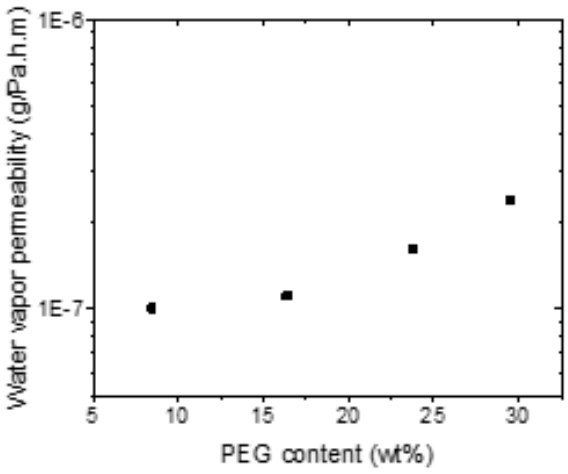

Figure 4.8 Water vapor permeability of the networks plotted as a function of PEG content of hybrid PEG and perfluorinated networks

Water vapor permeability of the hybrid networks increased as PEG concentration was increased (Figure 4.8), because of the enhancements in hydrogen bonding sites brought about by increasing PEG concentration, which in turn will increase water sorption, and thereby water vapor permeability.

4.5 Conclusions

Novel hybrid thiol-ene networks containing hydrophobic perfluorinated and hydrophilic PEG moieties were synthesized using a two-step approach. DSC analysis showed a single T_g in all networks and thereby confirmed that there was no phase separation in the networks. T_g of the networks decreased with increasing PEG concentration because of the plasticization effect of PEG moieties. $<v_h>$ of the networks decreased with increasing PEG concentration because of the increase in the number of attractive interactions as a result of an increase in the concentration of polar PEG moieties. Water vapor permeability of the networks increased with increasing PEG

concentration because of the affinity of PEG moieties for water. Gas permeability studies revealed that these networks have high CO_2 permeability and high selectivity for CO_2 over N_2, thereby making them suitable for CO_2 separation applications.

4.6 References

1. Aaron, D.; Tsouris, C., Separation of CO2 from Flue Gas: A Review. *Separation Science and Technology* **2005,** *40* (1-3), 321-348.

2. Figueroa, J. D.; Fout, T.; Plasynski, S.; McIlvried, H.; Srivastava, R. D., Advances in CO2 capture technology—The U.S. Department of Energy's Carbon Sequestration Program. *International Journal of Greenhouse Gas Control* **2008,** *2* (1), 9-20.

3. Merkel, T. C.; Lin, H.; Wei, X.; Baker, R., Power plant post-combustion carbon dioxide capture: An opportunity for membranes. *Journal of Membrane Science* **2010,** *359* (1), 126-139.

4. Brunetti, A.; Scura, F.; Barbieri, G.; Drioli, E., Membrane technologies for CO2 separation. *Journal of Membrane Science* **2010,** *359* (1), 115-125.

5. Hussain, A.; Hägg, M.-B., A feasibility study of CO2 capture from flue gas by a facilitated transport membrane. *Journal of Membrane Science* **2010,** *359* (1), 140-148.

6. Lin, H.; Kai, T.; Freeman, B. D.; Kalakkunnath, S.; Kalika, D. S., The Effect of Cross-Linking on Gas Permeability in Cross-Linked Poly(Ethylene Glycol Diacrylate). *Macromolecules* **2005,** *38* (20), 8381-8393.

7. Kawakami, M.; Yamashita, Y.; Yamasaki, M.; Iwamoto, M.; Kagawa, S., Effects of dissolved inorganic salts on gas permeabilities of immobilized liquid polyethylene glycol membranes. *Journal of Polymer Science: Polymer Letters Edition* **1982,** *20* (5), 251-257.

8. Lin, H.; Freeman, B. D., Materials selection guidelines for membranes that remove CO2 from gas mixtures. *Journal of Molecular Structure* **2005,** *739* (1), 57-74.

9. Car, A.; Stropnik, C.; Yave, W.; Peinemann, K.-V., Pebax®/polyethylene glycol blend thin film composite membranes for CO2 separation: Performance with mixed gases. *Separation and Purification Technology* **2008,** *62* (1), 110-117.

10. Yave, W.; Car, A.; Funari, S. S.; Nunes, S. P.; Peinemann, K.-V., CO2-Philic Polymer Membrane with Extremely High Separation Performance. *Macromolecules* **2010,** *43* (1), 326-333.

11. Kawakami, M.; Iwanaga, H.; Hara, Y.; Iwamoto, M.; Kagawa, S., Gas permeabilities of cellulose nitrate/poly(ethylene glycol) blend membranes. *Journal of Applied Polymer Science* **1982,** *27* (7), 2387-2393.

12. Hirayama, Y.; Kase, Y.; Tanihara, N.; Sumiyama, Y.; Kusuki, Y.; Haraya, K., Permeation properties to CO2 and N2 of poly(ethylene oxide)-containing and crosslinked polymer films. *Journal of Membrane Science* **1999,** *160* (1), 87-99.

13. Lin, H.; Freeman, B. D., Gas Permeation and Diffusion in Cross-Linked Poly(ethylene glycol diacrylate). *Macromolecules* **2006,** *39* (10), 3568-3580.

14. Lin, H.; Van Wagner, E.; Freeman, B. D.; Toy, L. G.; Gupta, R. P., Plasticization-Enhanced Hydrogen Purification Using Polymeric Membranes. *Science* **2006,** *311* (5761), 639-642.

15. Kwisnek, L.; Heinz, S.; Wiggins, J. S.; Nazarenko, S., Multifunctional thiols as additives in UV-cured PEG-diacrylate membranes for CO2 separation. *Journal of Membrane Science* **2011,** *369* (1–2), 429-436.

16. Kwisnek, L.; Goetz, J.; Meyers, K. P.; Heinz, S. R.; Wiggins, J. S.; Nazarenko, S., PEG Containing Thiol–Ene Network Membranes for CO2 Separation: Effect of Cross-Linking on Thermal, Mechanical, and Gas Transport Properties. *Macromolecules* **2014,** *47* (10), 3243-3253.

17. Hoyle, C. E.; Bowman, C. N., Thiol–Ene Click Chemistry. *Angewandte Chemie International Edition* **2010,** *49* (9), 1540-1573.

18. Hoyle, C. E.; Lee, T. Y.; Roper, T., Thiol–enes: Chemistry of the past with promise for the future. *Journal of Polymer Science Part A: Polymer Chemistry* **2004,** *42* (21), 5301-5338.

19. Kwisnek, L.; Kaushik, M.; Hoyle, C. E.; Nazarenko, S., Free Volume, Transport, and Physical Properties of n-Alkyl Derivatized Thiol−Ene Networks: Chain Length Effect. *Macromolecules* **2010,** *43* (8), 3859-3867.

20. Kirkegaard, P.; Eldrup, M.; Mogensen, O. E.; Pedersen, N. J., Program system for analysing positron lifetime spectra and angular correlation curves. *Computer Physics Communications* **1981,** *23* (3), 307-335.

21. Kwisnek, L.; Nazarenko, S.; Hoyle, C. E., Oxygen Transport Properties of Thiol−Ene Networks. *Macromolecules* **2009,** *42* (18), 7031-7041.

22. Hoyle, C. E.; Lowe, A. B.; Bowman, C. N., Thiol-click chemistry: a multifaceted toolbox for small molecule and polymer synthesis. *Chemical Society Reviews* **2010,** *39* (4), 1355-1387.

23. Avella, M.; Martuscelli, E., Poly-d-(−)(3-hydroxybutyrate)/poly(ethylene oxide) blends: phase diagram, thermal and crystallization behaviour. *Polymer* **1988,** *29* (10), 1731-1737.

24. Cohen, M. H.; Turnbull, D., Molecular Transport in Liquids and Glasses. *The Journal of Chemical Physics* **1959,** *31* (5), 1164-1169.

25. Lin, H.; Wagner, E. V.; Swinnea, J. S.; Freeman, B. D.; Pas, S. J.; Hill, A. J.; Kalakkunnath, S.; Kalika, D. S., Transport and structural characteristics of crosslinked poly(ethylene oxide) rubbers. *Journal of Membrane Science* **2006,** *276* (1–2), 145-161.

26. Park, J. Y.; Paul, D. R., Correlation and prediction of gas permeability in glassy polymer membrane materials via a modified free volume based group contribution method. *Journal of Membrane Science* **1997,** *125* (1), 23-39.

27. Haraya, K.; Hwang, S.-T., Permeation of oxygen, argon and nitrogen through polymer membranes. *Journal of Membrane Science* **1992,** *71* (1), 13-27.

28. Tanaka, K.; Okano, M.; Toshino, H.; Kita, H.; Okamoto, K.-I., Effect of methyl substituents on permeability and permselectivity of gases in polyimides prepared from methyl-substituted phenylenediamines. *Journal of Polymer Science Part B: Polymer Physics* **1992,** *30* (8), 907-914.

29. Nagel, C.; Günther-Schade, K.; Fritsch, D.; Strunskus, T.; Faupel, F., Free Volume and Transport Properties in Highly Selective Polymer Membranes. *Macromolecules* **2002,** *35* (6), 2071-2077.

30. Sanders, D. F.; Smith, Z. P.; Guo, R.; Robeson, L. M.; McGrath, J. E.; Paul, D. R.; Freeman, B. D., Energy-efficient polymeric gas separation membranes for a sustainable future: A review. *Polymer* **2013,** *54* (18), 4729-4761.

31. Hiltner, A.; Liu, R.; Hu, Y.; Baer, E., Oxygen transport as a solid-state structure probe for polymeric materials: A review. *Journal of Polymer Science Part B: Polymer Physics* **2005,** *43* (9), 1047-1063.

32. Robeson, L. M., The upper bound revisited. *Journal of Membrane Science* **2008,** *320* (1-2), 390-400.

CHAPTER V – EFFECT OF MOISTURE INGRESS ON FREE VOLUME, OXYGEN, AND WATER VAPOR TRANSPORT PROPERTIES OF EPOXY-AMINE NETWORKS

5.1 Abstract

A series of five different epoxy-amine networks were synthesized using 1:1 epoxide to amine hydrogen stoichiometry. The series consisted of rubbery networks having T_gs of -11 °C, -8 °C to glassy networks having T_gs of 61 °C, 136 °C, and 227 °C. Moisture sorption characteristics of the networks were evaluated using dynamic vapor sorption (DVS) analysis. The effect of water sorption on T_g was studied using RH-DMA analysis. Positron Annihilation Lifetime Spectroscopy (PALS) was used to understand the effect of water sorption on free volume. A novel PALS humidity chamber was built to maintain and control the required humidity during PALS experiments on epoxy-amine networks sorbed with water. For rubbery networks, water sorption did not show any effect on the average free volume hole size $<v_h>$ measured using PALS experiments. Whereas, glassy networks showed a V-shaped trend when $<v_h>$ was plotted as a function of RH, i.e., free volume gradually decreased with increasing relative humidity, and beyond 75% RH, $<v_h>$ increased. The competition between two processes, i.e., water molecules filling frozen-in free volume holes and plasticization of chains caused by water molecules were used to explain the V-shaped trend. The oxygen permeability of the glassy networks also showed a V-shaped trend, when it was plotted vs. relative humidity. The effect of water sorption on oxygen permeability was more complex as the sorbed water molecules affected both the oxygen solubility and diffusivity in different ways.

Whereas, water vapor permeability of glassy networks was unaffected until 75% RH, and beyond 75%RH, swelling of networks led to an increase in water vapor permeability.

5.2 Introduction

Organic coatings which are implemented to prevent or resist corrosion of metals need to have sufficient barrier properties against corrosive species such as oxygen, water, and electrolytes.[1] Epoxy-amine networks are often used as the matrix or the binder material for the primer or the intermediate coating layers which are tasked to prevent corrosion at the metal surface. Though most commercially used epoxy-amine chemistry based coatings have many beneficial characteristics such as good adhesion to metal, high hardness, and good chemical resistance, the presence of polar moieties and hydrogen bonding sites makes them absorb moisture, with maximum reported moisture content ranging between 1-7 wt%.[2-4] The absorbed moisture not only affects the water transport itself but also can affect the oxygen and electrolyte transport in a complex manner. There have been numerous previous reports that have tried to correlate factors such as network topology, polarity, and chain dynamics on moisture sorption and kinetics in epoxy-amine networks.[5-7] But an actual anti-corrosion application has mixed transport involving three penetrants, i.e. oxygen, water, and electrolytes which makes this transport phenomenon heavily convoluted. Also, the final coating formulation might contain additional substances such as pigments, solvents, fillers, and additives which further adds to the complexity. Hence the elucidation of the effect of epoxy-amine network structure and topology on mixed gas transport involving water and oxygen is still not available in the literature.

It is well known that the transport of small molecules such as oxygen etc. has a good correlation to the free volume in the material.[8-12] Whereas free volume or molecular level imperfections in networks are in turn affected by factors such as chain rigidity[13-14], cross-link density[15-20], intermolecular interactions or polarity of the network[21] etc. In addition to these network parameters, the presence of sorbed water[22-25] or solvent also affects the free volume of the material. The effect of water sorption or relative humidity on free volume has been mostly been studied on high barrier linear polymers such as polyamides[22, 24], ethylene-vinyl alcohol[23] copolymer etc. which are used as packaging films, or on highly permeable polymer like poly(arylene ether sulfone)[25] which is used for membrane application. Macqueen et al observed inconsistencies in the trends for free volume in epoxy-amine networks prior to and post saturation of networks with water. Thus, it can be said that the effect of water sorption on free volume of epoxy-amine networks is still not clear. Therefore, the goal of this study was to elucidate the effect of water sorption on free volume, oxygen, and water vapor transport properties of epoxy-amine networks having different structures.

5.3 Experimental

5.3.1 Materials

Cycloaliphatic epoxy resin, Eponex™ 1510 (E1510, epoxy equivalent weight (EEW) = 205-215 g/eq), and diglycidyl ether of bisphenol A (DGEBA) epoxy resin, Epon™ 825 (E825, EEW = 175-180 g/eq), were supplied by Hexion (Momentive Specialty Chemicals). Diamine crosslinking agents Jeffamine EDR 148 (amine hydrogen equivalent weight (AHEW) = 74 g/eq), Jeffamine ED900 (AHEW = 250 g/eq), and Jeffamine THF100 (AHEW = 260 g/eq) were supplied by Huntsman Corporation.

Whereas 4,4'-diaminodiphenyl methane (DDM, AHEW = 49.57 g/eq) was supplied by Acros Organics, and 4,4'-diaminodiphenyl sulfone (DDS, AHEW = 62.075 g/eq) was supplied by TCI America. Figure 5.1 displays their chemical structures. The chemicals were used as received.

5.4 Network preparation

The network was formulated on 1:1 stoichiometry (epoxy to amine-hydrogen). Table 5.1 shows the epoxy resin and diamine crosslinker combinations used in this study. Appropriate quantities of epoxy resin and diamine crosslinker were taken and hand stirred prior to mixing at high speeds using a FlackTek SpeedMixer. Diamine crosslinkers DDM and DDS are solids at room temperature, therefore compositions containing these crosslinkers were heated in an oven at 150 °C with periodic stirring until a homogeneous mixture was obtained. The monomer mixture was then placed in a vacuum oven at low pressure for approximately five minutes to remove air bubbles. Networks were prepared by curing the monomer mixtures while sandwiched between two glass plates with Teflon spacers having a thickness of ~300 μm placed at the corners between the plates to ensure uniform film thicknesses. Prior to the addition of monomer mixture, the plates were sprayed with a thin layer of silicone-free release agent and then placed in an oven pre-heated to the temperature corresponding to the primary cure temperature of that particular composition (Table 5.1). The degassed epoxy-amine mixture was then poured onto the bottom glass plate before slowly applying the top plate to avoid inclusions of air bubbles. The assembly was then placed in an oven and the cure profile shown in Table 5.1 was followed. After the curing process, the assembly was allowed to cool slowly to room temperature before separating the plates and removing the

solid epoxy-amine films. Larger volume samples were produced by curing bars in silicone molds with wells having dimensions of 76 x 15 x 12.7 mm (L x W x T).

5.5 Characterization

Water Sorption Analysis. Water sorption characteristics of the networks were studied using a TA Instruments Q5000 Sorption Analyzer. Circular discs having diameters of 6.3 mm and ~0.3 mm thickness were placed in quartz pans and subjected to a drying at 60 °C and 0% RH, following which the sorption characteristics were measured at 5, 22, 44, 57, 75, or 95% RH environments at 25 °C. At each RH condition, the weight change (%) was monitored until a saturation or near-equilibrium stage was achieved.

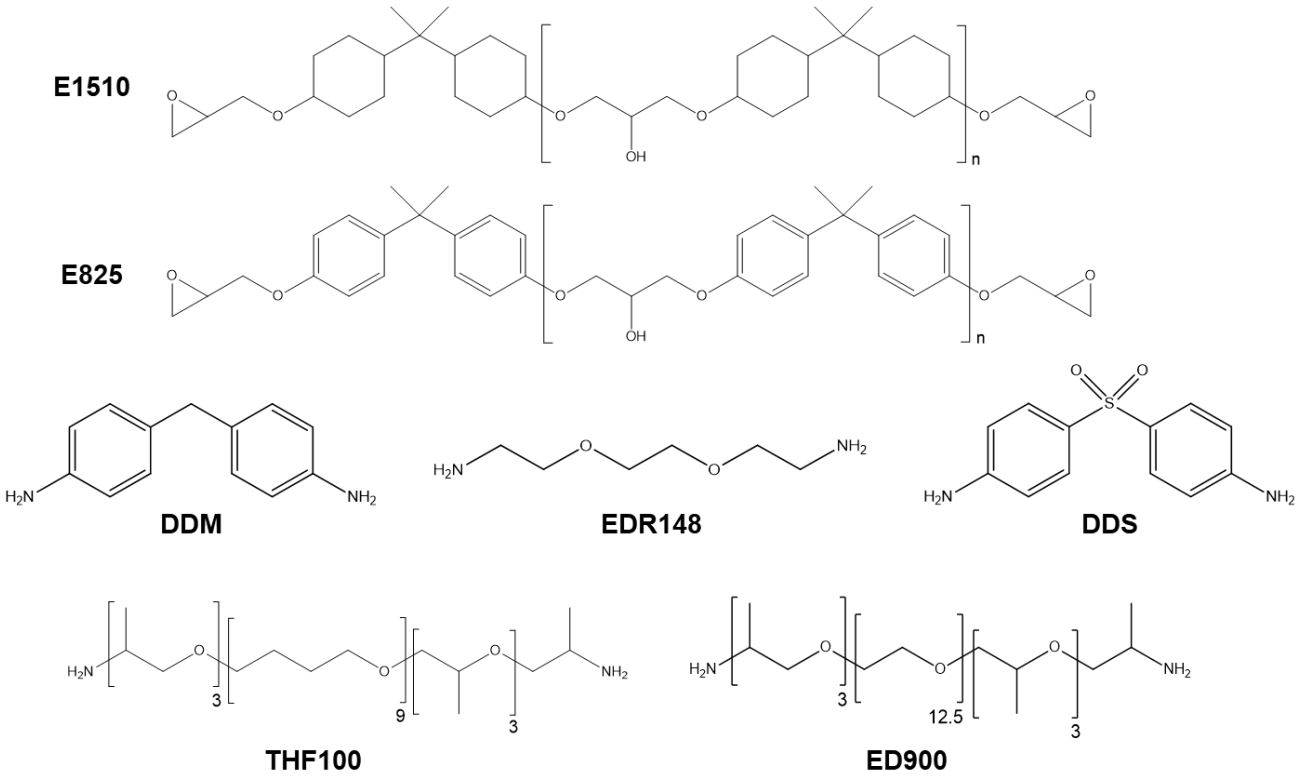

Figure 5.1 Chemical structure of the monomers used in this work

Table 5.1 Epoxy-amine networks prepared for this study and the curing profiles that were employed

Epoxy-Amine Combination	Primary Cure Temperature (°C)	Primary Cure Time (hours)	Secondary Cure Temperature (°C)	Secondary Cure Time (hours)
E1510-THF100	35	5	75	24
E1510-ED900	35	5	75	24
E1510-EDR148	60	2	120	2
E1510-DDM	90	2	150	1
E825-DDS	150	2	250	1

The dynamic mechanical analysis was carried out on free films with approximate dimensions of 12 x 5 x 0.3 mm on a TA instruments Q800 DMA outfitted with a RH controller. Single frequency temperature ramp testing was conducted in tensile mode with a heating rate of 1 °C/ minute from 15 – 115 °C, a strain rate of 0.1%, a pre-load force of 0.01 N, and frequency of 1 Hz. Storage Modulus (E′), Loss Modulus (E″), and Tan Delta (δ) signals were monitored over the entire temperature range.

Free Volume Analysis. Average free volume hole size $<v_h>$ of the networks, at different relative humidity conditions, were measured using positron annihilation lifetime spectroscopy (PALS). Discs having a diameter of 1 cm were punched out from the network films and were stacked to form thicknesses of 1 mm. Positron source, 30 μCi ^{22}Na, was sandwiched between two stacked discs, and the sample source assembly was wrapped using a Teflon tape and was placed inside a custom-built PALS humidity sample chamber (Figure 5.2(a)). The sample chamber was placed between two photomultiplier tubes (PMT) which are equipped with BaF_2 γ-radiation sensitive scintillators. PMTs are tuned such that one PMT can detect γ quanta and convert that into a signal associated with positron emission and the other with its annihilation. A

multichannel analyzer compiled the coincidences, i.e., the time difference between birth and death signal of positrons (lifetimes), with a time resolution of 290 ps.

Positrons thermalize in the sample and can form positronium species with secondary electrons. The longer lived ortho-positronium (o-Ps) species localizes within the less electron dense region, i.e. free volume holes within the sample. o-Ps gets annihilated when it gets "picked off" by an electron from the sample that has opposite spin and this phenomenon is called the pick-off mechanism. Therefore, the lifetime of the o-Ps is determined by the electron density of the sample and physical size of the free volume hole in which it is localized. o-Ps lifetime τ_3 was related to free volume hole radius R in accordance with the semi-empirical equation derived by Tao (equation 1).[26]

$$\tau_3 = 0.5\left[1 - \frac{R}{R_0+R} + \frac{1}{2\pi}\sin\left(\frac{2\pi R}{R_0+R}\right)\right]^{-1} ns \qquad (1)$$

Where, $_0$ = 0.1656 nm is the empirically derived electron layer thickness.[26] Assuming that the free volume holes are spherical, average free volume hole size of the networks can be calculated as follows, $< v_h > = \frac{4}{3}\pi R^3$.

Prior to PALS experiment, the sample was equilibrated for 24 hours in that RH condition by placing the sample discs in appropriate RH chambers. The equilibrated sample (along with the source) was then placed in the PALS humidity chamber. An automated technique was devised to accurately maintain the required RH% in the chamber (Figure 5.2(b)). In this technique, there is a constant influx of nitrogen gas bubbled through DI water (wet N_2) into the chamber. RH% is monitored at the gas outflux from the chamber by a humidity sensor. If the RH value goes beyond the set value, the humidity controller (which is connected to the humidity sensor) activates the

solenoid valve, which then lets dry nitrogen into the chamber. The dry nitrogen then brings down the RH% within the chamber, and once the RH% goes below the set value, the humidity controller turns off the solenoid valve, thereby stopping the influx of dry nitrogen, and the cycle continues. This automated dynamic technique accurately maintained any RH% value between 0 – 80% range. For tests at RH greater than 80%, a sponge containing a saturated salt solution or DI water was placed inside completely enclosed and sealed PALS sample chamber (Figure 5.2(c)). For RH values of 85% and 99%, sponge contained a saturated potassium chloride solution and DI water respectively.

At each relative humidity, seven spectra were generated. Each PALS spectrum was collected for one hour to get at least 1 million incidences using Ortec Positron Lifetime System (Advanced Measurement Technology, Oak Ridge, TN). Spectra were fit and deconvoluted using PATFIT-88 software assuming three lifetime components, to obtain τ_3, and thereby $<v_h>$ values.[27]

Oxygen Permeation was measured using a Mocon OX-TRAN® 2/21 instrument. Experiments were conducted at 23 °C and at a broad range of RHs. Prior to the oxygen permeation experiment at each RH condition, the sample was pre-conditioned at that particular RH for 24 hours. From the experimental oxygen flux *J(t)* data, oxygen permeability *P* and diffusivity *D* values were obtained by performing a two-parameter least-square fit to Fick's second law equation.

$$J(t) = \frac{Pp}{l}\left[-\sum_{n=1}^{\infty}(-1)^n \exp(-D\pi^2 n^2 t/l^2)\right] \qquad (2)$$

Using the solution-diffusion model, solubility *S* can then be calculated as $P = D \times S$.

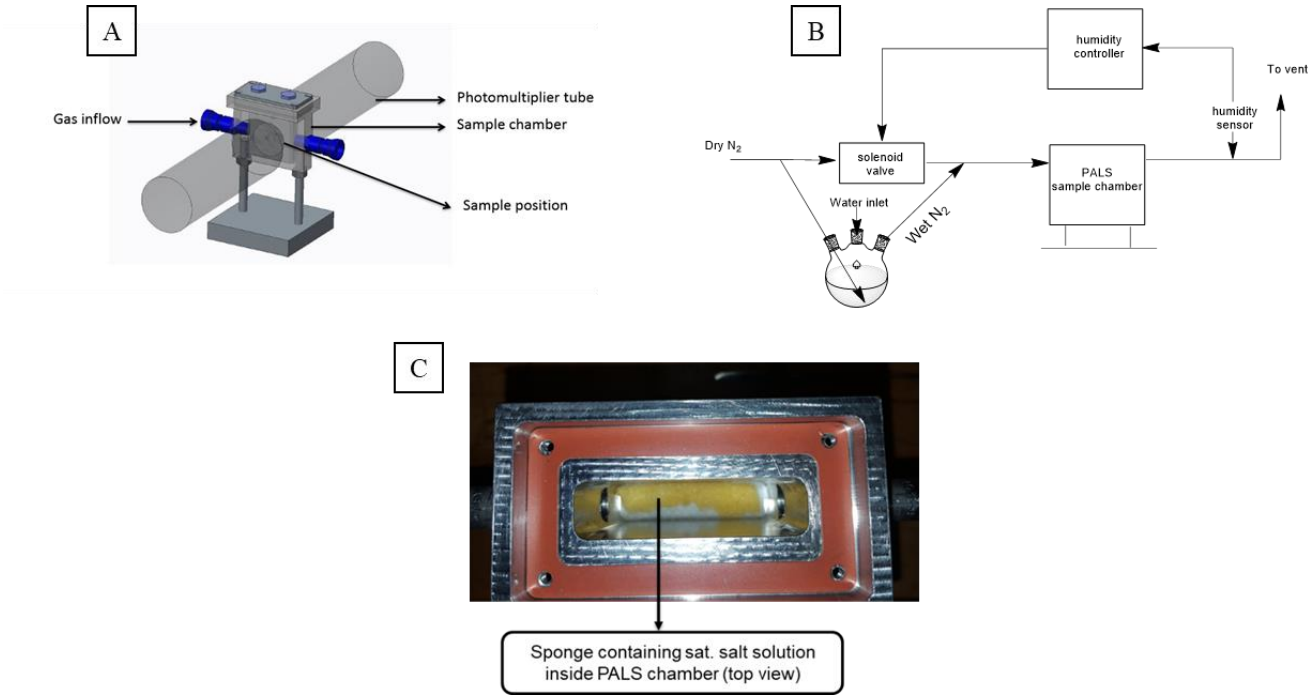

Figure 5.2 (a) Design of PALS humidity control chamber along with photomultiplier tubes (b) Automated technique devised to generate 0 – 80% RH. (c) The technique devised to achieve high humidities within the sample chamber (RH > 80%)

Bulk Volume Calculations. Cured E1510-EDR148 network samples having dimensions of approximately 15 x 12.7 x 6 mm were prepared and their masses were first measured on a Mettler Toledo XS104 analytical balance. Following which the densities of samples were determined via Archimedes method using a density kit attachment to the Toledo XS104 analytical balance, where water was used as the buoyant fluid. From the aforementioned steps, the dry mass and the dry density of the samples were obtained, from which the volume of the sample was calculated. Following which the samples were placed in different relative humidity chambers. The samples were exposed to different relative humidities for approximately 3 months to ensure that moisture absorption reached saturation. Following which the mass and the density of the samples were

measured. Through this, the bulk volume change of the E1510-EDR148 network was obtained at different %RH conditions.

Water Permeation Experiments. Water vapor permeability of the samples at different relative humidities was measured using desiccant cup test method described by ASTM E 96-95. In this method, an open mouth cup containing desiccant was covered by the test sample. The edges of the test specimen were sealed to the edges of the cup. The assembly was then placed in a relative humidity chamber, where the required relative humidity was controlled by having the appropriate saturated salt (potassium carbonate – 43% RH, sodium bromide – 57% RH, sodium chloride – 75% RH, potassium chloride – 85%) solution or DI water (for 99% RH) within the chamber. The mass of the cup test assembly was measured at periodic intervals, from which the water vapor transmission rate (WVTR) into the cup was calculated as follows.

$$WVTR = \frac{change\ in\ mass\ of\ the\ cup}{time \times A} \qquad (3)$$

Where *A* is the cup mouth area. The sample was allowed to equilibrate in the RH chamber for one day, after which the mass readings were taken at different time intervals. Change in mass of the cup assembly showed a linear trend as a function of time, and the slope of that line was used to obtain *change in mass of the cup/time*. Water vapor permeability (WVP) was calculated as follows:

$$WVP = WVTR\left(\frac{l}{\Delta p}\right) \qquad (4)$$

Where, *l* is the sample thickness and *Δp* is the water vapor pressure difference across the film, which can be calculated from the relative humidity difference across the film.

Experiments were conducted in different relative humidity chambers to generate water vapor permeability of the samples as a function of relative humidity.

5.6 Results and discussion

In this study epoxy-amine networks having different T_g values were chosen and Figure 5.3 shows the tan delta peaks of the networks obtained from DMA experiments and the figure also indicates the T_g of the networks. DGEBA based E825-DDS (T_g = 227 °C) was the most rigid among glassy networks, followed by the ones containing cyclohexyl derivative based E1510, i.e. E1510-DDM and E150-EDR148 which showed T_g of 136 °C and 61 °C respectively. Whereas, the networks containing long chain amine crosslinkers, i.e., E1510-ED900 and E1510-THF100 formed rubbery networks, because of lower cross-link density.

Figure 5.4 (a-e) shows the moisture sorption kinetics of the networks at different %RH conditions and it also indicates the moisture content at saturation or near saturation for all the networks at different %RH conditions obtained from DVS analysis. In rubbery networks, moisture absorption reaches saturation in about 200 minutes or lesser, except for the highly polar E1510-ED900 at 95% RH. Whereas in glassy networks, the moisture absorption reaches saturation within 1000 minutes (less than a day), except for the more polar E1510-EDR148 which at 75% and 95% RH does not reach saturation even after 2500 minutes of exposure, but the curve characteristics show that the moisture absorption is close to reaching saturation. Figure 5.4(f) compares the moisture absorption of the networks. After 1-day exposure to 95% RH, comparatively more polar glassy networks E1510-EDR148 and E1510-DDM absorbed more than 3.5 wt% moisture. Whereas, E825-DDS and E1510-THF100 contained less water, i.e., 1.9 and 2.5 wt% water

respectively after a 1-day exposure to 95% RH. The highly polar E1510-ED900 network absorbs 27 wt% water at 95% RH because of the presence of long chain PEG based amine cross-linker, i.e., ED900.

To study the effect of moisture on network plasticization, E1510-EDR148 network was studied using RH-DMA experiments. Figure 5.5 shows the decrease in T_g of the network with an increase in relative humidity. After 2 hours of exposure to 95% RH, the T_g of the network was reduced to 59.4 °C compared to the dry T_g of 70 °C.

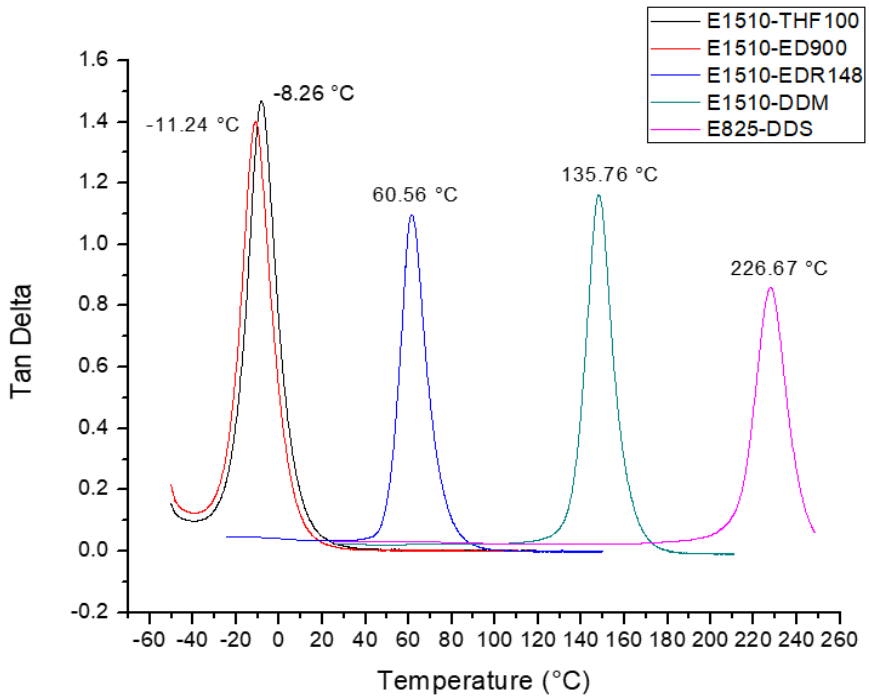

Figure 5.3 Tan delta vs. temperature obtained from DMA analysis plotted for all the networks. Number indicates the tan delta peak, i.e. T_g.

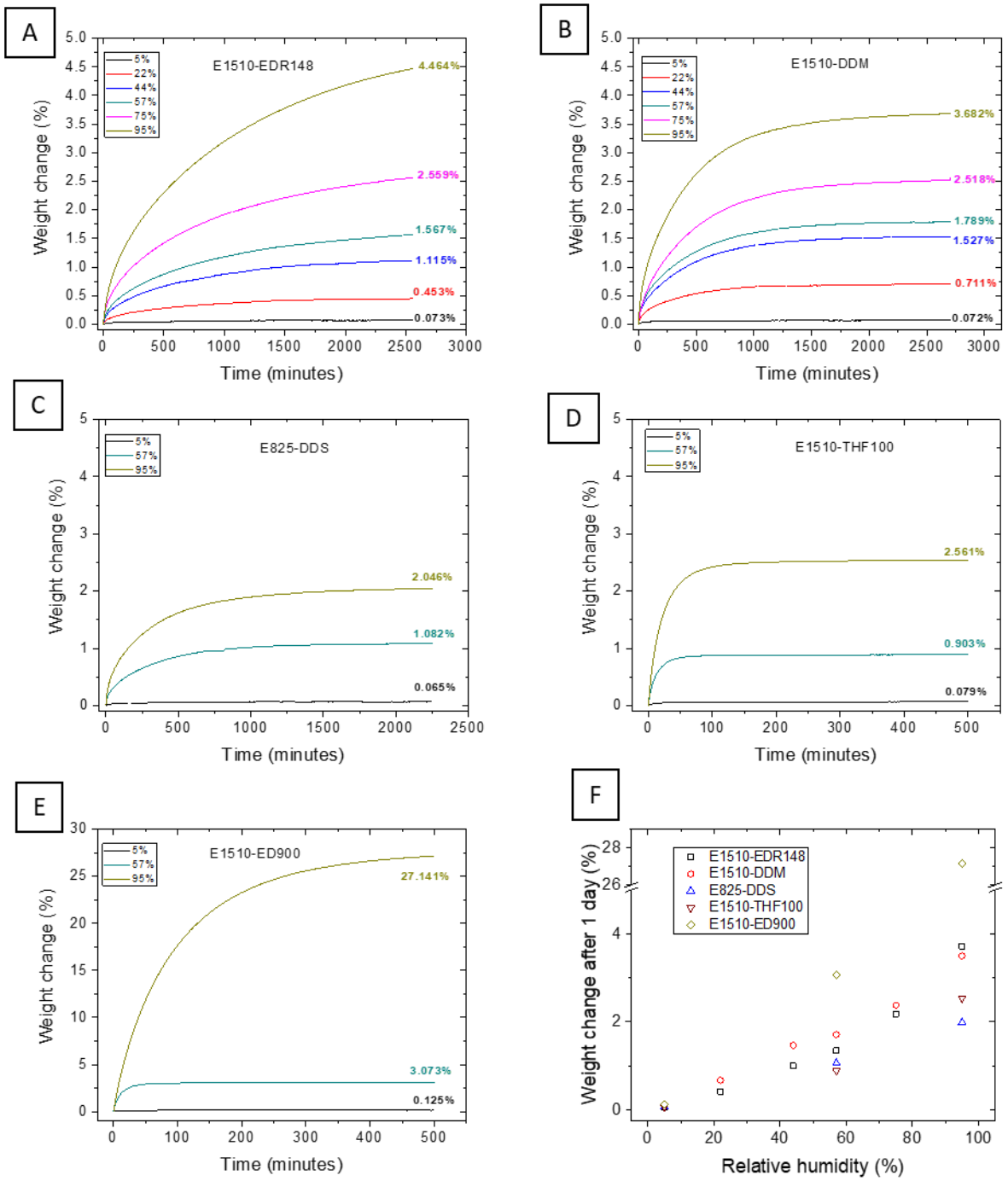

Figure 5.4 Water vapor sorption characteristics of (a) E1510-EDR148, (b) E1510-DDM, (c) E825-DDS, (d) E1510-THF100, (e) E1510-ED900 networks at different relative humidities. (f) shows the water content in the samples after 1-day exposure to different relative humidities

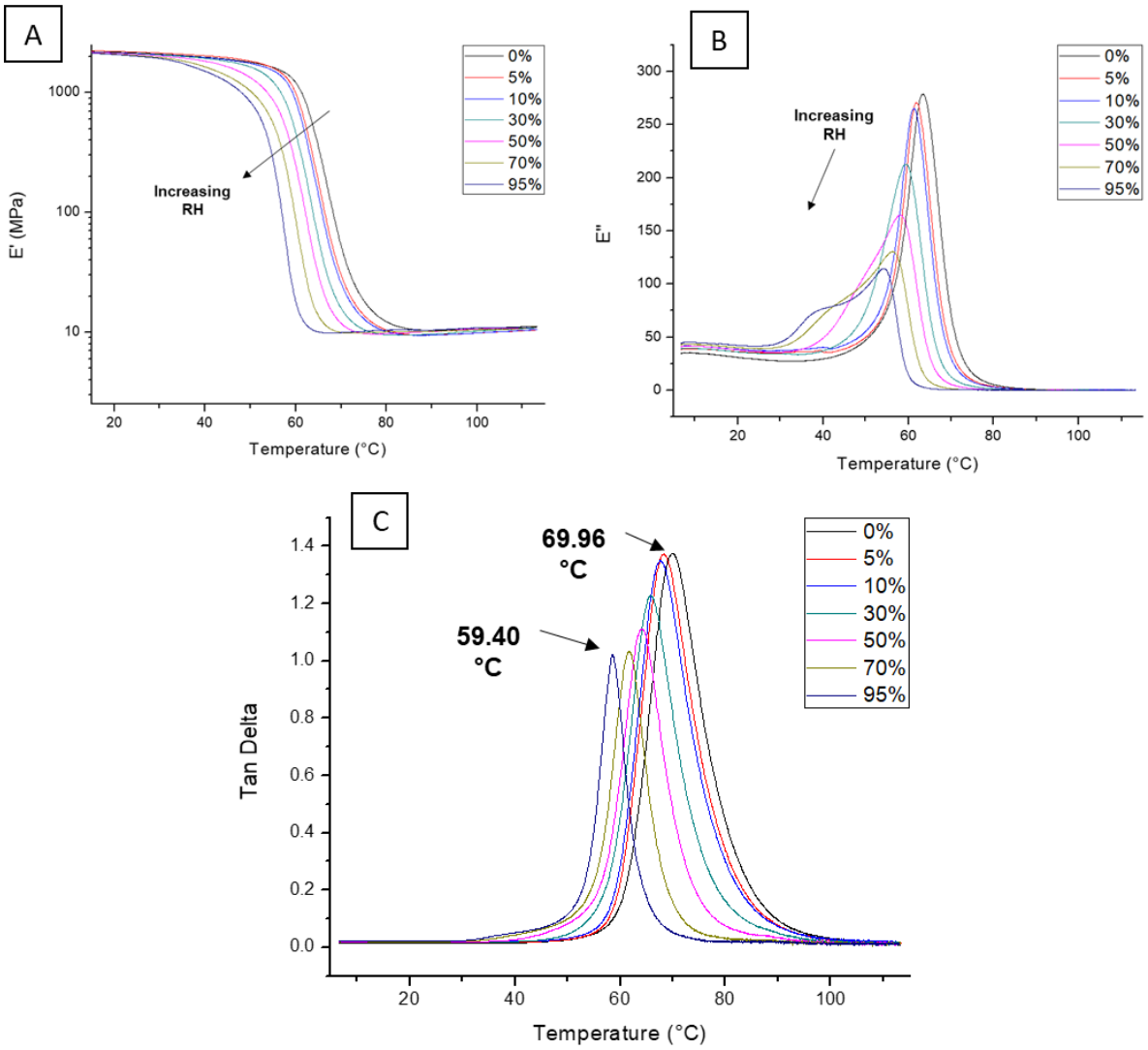

Figure 5.5 Storage Modulus *E'*, Loss Modulus *E''*, and Tan Delta plots of E1510-EDR148 at different RH% conditions.

Figure 5.6 shows the depression in T_g of the network (obtained from tan δ peak of RH-DMA analysis) as a function of water weight fraction in it. The water content of the network at different %RH conditions obtained from DVS experiments was used for the plot. The experimental T_g depression was compared with the Fox equation prediction[28], which is based on equation 5.

$$\frac{1}{T_g} = \frac{wt_1}{T_{g^1}} + \frac{wt_2}{T_{g^2}} \qquad (5)$$

Where T_g is the glass transition temperature of the network at different hydrated states. wt_1 and wt_2 are weight fraction of water and polymer respectively in the system. T_{g^1} is the glass transition temperature of water which was assumed as -137 °C[29] and T_{g^2} is the glass transition temperature of the dry network. The depression in T_g of the network showed a negative deviation from the Fox prediction (Figure 5.6). This negative deviation from Fox equation has been associated with weakening of the intermolecular interactions of the stiffer component by the second component.[30] In the case of hydration of E1510-EDR148 network, it can be assumed that in addition to the dilution effect, bound water also disrupts the intramolecular hydrogen bonding in the network leading to further lowering of T_g than what Fox equation predicts.

Figure 5.7(a) shows the effect of relative humidity on average free volume hole size of the networks obtained from PALS analysis. In the dry state, the average free volume hole size $<v_h>$ of the elastomeric networks, i.e., E1510-THF100 and E1510-ED900 were greater than 140 Å^3 and these values were significantly higher than that of the glassy networks that were analyzed in this study. Though the elastomeric networks had different amine crosslinkers they showed very similar free volume in the dry state and this can be attributed to the similarity of the chain lengths of the amine cross-linkers THF100 and ED900, i.e., the cross-link density or average molecular weight between cross-links of both the elastomeric networks were comparable, and it is well known that cross-link density is one of the important parameters affecting free volume in elastomers.[15-18] Among glasses, in the dry state $<v_h>$ values correlated with network rigidity (T_g). i.e. E825-DDS showed a higher free volume followed by E1510-DDM and

E1510-EDR148, and in general, it is known that glasses with higher chain rigidity have larger free volume.[13-14, 19-20]

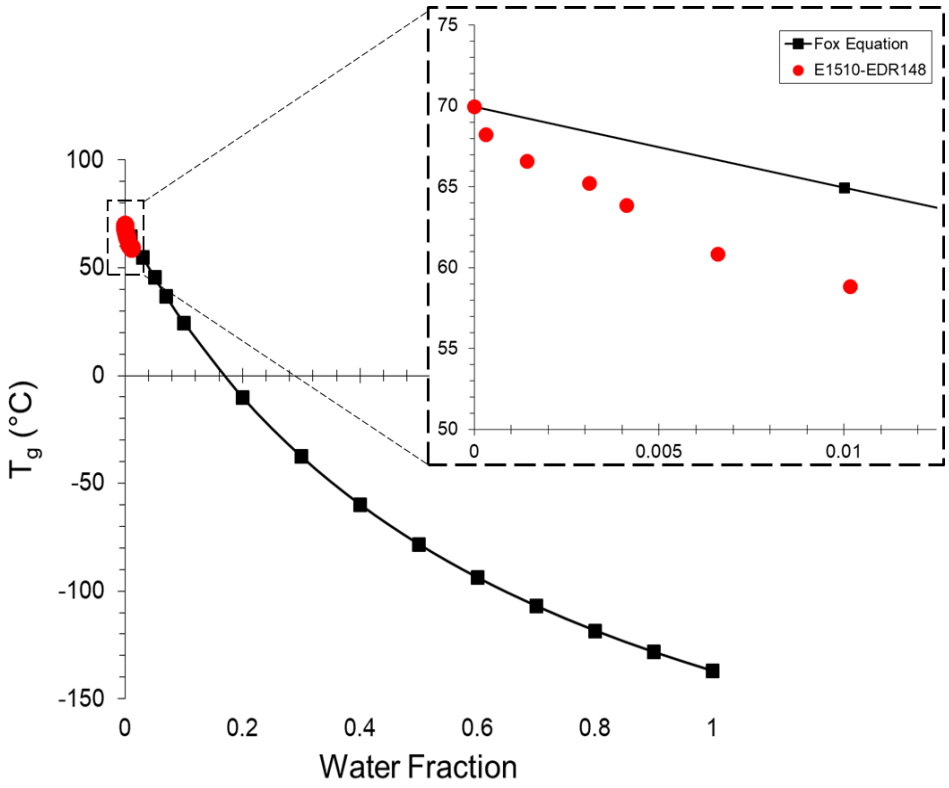

Figure 5.6 T_g vs. water fraction of the E1510-EDR148 network compared with Fox equation prediction

In both the elastomers, moisture sorption did not have any effect on $<v_h>$ (Figure 5.7(a)). The free volume holes in elastomers are dynamic in nature. In the case of E1510-THF100, even at 95% RH, the network absorbs only around 2.5 wt% moisture (Figure 5.4(d)) which probably was not enough to cause any substantial amount of swelling, and therefore relative humidity or moisture absorption did not have any effect on the free volume of E1510-THF100 network. Whereas E1510-ED900 absorbs about 27 wt% moisture at 95% RH (Figure 5.4(e)) and yet the free volume parameter $<v_h>$ measured by PALS at 85% and 99% RH surprisingly did not show any significant difference from that

of $<v_h>$ of E1510-ED900 measured at dry state. Swelling and plasticization of E1510-ED900 network by >20 wt% water would have significantly reduced the T_g of the network. DMA analysis of dry E1510-ED900 gave a T_g value of -11 °C and if -137 °C[29] is assumed as the T_g of water, then the network containing 0.2 weight fraction of water will have a T_g of ~-52 °C according to Fox equation (eq. 5)[28]. PALS measurements were performed at room temperature, i.e., 23 °C which is much greater than T_gs (< -52 °C) of water swollen E1510-ED900 network at 85% and 99% RH. It has been reported in the literature that when PALS measurements are performed at a $T>>T_g$, because of positronium bubble formation[31] or because o-Ps lifetimes are comparable to the relaxation times of polymer,[32-33] o-Ps lifetimes does not reflect the actual values of free volume hole sizes. Therefore, the aforementioned phenomenon can be assumed as the reason why RH did not have any effect on $<v_h>$ of E1510-ED900 network.

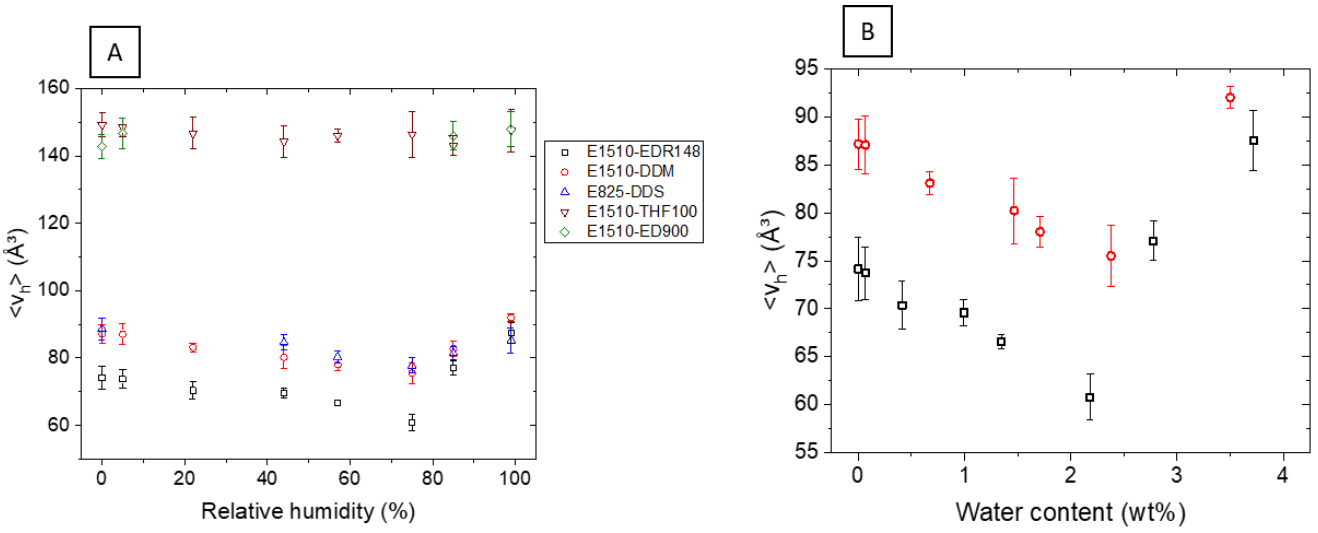

Figure 5.7 (a) Average free volume hole size $<v_h>$ vs. relative humidity of the networks. (b) $<v_h>$ vs. water content of E1510-EDR148 and E1510-DDM.

Whereas, the glassy networks showed a V-shaped trend for $<v_h>$ as a function of RH or water content (Figure 5.7). The V-shaped trend was more pronounced for E1510-

EDR148 and E1510-DDM networks than for E825-DDS network, and this is because the first two networks absorb more water (>3.5 wt% after a day in 95% RH), whereas the later network absorbs 2.5 wt% after a day's exposure to 95% RH (Figure 5.4(f)). The inherent differences in the polarity of the networks influence the moisture content in the networks at different RH conditions which in turn influences the free volume of the networks at different RH conditions. For E1510-EDR148, $<v_h>$ decreased from 74 Å^3 to 60 Å^3 after 1-day exposure to 75% RH. Similarly, for E1510-DDM $<v_h>$ decreased from 87 Å^3 to 75 Å^3. This decrease in $<v_h>$ was caused by 2.2 wt% and 2.4 wt% water for E1510-EDR148 and E1510-DDM networks respectively. This decrease in $<v_h>$ due to water sorption has previously been reported for linear glassy polymers such as ethylene-vinyl alcohol copolymer (EVOH)[23], polyamide 6[22], poly(arylene ether sulfone)[25], aromatic polyamides[24], and DGEBA based epoxy amine network[34]. In the aforementioned studies, the effect of water sorption on free volume was studied by pre-conditioning the polymer samples at different RH conditions or exposing the samples to liquid water, followed by $<v_h>$ measurements using PALS experiments. Except for the study on EVOH[23] and poly(arylene ether sulfone)[25], the other studies did not discuss maintaining the RH condition during the PALS experiment or how they took into account moisture desorption or absorption that can happen during the duration of PALS experiment. However, in the study on polyamide 6, the authors used Fick's law of diffusion and extrapolated the o-Ps lifetimes to zero time to obtain the values of $<v_h>$ at different RH conditions to account for moisture desorption and absorption during the experiments.[22] Whereas in our study since RH conditions were accurately maintained, $<v_h>$ values remained consistent across seven hours (or seven spectrums), i.e., during

one PALS experiment at any particular RH conditions, consistent $<v_h>$ values were obtained from all seven spectrums.

Most researchers agree that water molecules occupy the frozen-in (or static) free volume holes of glassy polymers which causes this decrease in $<v_h>$,[23, 25] i.e., Langmuir type of sorption. But they do not rule out the possibility of humidity-induced aging, i.e., the overall decrease in bulk volume caused by relaxation (or plasticization) of chains caused by water, leading to better packing[22]. Figure 5.8 compares the $<v_h>$ and the volume change of E1510-EDR148 network at different relative humidities. After exposure to 44% RH, there was negligible change in volume (i.e., 0.06%), whereas $<v_h>$ decreased from 74 Å^3 to 69 Å^3. This means that the 1.5 wt% (value obtained from DVS analysis) of water that was absorbed by E1510-EDR148 network after a 1-day exposure to 44% RH, mostly filled the frozen-in holes of the E1510-EDR148 network. From 44% to 75% RH, while the $<v_h>$ of the network decreased from 69 Å^3 to 60 Å^3, the volume of the network increased by 1%. This means that in E1510-EDR148 network, beyond 44% RH, in addition to the water molecules filling the pre-existing free volume holes, they also started to sorb into the network, i.e. Henry type sorption, which caused the increase in volume.

Beyond 75% RH, $<v_h>$ of all the glassy networks increased, which creates the V-shaped trend for $<v_h>$ as a function of RH. For the E1510-EDR148 network, the $<v_h>$ increased from 60 Å^3 to 88 Å^3 as RH was increased from 75% to 99%. This is because, beyond 75% RH, Henry type sorption dominates, i.e. sorbed water dissolves into the network causing the swelling of the networks. As water molecules swell into the network, they increase the distance between the chains, decrease the intermolecular interactions,

and thereby causing the increase in $<v_h>$ and bulk volume alike. Figure 5.8 shows that at 99% RH, the volume of E1510-EDR148 increased by 2.5%. Previous studies on glassy linear polymers such as polyamide 6[22], EVOH[23], poly(arylene ether sulfone)[25], aromatic polyamides[24], poly(ethylene imine)/poly(acrylic acid) multilayers[35] have shown this V-shaped trend and studies on poly(vinyl alcohol)[36], and poly(propylene glycol) based epoxy amine network[34] have shown an increase in free volume after sorption in liquid water. The study on EVOH showed a transition from the regime where free volume decreases to the regime where free volume increases, at 30% RH,[23] whereas for polyamide 6 it was at 50% RH,[22] and for aromatic polyamides at 54% RH[24]. In this study, all the networks showed a transition at around 75% RH. This difference in the region of transition for different polymers might be due to the differences in the amount of moisture absorbed by different polymers at different RH conditions, which in turn is due to the differences in polarity of the polymers, i.e., a more polar network might show a transition at a lower RH. EVOH and polyamide polymers are more polar and have more H-bonding sites for water compared to the glassy networks used in the present study and hence the linear polymers studied in the previous reports showed the transition at lower RHs. E1510-EDR148 and E1510-DDM both show transition at 75% RH because of the similar polarity of the networks, as they absorb similar levels of water at different RH conditions (Figure 5.4(f)), and hence the trends of $<v_h>$ as a function of water content (Figure 5.7(b)) looks similar for both E1510-EDR148 and E1510-DDM.

Figure 5.9 compares the oxygen transmission of E1510-EDR148 and E1510-DDM networks measured at different RH conditions by MOCON instrument. As expected, once equilibrium is attained, oxygen transmission of the E1510-DDM network

is much higher than that of the E1510-EDR148 because of the inherently higher free volume of the E1510-DDM network (Figure 5.7). To get a deeper understanding of oxygen transport, oxygen flux (transmission) data was fit using eq 2 as described in the experimental section.

Figure 5.10 shows that, in the dry state, the oxygen permeability of E1510-EDR148 is almost half as that of the E1510-DDM network. This difference is mainly due to the differences in oxygen solubility of the two networks, as there was not any significant difference in oxygen diffusivity. Oxygen gas sorbs in to the frozen-in free volume holes in glasses, and the transport happens by hoping of gas molecules between neighboring free volume holes towards the direction of lower chemical potential or lower oxygen partial pressure region.[37-39] Therefore, solubility is proportional to the amount of free volume in the material, and hence oxygen solubility and thus the oxygen permeability is higher in E1510-DDM when compared to E1510-EDR148.

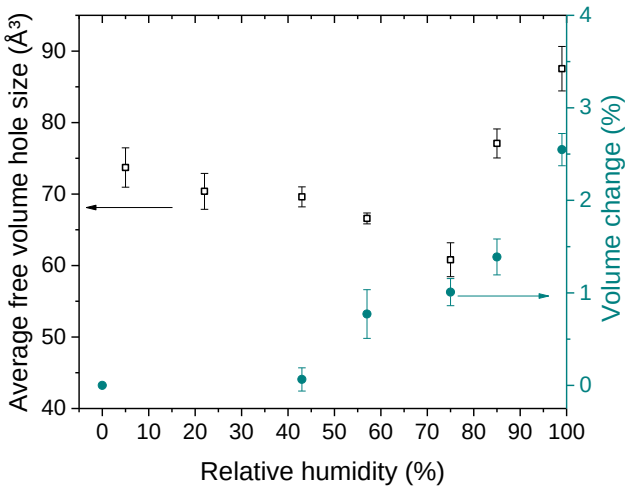

Figure 5.8 Average free volume hole size $<v_h>$ and bulk volume change of E1510-EDR148 network plotted as a function of relative humidity.

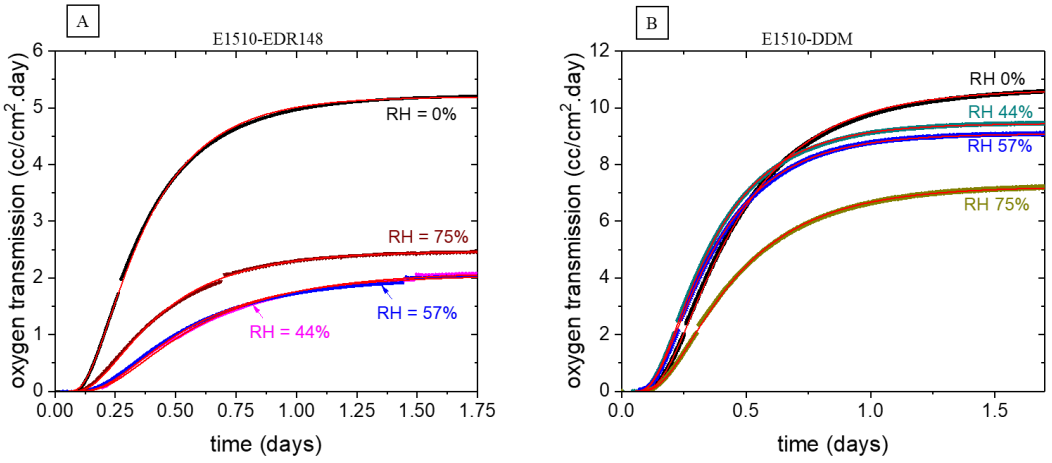

Figure 5.9 Oxygen transmission of (a) E1510-EDR148 and (b) E1510-DDM network films measured as a function of time by MOCON instrument.

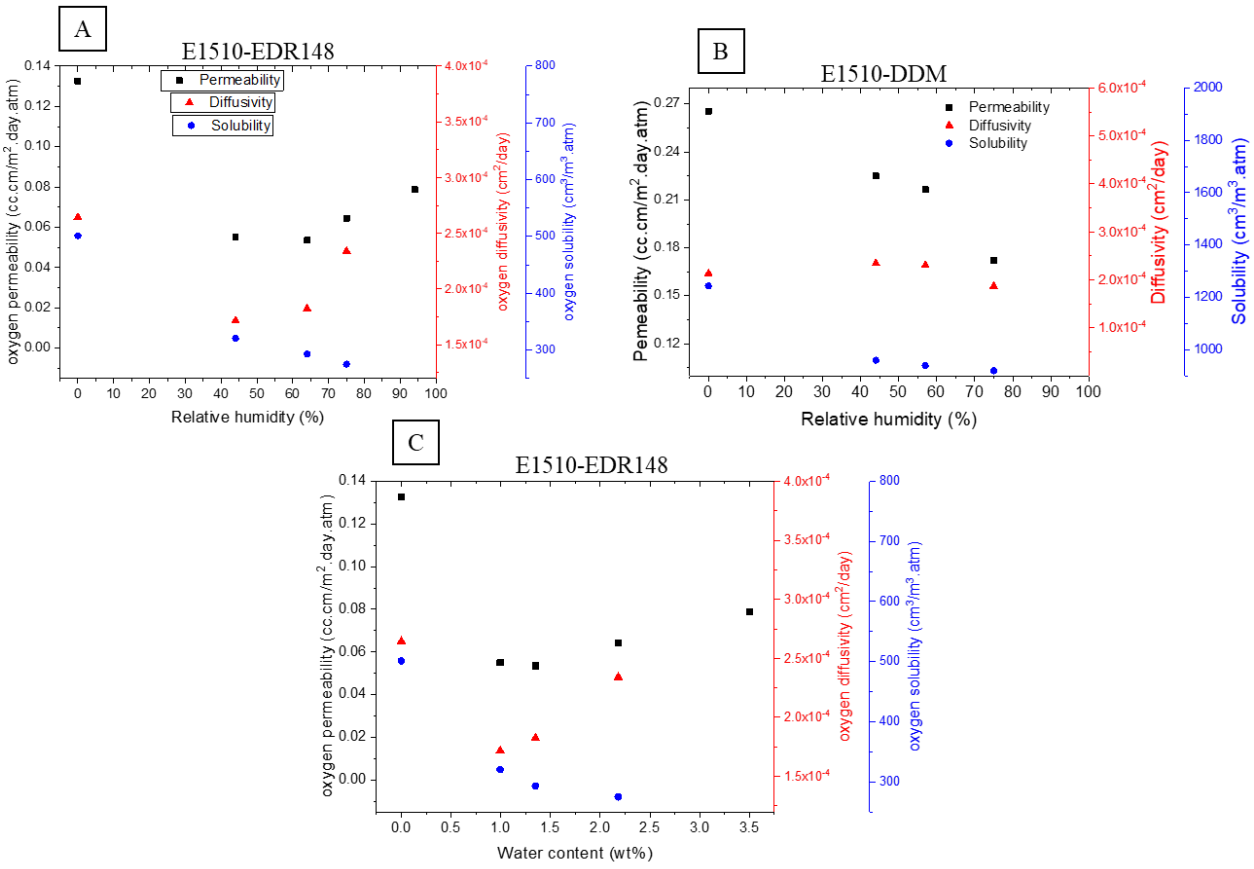

Figure 5.10 Oxygen transport parameters (permeability, diffusivity, and solubility) of (a) E1510-EDR148 and (b) E1510-DDM vs. relative humidity. 9(c) Oxygen transport parameters of E1510-EDR148 vs. water content in the network.

Like the $<v_h>$ vs. RH (or water content) trend (Figure 5.6), there is a dip or minimum for oxygen permeability for both E1510-EDR148 and E1510-DDM networks when plotted as a function of RH (or water content) (Figure 5.10). A similar trend for oxygen transport vs. RH has been previously been reported for Nylon 6[40-41], EVOH[23, 42], and aromatic polyamides[24]. In general, it is agreed that the oxygen permeability trend is more complex, as it is a product of diffusivity and solubility. For both E1510-EDR148 and E1510-DDM networks, oxygen solubility decreases when relative humidity (or water content) is increased (Figure 5.10). As relative humidity increases, the water content in the networks increase, and these water molecules sorb and occupy the frozen-in free volume of the networks, which means there is less free volume available for oxygen sorption and this causes the decrease in oxygen solubility for both the networks when RH is increased. A similar trend for oxygen solubility vs. RH was seen in aromatic polyamides.[24]

The water sorption did not have any effect on oxygen diffusivity for the E1510-DDM network (Figure 5.10(b)), whereas 44% RH (or 1 wt% water sorption) caused ~30% decrease in oxygen diffusivity for the E1510-EDR148 network (Figures 5.10(a) and 10(c)). The conformational changes and chain motions let gas molecules hop between different frozen-in (or static) free volume holes.[43] In the case of E1510-EDR148, since the free volume is lesser, even 1 wt% water probably fills up most of the free volume holes, which probably increases the average distance between the remaining free volume holes, and therefore increasing the hoping or jump distance for oxygen molecules which caused the decrease in oxygen diffusivity at 44% RH (Figure 5.10(a)). Whereas, in the case of E1510-DDM, since the free volume is higher, to begin with, the average

hopping distance or jump distance for oxygen gas molecules remains constant even though water molecules fill some free volume holes, which explains the reason why water sorption did not have any effect on oxygen gas diffusivity of E1510-DDM network.

Beyond 44% RH, oxygen diffusivity through E1510-EDR148 network increased. As the chain motions increase, the activation energy required for oxygen gas molecules to hop between free volume holes decreases and therefore increasing the oxygen diffusivity.[43] It can be hypothesized that in the case of E1510-EDR148, water starts to sorb into the network beyond 44% RH disrupting the intermolecular Hydrogen bonding, which caused the improvements in chain dynamics resulting in oxygen diffusivity upswing. As discussed earlier this Henry-type sorption also caused volume increase beyond 44% RH (Figure 5.8) in E1510-EDR148 network.

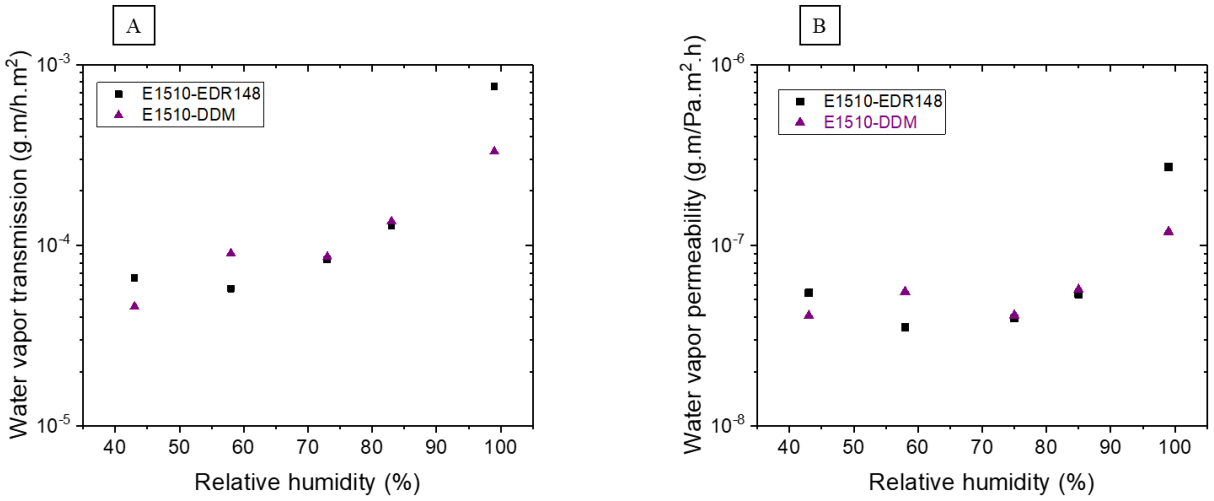

Figure 5.11 Effect on relative humidity on (a) water vapor transmission and (b) water vapor permeability in E1510-EDR148 and E1510-DDM networks.

Figure 5.11(b) shows that there is no significant difference between the water vapor permeability values of E1510-EDR148 and E1510-DDM networks up till 85% RH. Also, RH had no significant effect on water vapor permeability up till 75% RH, and

beyond 75% RH, water vapor permeability increases. Similar trends were seen in EVOH polymers, but the upswing in water vapor permeability happened at a much lower RH.[42] This trend is different from that of oxygen permeability vs. RH trend. The water molecules that are sorbed into the free volume holes will not act as a barrier for water transport, whereas they do reduce oxygen sorption, and hence water vapor permeability remains almost constant up till 75% RH. Beyond 75% RH, higher water absorption results in network swelling which results in increased free volume, and thereby the water vapor permeability upswing beyond 75% RH.

5.7 Conclusions

A comprehensive study on the complex effect of water sorption on free volume, oxygen, and water vapor permeability of epoxy-amine networks was performed. In glasses, free volume showed a V-shaped trend when plotted against water content. The decrease in free volume was caused by the filling of free volume holes by water molecules. Beyond a certain limit, further ingress of water molecules into the network resulted in swelling which caused the increase in free volume and thereby the V-shaped trend.

The oxygen permeability of the E1510-EDR148 network showed a V-shaped trend when plotted as a function of water content. But the trend was more complex as water sorption affected both oxygen solubility and oxygen diffusivity. The Langmuir-type sorption of water, i.e. filling of free volume holes by water molecules reduced the oxygen solubility because of the reduction in free volume spaces for oxygen sorption. Initially, i.e., at lower water content, oxygen diffusivity also decreased for E1510-EDR148 because of the increase in average jump distance or hoping distance for oxygen

molecules, as the water molecules filled most of the free volume holes. With further ingress, the water molecules started to penetrate the network (i.e., Henry-type sorption) and disrupt the intermolecular interactions and plasticize the chains, leading to an increase in oxygen diffusivity values.

Water vapor permeability values remained almost constant until the networks started to swell (i.e., for E1510-EDR148 and E1510-DDM up till 75% RH). Because the water molecules which fill the free volume holes do not act as barrier for water vapor transport. Whereas, beyond 75% RH, as the networks started to swell or as the free volume started to increase, water vapor permeability increased.

5.8 References

1. Wicks, Z. W., Jr.; Jones, F. N.; Pappas, S. P., *Organic Coatings: Science and Technology*. Second ed.; Federation of Societies for Coatings Technology: 1999; Vol. 71.

2. Vanlandingham, M.; Eduljee, R.; Gillespie Jr, J., Moisture diffusion in epoxy systems. *Journal of Applied Polymer Science* **1999,** *71* (5), 787-798.

3. Musto, P.; Mascia, L.; Ragosta, G.; Scarinzi, G.; Villano, P., The transport of water in a tetrafunctional epoxy resin by near-infrared Fourier transform spectroscopy. *Polymer* **2000,** *41* (2), 565-574.

4. Van der Wel, G.; Adan, O., Moisture in organic coatings—a review. *Progress in Organic Coatings* **1999,** *37* (1-2), 1-14.

5. Soles, C. L.; Chang, F. T.; Bolan, B. A.; Hristov, H. A.; Gidley, D. W.; Yee, A. F., Contributions of the nanovoid structure to the moisture absorption properties of epoxy resins. *Journal of Polymer Science Part B: Polymer Physics* **1998,** *36* (17), 3035-3048.

6. Soles, C. L.; Chang, F. T.; Gidley, D. W.; Yee, A. F., Contributions of the nanovoid structure to the kinetics of moisture transport in epoxy resins. *Journal of Polymer Science Part B: Polymer Physics* **2000,** *38* (5), 776-791.

7. Soles, C. L.; Yee, A. F., A discussion of the molecular mechanisms of moisture transport in epoxy resins. *Journal of Polymer Science Part B: Polymer Physics* **2000,** *38* (5), 792-802.

8. Lin, H.; Wagner, E. V.; Swinnea, J. S.; Freeman, B. D.; Pas, S. J.; Hill, A. J.; Kalakkunnath, S.; Kalika, D. S., Transport and structural characteristics of crosslinked poly(ethylene oxide) rubbers. *Journal of Membrane Science* **2006,** *276* (1–2), 145-161.

9. Cohen, M. H.; Turnbull, D., Molecular Transport in Liquids and Glasses. *The Journal of Chemical Physics* **1959,** *31* (5), 1164-1169.

10. Park, J. Y.; Paul, D. R., Correlation and prediction of gas permeability in glassy polymer membrane materials via a modified free volume based group contribution method. *Journal of Membrane Science* **1997,** *125* (1), 23-39.

11. Haraya, K.; Hwang, S.-T., Permeation of oxygen, argon and nitrogen through polymer membranes. *Journal of Membrane Science* **1992,** *71* (1), 13-27.

12. Sanders, D. F.; Smith, Z. P.; Guo, R.; Robeson, L. M.; McGrath, J. E.; Paul, D. R.; Freeman, B. D., Energy-efficient polymeric gas separation membranes for a sustainable future: A review. *Polymer* **2013,** *54* (18), 4729-4761.

13. Paul, D. R.; Yampol'skii, Y. P., *Polymeric gas separation membranes*. CRC press: 1993.

14. Freeman, B.; Yampolskii, Y.; Pinnau, I., *Materials science of membranes for gas and vapor separation*. John Wiley & Sons: 2006.

15. Fox, T. G.; Loshaek, S., Influence of molecular weight and degree of crosslinking on the specific volume and glass temperature of polymers. *Journal of Polymer Science* **1955,** *15* (80), 371-390.

16. Kwisnek, L.; Goetz, J.; Meyers, K. P.; Heinz, S. R.; Wiggins, J. S.; Nazarenko, S., PEG Containing Thiol–Ene Network Membranes for CO2 Separation: Effect of Cross-Linking on Thermal, Mechanical, and Gas Transport Properties. *Macromolecules* **2014,** *47* (10), 3243-3253.

17. Morgan, D. R.; Stejskal, E. O.; Andrady, A. L., 129Xe NMR Investigation of the Free Volume in Dendritic and Cross-Linked Polymers. *Macromolecules* **1999,** *32* (6), 1897-1903.

18. Consolati, G.; Kansy, J.; Pegoraro, M.; Quasso, F.; Zanderighi, L., Positron annihilation study of free volume in cross-linked amorphous polyurethanes through the glass transition temperature. *Polymer* **1998,** *39* (15), 3491-3498.

19. Finkelshtein, E. S.; Makovetskii, K.; Gringolts, M.; Rogan, Y. V.; Golenko, T.; Starannikova, L.; Yampolskii, Y. P.; Shantarovich, V.; Suzuki, T., Addition-type polynorbornenes with Si (CH3) 3 side groups: synthesis, gas permeability, and free volume. *Macromolecules* **2006,** *39* (20), 7022-7029.

20. Yu, X.; Jia, J.; Xu, S.; Lao, K. U.; Sanford, M. J.; Ramakrishnan, R. K.; Nazarenko, S. I.; Hoye, T. R.; Coates, G. W.; DiStasio, R. A., Unraveling substituent effects on the glass transition temperatures of biorenewable polyesters. *Nature communications* **2018,** *9* (1), 2880.

21. Kusuma, V. A.; Freeman, B. D.; Borns, M. A.; Kalika, D. S., Influence of chemical structure of short chain pendant groups on gas transport properties of cross-linked poly(ethylene oxide) copolymers. *Journal of Membrane Science* **2009,** *327* (1), 195-207.

22. Dlubek, G.; Redmann, F.; Krause-Rehberg, R., Humidity-induced plasticization and antiplasticization of polyamide 6: A positron lifetime study of the local free volume. *Journal of Applied Polymer Science* **2002,** *84* (2), 244-255.

23. Muramatsu, M.; Okura, M.; Kuboyama, K.; Ougizawa, T.; Yamamoto, T.; Nishihara, Y.; Saito, Y.; Ito, K.; Hirata, K.; Kobayashi, Y., Oxygen permeability and free

volume hole size in ethylene–vinyl alcohol copolymer film: temperature and humidity dependence. *Radiation Physics and Chemistry* **2003,** *68* (3), 561-564.

24. Hu, Y. S.; Mehta, S.; Schiraldi, D. A.; Hiltner, A.; Baer, E., Effect of water sorption on oxygen-barrier properties of aromatic polyamides. *Journal of Polymer Science Part B: Polymer Physics* **2005,** *43* (11), 1365-1381.

25. Xie, W.; Ju, H.; Geise, G. M.; Freeman, B. D.; Mardel, J. I.; Hill, A. J.; McGrath, J. E., Effect of free volume on water and salt transport properties in directly copolymerized disulfonated poly (arylene ether sulfone) random copolymers. *Macromolecules* **2011,** *44* (11), 4428-4438.

26. Tao, S. J., Positronium Annihilation in Molecular Substances. *The Journal of Chemical Physics* **1972,** *56* (11), 5499-5510.

27. Kirkegaard, P.; Eldrup, M.; Mogensen, O. E.; Pedersen, N. J., Program system for analysing positron lifetime spectra and angular correlation curves. *Computer Physics Communications* **1981,** *23* (3), 307-335.

28. Fox, T. G., Influence of Diluent and of Copolymer Composition on the Glass Temperature of a Poly-mer System. *Bull. Am. Phys. Soc.* **1956,** *1*, 123.

29. Tsavalas, J. G.; Sundberg, D. C., Hydroplasticization of polymers: model predictions and application to emulsion polymers. *Langmuir* **2010,** *26* (10), 6960-6966.

30. Kalogeras, I. M.; Brostow, W., Glass transition temperatures in binary polymer blends. *Journal of Polymer Science Part B: Polymer Physics* **2009,** *47* (1), 80-95.

31. Mikhin, K. V.; Stepanov, S. V.; Byakov, V. M., Formation of the Ps bubble in liquid media. *Radiation Physics and Chemistry* **2003,** *68* (3-4), 415-417.

32. Bartos, J.; Sausa, O.; Kristiak, J.; Blochowicz, T.; Rössler, E., Free-volume microstructure of glycerol and its supercooled liquid-state dynamics. *Journal of Physics: Condensed Matter* **2001,** *13* (50), 11473.

33. Bamford, D.; Dlubek, G.; Reiche, A.; Alam, M.; Meyer, W.; Galvosas, P.; Rittig, F., The local free volume, glass transition, and ionic conductivity in a polymer electrolyte: A positron lifetime study. *The Journal of Chemical Physics* **2001,** *115* (15), 7260-7270.

34. MacQueen, R. C.; Granata, R. D., A positron annihilation lifetime spectroscopic study of the corrosion protective properties of epoxy coatings. *Progress in Organic Coatings* **1996,** *28* (2), 97-112.

35. Song, Y.; Meyers, K. P.; Gerringer, J.; Ramakrishnan, R. K.; Humood, M.; Qin, S.; Polycarpou, A. A.; Nazarenko, S.; Grunlan, J. C., Fast Self-Healing of Polyelectrolyte Multilayer Nanocoating and Restoration of Super Oxygen Barrier. *Macromolecular Rapid Communications* **2017**, 1700064-n/a.

36. Hodge, R.; Bastow, T.; Edward, G.; Simon, G.; Hill, A., Free volume and the mechanism of plasticization in water-swollen poly (vinyl alcohol). *Macromolecules* **1996,** *29* (25), 8137-8143.

37. Weiss, G. H.; Bendler, J. T.; Shlesinger, M. F., Continuous-site model for Langmuir gas sorption in glassy polymers. *Macromolecules* **1992,** *25* (2), 990-992.

38. Polyakova, A.; Liu, R.; Schiraldi, D.; Hiltner, A.; Baer, E., Oxygen-barrier properties of copolymers based on ethylene terephthalate. *Journal of Polymer Science Part B: Polymer Physics* **2001,** *39* (16), 1889-1899.

39. Polyakova, A.; Connor, D.; Collard, D.; Schiraldi, D.; Hiltner, A.; Baer, E., Oxygen-barrier properties of polyethylene terephthalate modified with a small amount of aromatic comonomer. *Journal of Polymer Science Part B: Polymer Physics* **2001,** *39* (16), 1900-1910.

40. Gavara, R.; Hernandez, R. J., The effect of water on the transport of oxygen through nylon-6 films. *Journal of Polymer Science Part B: Polymer Physics* **1994,** *32* (14), 2375-2382.

41. Khanna, Y.; Day, E.; Tsai, M.; Vaidyanathan, G., Re-examining the oxygen barrier of nylon 6 films. I. Role of moisture and processing induced variables. *Journal of Plastic Film & Sheeting* **1997,** *13* (3), 197-211.

42. Zhang, Z.; Britt, I. J.; Tung, M. A., Permeation of oxygen and water vapor through EVOH films as influenced by relative humidity. *Journal of Applied Polymer Science* **2001,** *82* (8), 1866-1872.

43. Hiltner, A.; Liu, R.; Hu, Y.; Baer, E., Oxygen transport as a solid-state structure probe for polymeric materials: A review. *Journal of Polymer Science Part B: Polymer Physics* **2005,** *43* (9), 1047-1063.